

LARGE LOW SPEED HYDROGENERATORS - UMP AND ADDITIONAL DAMPER LOSSES IN ECCENTRICITY CONDITIONS

THÈSE N° 3773 (2007)

PRÉSENTÉE LE 13 AVRIL 2007

À LA FACULTÉ DES SCIENCES ET TECHNIQUES DE L'INGÉNIEUR

Laboratoire de machines électriques

PROGRAMME DOCTORAL EN ENERGIE

ÉCOLE POLYTECHNIQUE FÉDÉRALE DE LAUSANNE

POUR L'OBTENTION DU GRADE DE DOCTEUR ÈS SCIENCES

PAR

Stefan KELLER

ingénieur électricien diplômé EPF
de nationalité suisse et originaire de Zurich (ZH)

acceptée sur proposition du jury:

Prof. A. Rufer, président du jury
Prof. J.-J. Simond, Dr M. Tu Xuan, directeurs de thèse
Prof. J.-M. Kauffmann, rapporteur
Prof. J. R. Mosig, rapporteur
Dr A. Schwery, rapporteur



ÉCOLE POLYTECHNIQUE
FÉDÉRALE DE LAUSANNE

Suisse
2007

Remerciements

Par ces quelques lignes, je souhaiterais remercier les personnes qui ont contribué à ce travail de doctorat.

Avant tout, j'aimerais faire part de ma reconnaissance au Professeur Jean-Jacques Simond, qui m'a permis de réaliser ce projet au sein de son laboratoire, le LME, ainsi qu'au Docteur Mai Tu Xuan pour sa participation très active tout au long de cette étude. Ils ont partagé avec moi leur vaste expérience et leurs connaissances dans ce domaine, tout en m'accordant une grande liberté.

Merci également aux membres du jury, Professeur Jean-Marie Kaufmann, Professeur Juan Mosig, Professeur Alfred Rufier et Docteur Alexander Schwery qui m'ont aidé, par leurs critiques constructives, à améliorer ce rapport de thèse.

Je remercie aussi mes collègues du LME. Grâce à eux, j'ai pu travailler durant ces trois ans dans une atmosphère à la fois agréable, détendue, fructueuse et inspirante.

Je tiens également à remercier Carlos Ramirez et Alexander Schwery, de la firme ALSTOM. Leurs commentaires et réactions d'un point de vue industriel ont élargi mon horizon et beaucoup contribué à ma motivation.

Mes remerciements vont aussi à la Commission pour la Technologie et l'Innovation, CTI, aux Electriciens Romands, au fonds pour projets et études de l'économie électrique, PSEL, ainsi qu'à la firme ALSTOM, qui ont soutenus financièrement ce projet.

Pour conclure, je remercie ma famille et tout particulièrement mes parents. Ils m'ont appris à poursuivre mes objectifs et à affronter les défis avec plaisir et ouverture d'esprit.

Résumé

Cette thèse est une contribution avancée à la conception des grands alternateurs synchrones à haute polarité. Elle propose deux apports originaux permettant, l'un une prédiction très précise de l'onde de tension induite à vide et des pertes supplémentaires dans l'enroulement amortisseur, l'autre le calcul rigoureux des efforts d'attraction magnétiques non compensés (UMP – Unbalanced Magnetic Pull) et des pertes supplémentaires associées dans l'enroulement amortisseur lorsque la machine est affectée par une excentricité ou lorsque sa géométrie statorique ou rotorique est déformée de manière quelconque. Les deux apports sont basés sur la même stratégie, à cela près qu'il y a lieu de tenir compte que la géométrie n'est pas la même dans les deux cas, elle est supposée parfaite pour le premier, dégradée pour le second.

La méthode des éléments finis (FEM) magnétostatique en 2D est utilisée pour déterminer les couplages magnétiques entre les conducteurs de la machine en fonction de la position du rotor. Ces valeurs de couplages magnétiques sont ensuite utilisées dans les équations de tension des circuits électriques de la machine qui sont résolues grâce à une méthode numérique. L'astuce utilisée revient au calcul du flux magnétique couplé avec un conducteur dans deux situations, la première où seule l'excitation polaire intervient et fixe les niveaux de saturation, la seconde où intervient simultanément un courant dans l'une des barres amortisseur. Cette stratégie conduit à la notion d'inductances différentielles.

Les deux apports se différencient en raison du fait que pour le premier la périodicité cyclique géométrique de la machine est d'un pas d'encoche statorique, alors qu'il n'y a plus de périodicité courte pour une géométrie dégradée.

Dans le premier cas les valeurs de couplages magnétiques et les inductances nécessaires à la prédiction de l'onde de tension induite sont ainsi calculées uniquement pour un certain nombre de positions du rotor sur un pas d'encoche statorique. Ces valeurs sont ensuite réutilisées pour toutes les autres positions du rotor. Cette méthode permet de prédéterminer les courants et les pertes dans l'amortisseur, ainsi que l'onde de tension induite à vide avec la même précision que celle livrée par un calcul FEM magnéto-évolutif en 2D, mais en réduisant le temps de calcul d'un facteur d'environ 20. Des comparaisons avec des mesures et des calculs FEM magnéto-évolutifs effectuées sur plusieurs unités en exploitation quittent l'extrême précision garantie par cette démarche.

Le calcul des efforts d'attraction magnétiques non compensés et des pertes supplémentaires associées pour une machine dont la géométrie est dégradée ne pouvant pas exploiter une périodicité géométrique courte, il y a lieu de procéder autrement. Les couplages magnétiques entre les divers circuits sont à nouveau calculés préalablement par FEM magnétostatique, mais sans rotation du rotor. L'encoche statorique peut être négligé parce qu'il n'influence pas le résultat visé. Une déformation géométrique

quelconque est traduite par des segments contigus, disposés sur l'alésage, segments qu'il est possible de déplacer radialement dans les deux directions. L'ajustement correct dans le temps de la valeur d'entrefer de chaque segment permet de modéliser toutes les combinaisons possibles de déformations statiques et dynamiques de l'entrefer pour toutes les positions du rotor. En utilisant une superposition linéaire des influences linéarisées de tous les segments sur les valeurs de couplages magnétiques et les inductances, le nombre de calculs préliminaires FEM magnéto-statiques peut être minimisé. Il y a lieu de relever que les calculs préliminaires en magnéto-statique 2D ne sont réalisés qu'une seule fois pour une machine donnée. Ils sont alors utilisables pour plusieurs déformations de la géométrie. Si l'on utilise un calcul magnéto-évolutif 2D l'entier de l'approche est à répéter pour chaque déformation géométrique à analyser. Les résultats obtenus ont été systématiquement comparés à ceux livrés par un calcul FEM en magnéto-évolutif, la concordance est excellente et le gain en temps de calcul est énorme.

Les deux apports sont traduits par deux logiciels hautement automatisés et donc très adaptés à une exploitation industrielle.

Mots clés – modélisation, onde de tension induite à vide, courants amortisseur, excentricité, force magnétique non-compensée (UMP), machine synchrone

Abstract

The present thesis is an advanced contribution to the design process of large synchronous generators with high number of poles. It proposes two original contributions, the first one allowing a very precise prediction of the no-load voltage and of the no-load losses in the damper winding, the second one allowing a rigorous calculation of the unbalanced magnetic pulls and of the associated losses in the damper winding in the case of a machine in eccentricity conditions or with any kind of rotor and stator deformation. Both contributions are based on the same strategy, apart from the fact that it has to be taken into account that the geometry is not the same in both cases, it is supposed perfect in the first case and damaged in the second.

The magnetostatic 2D finite element method (FEM) is used to determine the magnetic coupling of the machine conductors as a function of the rotor position. These values of magnetic coupling are then used in the voltage equations of the machine which are solved using a numerical method. A particularity is the calculation of the magnetic flux coupled with a conductor in two situations, once with only the field winding currents, fixing the levels of saturation, and once with field winding currents and a current in one damper bar. This strategy leads to the concept of differential inductances.

The two contributions are different because for the first one the geometric, cyclic periodicity of the machine is of one stator slot pitch and for the damaged machine no short cyclic periodicity can be found.

In the first case the values of flux linkage and the inductances necessary for the voltage prediction are therefore calculated only for some rotor positions within one stator slot pitch. These values are then reused for all other rotor positions. This method allows to predict the currents and the losses in the damper winding, as well as the no-load voltage waveform with the same precision as a transient magnetic FEM simulation but reducing the simulation time by a factor of about 20. Comparisons with measurements and with transient magnetic FEM simulations on several operating units prove the precision of this approach.

As in the case of the calculation of the unbalanced magnetic pulls and of the associated losses in the damper winding for a machine with damaged geometry one can not take advantage of a short geometric periodicity, the procedure has to be different. Again the magnetic coupling of the different circuits is calculated in advance using the magnetostatic FEM, but in this case without rotation of the rotor. The stator slotting can be neglected because it does not influence the aimed results. Any kind of geometric deformation is represented by contiguous segments, placed on the interior stator surface, which can be displaced radially in both directions. A correct adjustment in time of the air gap value of each segment allows to represent any combination of static and dynamic deformation of the air gap for any position of the rotor. The use of a linear superposition of the linearized influences of all segments on the values of magnetic

coupling and on the inductances allows to reduce the number of preliminary magnetostatic FEM calculations to the minimum. It has to be specified that the preliminary magnetostatic 2D FEM calculations are carried out only once for a given machine. They can then be used for different deformations of the geometry. If one wants to use the transient magnetic 2D FEM the whole approach has to be repeated for every geometric deformation to be analyzed. The results obtained have been systematically compared to results obtained through transient magnetic FEM calculations. The agreement is excellent and the reduction of calculation time is enormous.

Both contributions were implemented in highly automatized tools; they are therefore well adapted to an industrial application.

Key words – Modeling, no-load voltage waveform, damper winding currents, eccentricity, unbalanced magnetic pull (UMP), synchronous machine

Table of contents

1	Introduction	1
1.1	Eccentricities in hydrogenerators	1
1.2	Contribution of this thesis.....	2
1.3	Structure of this report	3
2	Method for calculation of the no-load voltage of hydrogenerators	5
2.1	Introduction.....	5
2.1.1	Existing methods.....	5
a)	Numerical methods	5
b)	Analytical methods.....	7
c)	Combined analytical and numerical methods	8
2.1.2	Suggested method	8
2.2	Summary of the suggested method.....	9
2.3	Hypotheses.....	10
2.4	Determination of the flux linkages	10
2.4.1	Principles.....	10
a)	Inductances.....	10
b)	Differential inductances	10
c)	Taking into account the machine rotational symmetry	12
d)	Determination of the differential inductances using the FEM	12
2.5	Differential equations and numerical resolution.....	15
2.5.1	Principles.....	15
2.5.2	Calculation of the damper bar currents	15
a)	Circuits and equations describing the connection of the conductors	15
b)	Differential equations in matrix form.....	18
c)	Numerical resolution of the differential equations.....	20
2.5.3	Calculation of the no-load voltage	20
2.6	Practical application of the method	22
2.6.1	FEM calculations	22
2.6.2	Tool for solving the circuit equations	22
3	Verification and applications	25
3.1	Introduction.....	25
3.2	Verification on unit 1	25
3.2.1	Unit 1	25
3.2.2	Comparison of the results	26
a)	Damper bar currents	26
b)	No-load voltage and THF.....	27
3.3	Application to unit 2.....	30
3.3.1	Unit 2	30
3.3.2	Comparison of two damper cage layouts.....	31
a)	No-load voltage and damper bar currents for two cases	31
b)	Analysis of the damper bar currents.....	32
3.4	Comparison of the simulation time.....	36

4	Prediction of the damper bar currents and of unbalanced magnetic pulls in deformed synchronous machines	37
4.1	Introduction	37
4.1.1	Types of deformations	37
a)	Static deformation	37
b)	Dynamic deformation	38
4.1.2	Existing methods for eccentricity analysis	39
4.1.3	Extensions of the method described in chapter 2	39
4.2	Hypothesis and simplifications	41
4.2.1	Machines used for verification	41
a)	Unit 3	42
b)	Unit 4	43
4.2.2	Neglect stator slotting	44
a)	Modification of the air gap according to Carter	44
b)	Stator conductors on smooth stator	45
4.2.3	Verifications concerning stator slotting	46
a)	Carter correction of the air gap	46
b)	Neglecting stator slotting	47
4.2.4	Modeling of the variable air gap	49
a)	Variable air gap representation for FEM calculations	49
b)	Calculation of magnetic coupling without rotating the rotor	51
c)	Representation of the effects of each air gap segment	52
d)	Combination of the effects of each air gap segment	55
e)	Resolution of the circuit equations	56
4.2.5	Verifications of the air gap modeling	57
a)	Representation of air gap deformations using line region segments	57
b)	Linear superposition of the influences of several air gap segments	59
4.2.6	Re-using inductance values	63
4.3	Unbalanced magnetic pull calculation	64
4.3.1	Deformation of the air gap induction	64
4.3.2	Unbalanced magnetic pull calculation	65
4.4	Summary of the method	66
4.4.1	Number of FEM calculations	67
4.4.2	Description of the calculation steps	68
a)	FEM calculations	68
b)	Calculation of flux linkage and inductance values	69
c)	Resolution of differential equations	69
d)	Calculation of the unbalanced magnetic pulls	69
4.4.3	Tool for practical application of the method	69
a)	Generalities	70
b)	Introduction of machine data	70
c)	Description of the deformation	71
d)	Calculation of the damper bar currents, stator voltages and unbalanced magnetic pulls	72
e)	Visualization of the results	73
4.4.4	Calculation of additional losses due to eccentricities	74
4.5	Verifications	74

4.5.1	Machines used for verifications	75
a)	Unit 5.....	75
b)	Unit 6.....	76
4.5.2	Damper bar currents.....	77
a)	1st order static eccentricity.....	77
b)	Higher order static deformations.....	79
c)	Combined static and dynamic deformation.....	82
4.5.3	Induced stator voltages	83
a)	Static deformations.....	83
b)	Dynamic deformations	85
c)	Combined static and dynamic deformations	88
4.5.4	Unbalanced magnetic pulls	89
4.5.5	Limits of precision of the presented method.....	91
a)	Influence of the number of air gap segments	91
b)	Influence of the number of rotor positions per revolution	94
c)	Amplitudes of air gap deformations and linearization with one or two line segments	96
d)	General assessment of the limits of precision	99
4.6	Application example	100
4.6.1	Unit 5, geometries with 3 and 4 damper bars	100
5	Outlook	103
5.1	Calculation of circulating currents in stator parallel circuits and equipotential connections	103
5.2	Calculation for other operating points	103
6	Conclusion	105
7	Bibliography.....	107
8	Glossary	109

1 Introduction

1.1 Eccentricities in hydrogenerators

Large low speed synchronous machines used in run of river hydro power plants are characterized by a considerable stator bore diameter (up to 22m) and a relatively small minimum air gap width (20mm to 30mm). This very small air gap to stator bore diameter ratio makes it virtually impossible to center the rotor perfectly within the stator during the assembly process (see figure 2). Figure 1 shows a cross-section of the magnetic circuits of a bulb type machine; it shows clearly the very low air gap to stator bore diameter ratio.

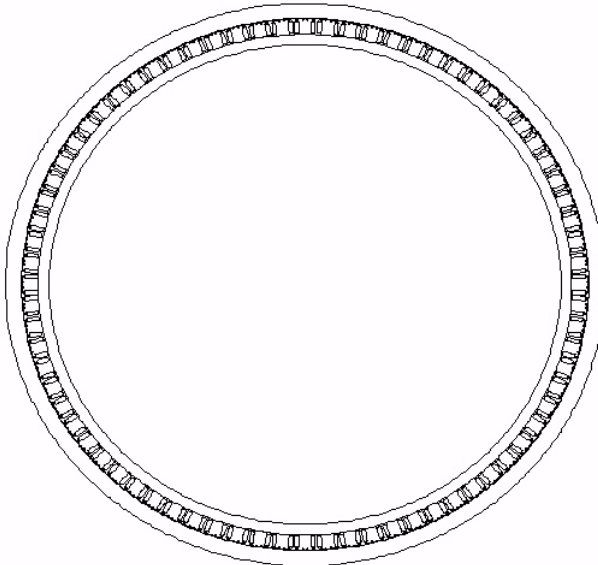


Figure 1: Bulb type machine

Another problem is the rigidity of stator and rotor. Especially in bulb type machines the stator can deform because of the very thin stator core (see also figure 1). Stator deformations of up to 2mm, caused only by the pressure of the water around the bulb, were measured on some generators. In vertical machines the stator can deform due to its own weight and depending on the way it is fixed on its foundations. Rotor deformations can occur due to the centrifugal force.

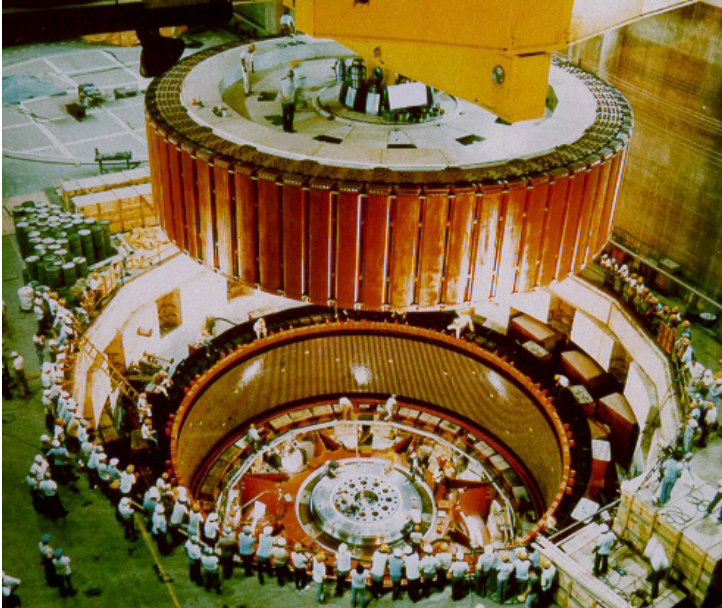


Figure 2: Assembly of a hydrogenerator

These machines are therefore operated with an eccentricity that, though small, is not negligible, and is the cause of undesirable effects:

- vibrations
- additional losses in the damper cage and in parallel circuits of the stator windings
- unbalanced magnetic pulls

These undesirable effects either reduce the machine performance or even make secure operation of the machine impossible. A profound and scientific knowledge of the physical effects of an eccentricity on the magnetic and electric circuits is therefore very desirable for the manufacturer of salient-pole synchronous machines.

1.2 Contribution of this thesis

The knowledge of the physical effects of eccentricities on the magnetic and electric circuits of large, low speed salient-pole synchronous generators is not yet very complete. This lack of knowledge is at least partially due to a lack of computational tools and calculation methods. Analytical calculation methods, as used by

manufacturers during the design process, do generally not allow to take into account eccentric geometries. Purely numerical methods, such as the finite element method (FEM), allow to calculate all electric and magnetic values of an electrical machine in almost any operating mode. Unfortunately their application is very time consuming, especially in the case of a machine with eccentric rotor or deformed rotor or stator.

During this thesis, as a first step, a combined numerical and analytical method for calculation of damper bar currents and stator voltages of perfectly centered, large salient-pole synchronous generators in no-load conditions was developed. This method allows fast and precise prediction of the damper bar currents and of the no-load voltage waveform and therefore also of the no-load losses in the damper bars and of the Telephone Harmonic Factor (THF). The method takes precisely into account the geometry of the machine as well as saturation effects and is significantly faster than the FEM (10 to 20 times faster). It was implemented in a user-friendly tool allowing convenient industrial application.

This method was then extended to the calculation of damper bar currents and unbalanced magnetic pulls in large, low speed salient-pole synchronous generators in any kind of eccentricity condition (rotor eccentricity, stator or rotor deformation). This calculation method is also easy to apply and, compared to the FEM, very fast. The presented method was verified on several examples and was also implemented in a user-friendly, graphical tool, allowing easy industrial application of the method.

The unbalanced magnetic pull calculation integrated in the extended method is inspired by an approach developed in the laboratory for electrical machines of the EPFL for an unbalanced magnetic pull monitoring system (see [24]). Monitoring aspects are obviously essential regarding the dangers due to eccentricities, but they are not the subject of this thesis and are therefore not discussed in this report.

1.3 Structure of this report

The structure of this report follows the sequence of the developments of this thesis.

Chapter 2 describes the method for prediction of the no-load voltage waveform and of the damper bar currents in perfectly centered salient-pole synchronous generators and chapter 3 presents verifications and some application examples.

The extension of the method presented in chapter 2 to the calculation of the damper bar currents in the case of large, low speed salient-pole generators in eccentricity conditions is described in chapter 4. This same chapter presents also the verifications carried out concerning this extension. At the end of chapter 4 an application example of the extended method is presented and in chapter 5 the work carried out throughout this thesis is summarized.

2 Method for calculation of the no-load voltage of hydrogenerators

2.1 Introduction

In the following a combined analytical and finite element method for calculation of the no-load voltage waveform of perfectly centered and not deformed laminated salient-pole synchronous generators will be described. The method allows to calculate the currents in the damper bars and the no-load voltage, taking into account the damper bar currents. It takes also into account saturation as well as the geometry of the machine, like pole shoe shape, damper bar distribution and stator slotting.

It is very important for the designer of salient-pole synchronous generators to be able to predict the no-load voltage waveform in a fast and reliable way. This is above all true in the case of a design where a low number of stator slots per pole and per phase have been chosen to reduce costs. Knowing in advance the harmonic content of the no-load voltage is important for satisfying standards requirements (Telephone Harmonic Factor, etc.). Also the computation of the losses due to currents in the damper bars, induced by the slot pulsation field, is important for the design.

In the context of this thesis this method is the first step towards the analysis of the damper bar currents in eccentricity conditions. The method presented in this chapter gives us already a general idea of the way the eccentricity problem will be approached.

The described method was presented at the IEEE IAS Annual Meeting 2005 in Hong Kong; the corresponding article was published in the IEEE Transactions on Industry Applications [27].

2.1.1 Existing methods

Several different methods exist to calculate the no-load voltage waveform of salient-pole synchronous generators. Often they are either too slow, not precise enough, not very well adapted to the problem or their application is complicated. In the following the 3 main categories of methods for no-load voltage calculation will be presented.

a) Numerical methods

Among others (finite differences, etc.) the most widespread numerical method and also often the reference method for electromagnetic calculations in electrical machines is clearly the finite element method (FEM). Application of the FEM starts with the geometric definition of the domain of interest which is then divided in small pieces, so-called finite elements. This operation is generally called 'meshing' of the domain; it is a spatial discretization of the domain of interest. Then boundary conditions are imposed on the boundaries of the domain (for example imposed magnetic flux or

symmetry conditions, etc.) and current distributions can be imposed in different regions of the domain. Finally the Maxwell equations are solved for each finite element, taking into account its physical properties (magnetic saturation, etc.) as well as the boundary conditions and the current distributions.

The FEM can be used either in 3D or in 2D. In most of the cases in electrical machine analysis the 2D FEM is used. This means that the magnetic flux in direction of one axis (generally the z-axis) is considered equal to 0 and that the currents flow only in the direction of this axis. The calculation is therefore carried out only in a slice of the machine and it is considered that one finds exactly the same magnetic field and current distributions in every plane along the whole active length of the machine. This allows to considerably reduce the number of elements and thus also the calculation time. For this reason the 3D FEM will not be mentioned any more in this report.

The meshing of the domain is one of the most sensitive points when the FEM is applied. A too fine mesh results in a high number of elements and therefore in a long calculation time. A too coarse mesh reduces calculation time but can provide imprecise or even wrong results. Normally the mesh is adapted to the geometry; fine mesh for regions with small details (damper bars, air gap, etc.) and coarse mesh for large surfaces (pole bodies, etc.). Figure 3 shows a detail of a meshed geometry.

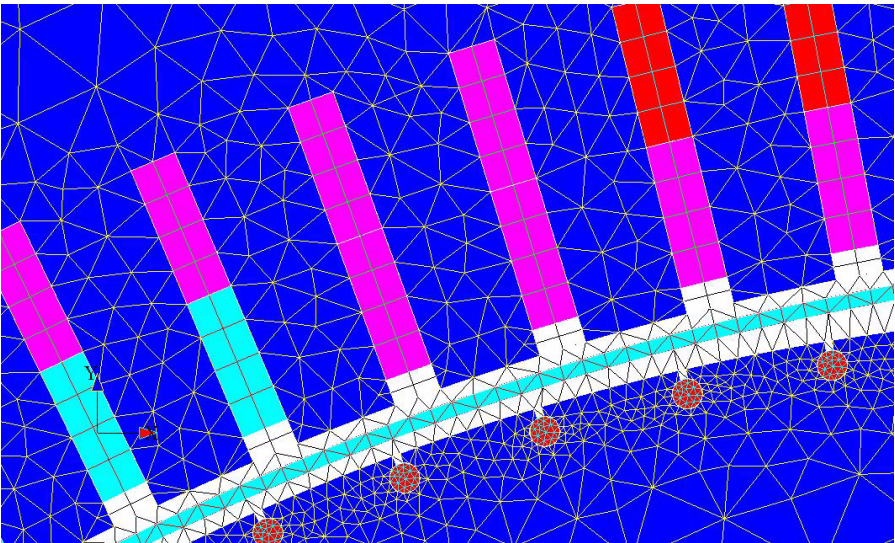


Figure 3: FEM: mesh detail

The FEM can be used for calculations in either magnetostatic or transient magnetic conditions. In the case of the magnetostatic FEM application the magnetic field

distribution is calculated only once for a given geometry, given boundary conditions and a given current distribution.

The FEM can also be used coupled to electrical circuits describing the way the different regions of the domain are electrically interconnected. This allows also to take into account, up to a certain point, end region effects through resistances and leakage inductances in the electrical circuit (one could call this 2.5D FEM). In this case the FEM is applied repetitively, alternating with the resolution of the equations of the electrical circuits. At each time step the currents calculated using the equations of the electrical circuits at the end of the previous step are used in the FEM calculations. The distribution of the magnetic field calculated by the FEM is used to calculate the induced voltages in each conductor represented in the coupled electrical circuit. One speaks in this case of time-stepping or transient magnetic FEM calculations.

Transient magnetic FEM calculations allow to predict the machine behavior very precisely, taking into account the exact geometry of the machine, saturation, skin effects and eddy currents. On the other hand transient magnetic FEM calculations are very time-consuming.

In [1] and [2] transient magnetic FEM analysis is used for computation of the no-load voltage shape and for the design of the damper winding respectively.

As often measured reference values are not at hand or do not exist, transient magnetic FEM calculations were used as reference throughout this thesis.

b) Analytical methods

Analytical methods allow very fast prediction of some machine characteristics. The drawbacks are low precision and difficulties to take into account non-linear effects (saturation) and exact geometric parameters. Nevertheless analytical methods allow the qualitative comparison of a high number of variants (different number of stator slots or damper bars, etc.).

In [3] a fast analytical method is used as a criterion for the selection of the number of stator slots. In [4] an analytical method is developed for the calculation of the no-load voltage waveform of turbogenerators. This method does not take into account saturation effects; it is applied for the calculation of the Telephone Harmonic Factor (see also paragraph 3.2.2). This same method is extended in [5] to the calculation of the no-load voltage waveform of salient-pole synchronous generators. Especially the influences of skewing, slotting, pole shoe shaping and the type of the stator winding are studied.

c) **Combined analytical and numerical methods**

Different combined analytical and numerical methods exist for electrical machine analysis. Often numerical methods (e.g. the FEM or the finite differences method) are used to calculate some values and then analytical equations are solved using these values.

In [6] a combined analytical and finite element modeling method is used for calculation of the currents induced in the damper winding and for calculation of the force-density harmonics including the effects of these currents. In [7] and [8] the modified winding function approach and the magnetics circuits approach have been used for modeling the synchronous machine performance under dynamic air gap eccentricity. In [9] a combined analytical and finite element approach, similar to the one presented in this article, is proposed. Finally in [10] the Harmonic Balance Finite Element method is used to calculate the synchronous machine no-load voltage.

Often these methods were developed for a very specific application. The method proposed in this thesis is also a combined analytical and numerical method. It is much faster than the transient magnetic FEM, but provides results of very similar precision and allows the user to understand better the magnetic coupling of the machine conductors and therefore the functioning of the synchronous machine.

2.1.2 Suggested method

The proposed method combines magnetostatic 2D FEM calculations and a numerical resolution of electrical circuit differential equations. This results in very precise prediction of the no-load voltage and, at the same time, dramatically reduced simulation time compared to the transient magnetic 2D FEM.

The method is based on the determination of the flux linkage of the different machine conductors in function of the rotor position and for a given main flux using the magnetostatic FEM. This and taking into account the machine rotational symmetry allows to limit the necessary FEM calculations to the minimum. The described approach will be the basis for a method for analysis of machines with eccentric rotor or deformed rotor or stator (see chapter 4).

2.2 Summary of the suggested method

Unlike transient magnetic FEM simulations, where the magnetic coupling of the different electrical conductors of the machine is re-calculated at every time-step, this combined method takes into account the machine symmetries. The magnetic coupling of the conductors is calculated only for some positions of the rotor within one stator slot pitch and the values for all other positions are obtained by consideration of the machine symmetries. As in the case of the transient magnetic FEM, according to the machine rotational symmetries, only a part of the machine is modelled (typically one pole pair for a machine with integer slot winding).

Due to the fact that the machine is in no-load conditions, it is assumed that the most important part of the magnetic flux in the machine is caused by the current in the field windings. As the field winding current is considered constant, this part of the flux depends only on the position of the rotor and fixes the level of saturation in the machine. The effect of the damper bar currents can therefore be modelled through so-called differential inductances (inductances for a given operating point). The total flux linked to one conductor can then be written as the sum of the flux caused by the field windings and of small flux variations due to the currents in the other machine conductors (the damper bars). These flux variations are described through so-called differential inductances. The flux linkage values and differential inductances are calculated only for some rotor positions within one stator slot pitch using the magnetostatic FEM. The machine rotational symmetry is then used to obtain the values for all other rotor positions.

The differential equations describing the electrical behavior of the machine, can be formed using the resistance of the machine conductors and the inductance and flux linkage values described above. These differential equations are finally solved numerically.

Summarized the method consists roughly of two stages:

1. Calculation of the differential mutual and self inductances as well as the flux linkage values with the field windings for all electrical conductors of the machine for different positions of the rotor within one stator slot pitch using the magnetostatic FEM.
2. Numerical resolution of the analytical equations describing the electrical circuit composed of the machine conductors using the values calculated in the first stage.

2.3 Hypotheses

For application of the described method the following hypotheses are assumed:

- The machine is rotating at constant speed in no-load conditions.
- The resistance of the damper bars is given for the slot pulsation frequency (for example according to [12]).
- The field winding currents are constant.
- The saturation level is constant and given by the flux created by the field winding currents.
- End region effects (including leakage reactances of the damper cage short-circuit rings) are neglected.
- The poles are laminated, therefore no eddy currents are considered.

2.4 Determination of the flux linkages

2.4.1 Principles

a) Inductances

The effect through magnetic coupling of the current in one electrical conductor on another conductor and on itself can be modeled through inductances. The definition of an inductance is given in equation 1:

$$L_{ij} = \frac{\Phi_j}{i_i} \quad (1)$$

An inductance is the quotient of the flux created by the current in conductor 'i' linked with conductor 'j' and the current in conductor 'i'. The knowledge of the mutual inductance allows therefore to calculate the flux linkage between two conductors, knowing the current in the conductors. This definition clearly shows the linear dependency of the flux linked with conductor 'j' caused by the current in 'i', any variation of flux in a saturated environment can therefore not be represented with an inductance.

b) Differential inductances

As soon as the materials surrounding the conductors show a non linear magnetic behavior the above mentioned definition is not any longer usable to represent flux variations. As the iron in synchronous generators is generally already saturated in no-load conditions the use of inductances as described before is not suitable for describing the magnetic coupling of the machine conductors.

For this reason the magnetic flux in the machine in no-load conditions is separated into two parts. The main flux is caused by the constant current in the field windings. The only other currents in no-load conditions are the damper bar currents. As their magneto motive force (MMF) is significantly lower than the MMF of the field winding currents their contribution to the flux is also significantly lower. It can therefore be assumed that the flux created by the field winding currents sets the saturation level. The damper bar currents cause only small variations around this saturation level, the saturation curve can therefore be linearized around the operating point given by the field winding currents.

Figure 4 illustrates this linearization. The blue lines indicate the operating point imposed by the field winding currents, the red lines indicate the deviation from this operating point by adding the effect of the damper bar currents, the green line is the linearization of the saturation curve around the chosen operating point. It is evident that this linearization only works well if one does not deviate too much from the operating point. In no-load conditions the damper bar currents are normally very low and one remains therefore on the local tangent very close to the no-load characteristic. One can observe that this linearization will always overestimate the flux created by a current. Damping effects due to saturation will therefore generally be underestimated.

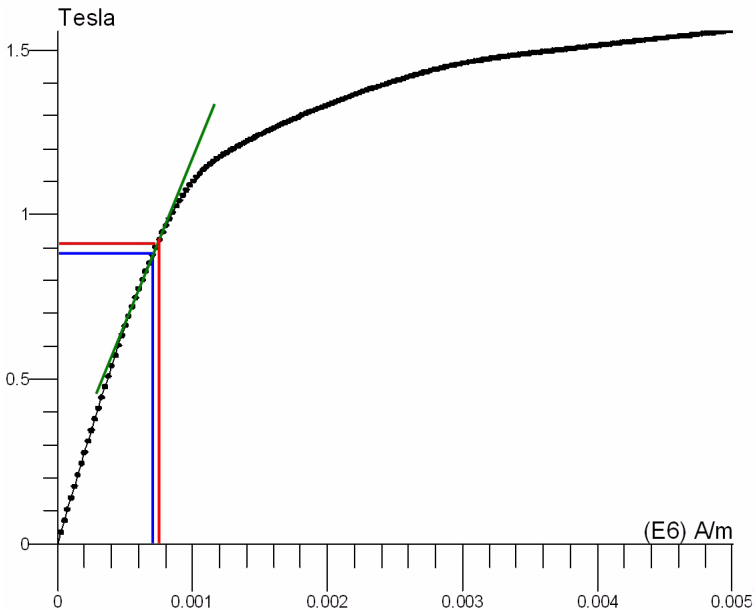


Figure 4: Linearization of the saturation curve

Thus the flux linked to one machine conductor can be expressed as the sum of the contributions of the flux due to field winding currents and the flux due to the much smaller current in each damper bar (i_k):

$$\varphi_j = \varphi_{exc,j} + \sum_{k=1}^N \Delta\varphi_{k,j} = \varphi_{exc,j} + \sum_{k=1}^N L_{diff_{k,j}} i_k \quad , \text{with } \Delta\varphi_{k,j} \ll \varphi_{exc,j} \quad (2)$$

The differential inductances used in equation 2 are the mathematical expression of the linearization of the iron saturation curve as described above. They are inductances describing the influence of the current in one conductor on another conductor in an already magnetically saturated environment. The use of differential inductances allows to take into account saturation effects for a given operating point (a given current in the field windings).

As can be seen in equation 2, knowledge of $\varphi_{exc,j}$ and all $L_{diff_{k,j}}$ as well as the currents in all damper bars allows to calculate the flux linked with conductor 'j'. As the field winding currents are considered constant these values only depend on the rotor position.

c) Taking into account the machine rotational symmetry

As mentioned in section b) the values of $\varphi_{exc,j}$ and $L_{diff_{k,j}}$ depend only on the rotor position. Considering the machine rotational symmetry, one can easily see that after a rotation of the rotor of one stator slot pitch the machine is geometrically in exactly the same conditions as at the beginning of the rotation. It is therefore sufficient to know the values of $\varphi_{exc,j}$ and $L_{diff_{k,j}}$ for some rotor positions within one stator slot pitch. These values can then be re-used for all other rotor positions.

The number of rotor positions within one stator slot pitch (resolution of the spatial discretization) determines the sampling rate for the resolution of the differential equations which will be described in paragraph 2.5. The number of rotor positions should be chosen high enough to allow the representation of the no-load voltage harmonics one is interested in. 20 rotor positions within one stator slot pitch allows generally very precise prediction of the harmonics due to the slot pulsation field. This appeared to be largely fulfilling the requirements for calculating the telephone harmonic factor (THF) of the no-load line voltage (see paragraph 3.2.2).

d) Determination of the differential inductances using the FEM

The flux linkage values and differential inductances presented in section b) are calculated using the 2D magnetostatic FEM. This allows to take precisely into account all geometrical properties of the machine (stator slotting, damper bar distribution, pole shoe shape, etc.) as well as saturation effects.

As in the case of transient magnetic FEM simulations, the part of the machine which has to be considered depends on the geometry of the poles, the distribution of the damper bars and the number of stator slots per pole and per phase. In the following the machine unit 2 (see paragraph 3.3.1) is used as an example. In the case of unit 2 'q' equals 5 and the damper cage is shifted by $\pm\tau_s/4$ on the pole shoes, therefore one pole pair is modeled (τ_s being one stator slot pitch) and cyclic boundary conditions are applied. One could also model only one pole and apply anti-cyclic boundary conditions, but the proposed choice is easier to implement.

For the FEM calculations the following settings were used:

- The field winding currents are imposed as uniform current densities in the corresponding regions.
- The real, non-linear magnetic characteristics are used for rotor and stator materials (introduced as B-H curves).

The distribution of the magnetic field in the case of unit 2 in no-load conditions, calculated using one magnetostatic FEM calculation, is shown in figure 5.

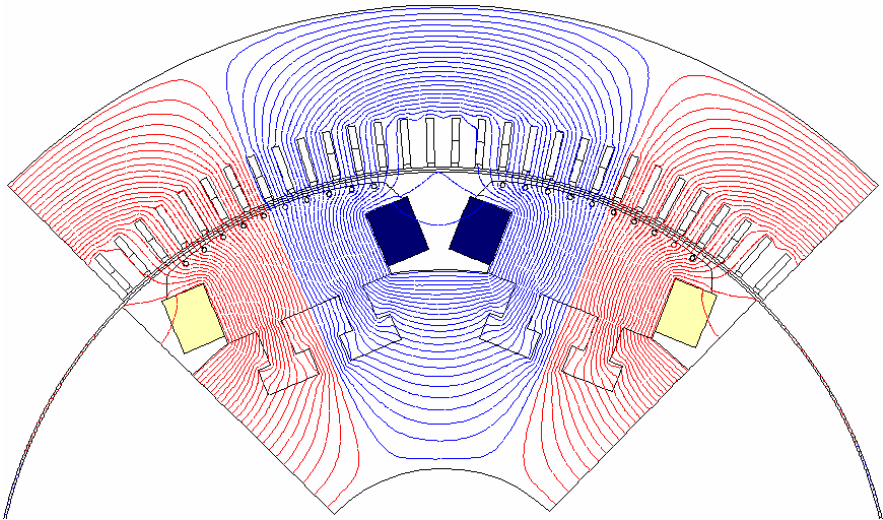


Figure 5: Magnetic field in no-load conditions

The differential inductances are obtained through the following equation:

$$L_{diff_{k,j}} = \frac{\varphi_{exc_{k,j}} - \varphi_{exc,j}}{i_k} \quad (3)$$

Where:

- $L_{diff_{k,j}}$: mutual differential inductance of conductors 'k' and 'j'
- $\varphi_{exc_{k,j}}$: flux created by the field winding and the current i_k in conductor 'k', linked to conductor 'j'
- $\varphi_{exc,j}$: flux created only by the field windings, linked to conductor 'j'
- i_k : small current in conductor 'k'

The values of $\varphi_{exc_{k,j}}$ and $\varphi_{exc,j}$ are respectively the flux linked to conductor 'j' (damper bar or conductor on the stator) obtained from a FEM calculation with currents in the field windings and conductor 'k' and the flux linked to the same conductor obtained from a FEM calculation with only the field windings supplied. The determination of the mutual inductances of one damper bar with all other conductors needs therefore 2 FEM calculations. The flux due to field winding currents only, linked with each conductor can also be obtained from one of these 2 calculations. This procedure has to be repeated for all damper bars and for the number of rotor positions considered (according to section c)). The value of the current i_k should be chosen as small as possible so as to calculate as precisely as possible the value of the differential inductance (slope of the green line in figure 4) but big enough for being insensitive to noise. A value of 50A provided very good results for all the cases studied.

The necessary number of FEM calculations can be determined easily. Let 'n' be the number of damper bars represented in the chosen geometry and 'm' the number of rotor positions within one stator slot pitch considered (unit 2: n = 20, m = 20). For every position of the rotor and for every damper bar represented one magnetostatic FEM calculation has to be performed, where the current corresponding to the chosen operating point circulates in the field windings and a low current is imposed in that damper bar. Finally one more magnetostatic FEM calculation has to be performed for every position with only the field windings supplied. In the case of unit 2 this results in $m*(n+1) = 420$ magnetostatic FEM calculations.

In the case of our example (one pole pair of unit 2, 20 damper bars, 60 stator conductors and 20 different positions of the rotor) this provides us with a set of 28200 differential mutual and self inductances linking the different conductors of the machine for any position of the rotor ($28200 = 20$ positions * (190 damper bar mutual inductances + 20 damper bar self inductances + 1200 damper bar - stator conductor

mutual inductances)). Additionally the 1600 values of flux linkage of the field windings with all conductors for all positions are stored ($1600 = 20 \text{ positions} * (20 \text{ damper bars} + 60 \text{ stator conductors})$). These values describe the magnetic coupling of all electrical conductors in the machine for every position of the rotor.

2.5 Differential equations and numerical resolution

2.5.1 Principles

The calculation of the no-load voltage is done in two steps:

1. Calculation of the damper bar currents.
2. Calculation of the phase voltages using the damper bar currents.

In the following the differential equations describing the connection of the different conductors are explained as well as the way they are solved.

2.5.2 Calculation of the damper bar currents

a) Circuits and equations describing the connection of the conductors

The different electrical conductors of the machine form several galvanically separated circuits:

- The field windings.
- The damper bars forming the damper cage.
- The stator windings forming the three phases on the stator.

As the field windings are supplied by a constant current, no circuit is associated to the field windings. The phase windings are also not considered because there is no current circulating in a no-load situation in the case of a perfectly centered and not deformed machine. The electrical circuit of figure 6 is associated to the damper bars. The circuit associated to the damper cage represents the same number of damper bars as was considered for calculating the inductances.

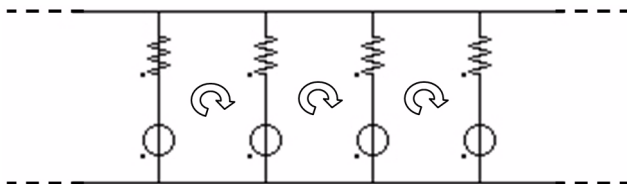


Figure 6: Circuit associated to the damper cage

In figure 6 only a part of the circuit associated to one pole pair of unit 2 is represented, the whole circuit includes one branch for every damper bar. Every damper bar is modeled as one branch composed of a resistance and a voltage source. The resistance models obviously the resistance of the damper bar, the voltage source models the voltage induced through the variation of the flux linked to the damper bar.

As can be seen in figure 6, the resistance and leakage inductances of the damper cage are neglected; this provides nevertheless very good results. In all the machines studied during this thesis all damper bars on all poles were short-circuited. There also exist machines with galvanically separated damper cages on each pole (no inter-pole links). These machines could also be analyzed with the same method; the equation system developed in the following would simply have to be developed in a different way. Even if the longer inter-pole links are not graphically represented in the circuit of figure 6, the geometrical distribution of the damper bars (as all geometric parameters) is precisely taken into account in the induced voltage terms.

The electrical behavior of this circuit can be described using the Kirchhoff laws. For each loop in the electrical circuit (figure 6) the following equation can be written:

$$R_j i_j - R_{j+1} i_{j+1} + \frac{d\phi_j}{dt} - \frac{d\phi_{j+1}}{dt} = 0 \quad (4)$$

Where ϕ_j is the flux linked to conductor 'j' as in equation 2.

As described in equation 2 the flux linked to one conductor can be written as the sum of the contributions of the field windings and the damper bars.

In the case of the flux caused by the damper bars the derivation in time of the flux is replaced by its partial derivatives:

$$\frac{d\phi_{i,j}}{dt} = \frac{\partial \phi_{i,j}}{\partial i_i} \frac{di_i}{dt} + \frac{\partial \phi_{i,j}}{\partial \alpha} \frac{d\alpha}{dt} \quad (5)$$

Where α is the position of the rotor and its derivative the rotating speed ω :

$$\frac{d\phi_{i,j}}{dt} = \frac{\partial \phi_{i,j}}{\partial i_i} \frac{di_i}{dt} + \frac{\partial \phi_{i,j}}{\partial \alpha} \omega \quad (6)$$

The derivation of the flux with respect to the current can be replaced with a differential inductance as described in section b) of paragraph 2.4.1:

$$\frac{\partial \phi_{i,j}}{\partial i_i} = L_{diff,i,j} \quad (7)$$

Therefore and expressing $\varphi_{i,j}$ also using the differential inductances:

$$\frac{d\varphi_{i,j}}{dt} = L_{diff_{i,j}} \frac{di_i}{dt} + \frac{\partial L_{diff_{i,j}}}{\partial \alpha} i_i \omega \quad (8)$$

Replacing equation 2 and equation 8 in equation 4:

$$\begin{aligned} R_j i_j - R_{j+1} i_{j+1} & \quad (9) \\ + \frac{d\varphi_{exc,j}}{dt} + \sum_{k=1}^n \left(L_{diff_{k,j}} \frac{di_k}{dt} + \frac{\partial L_{diff_{k,j}}}{\partial \alpha} i_k \omega \right) \\ - \left(\frac{d\varphi_{exc,j+1}}{dt} + \sum_{k=1}^n \left(L_{diff_{k,j+1}} \frac{di_k}{dt} + \frac{\partial L_{diff_{k,j+1}}}{\partial \alpha} i_k \omega \right) \right) & = 0 \end{aligned}$$

An equation like this can be written for every loop in the damper cage except the last one. The current in the last bar can be expressed as the sum of the currents in all other damper bars (Kirchhoff law):

$$i_n = - \sum_{k=1}^{n-1} i_k \quad (10)$$

Introducing equation 10 in equation 9 and regrouping the inductances:

$$\begin{aligned} R_j i_j - R_{j+1} i_{j+1} & \quad (11) \\ + \sum_{k=1}^{n-1} \frac{di_k}{dt} (L_{diff_{k,j}} - L_{diff_{n,j}} - L_{diff_{k,j+1}} + L_{diff_{n,j+1}}) \\ + \omega \sum_{k=1}^{n-1} i_k \left(\frac{\partial L_{diff_{k,j}}}{\partial \alpha} - \frac{\partial L_{diff_{n,j}}}{\partial \alpha} - \frac{\partial L_{diff_{k,j+1}}}{\partial \alpha} + \frac{\partial L_{diff_{n,j+1}}}{\partial \alpha} \right) \\ + \frac{d\varphi_{exc,j}}{dt} - \frac{d\varphi_{exc,j+1}}{dt} & = 0 \end{aligned}$$

The linear differential equation system composed of 'n-1' equations (in the case of 'n' damper bars) of the form of equation 11 can then be solved using a numerical method.

b) Differential equations in matrix form

The differential equation system has to be written in matrix form for being solved with a numerical method:

$$\dot{\vec{i}}(t) = f(\vec{i}(t), t) \quad (12)$$

With:

$$\dot{\vec{i}}(t) = \frac{d}{dt} \begin{bmatrix} i_2(t) \\ i_2(t) \\ \vdots \\ i_{n-1}(t) \end{bmatrix} \quad \vec{i}(t) = \begin{bmatrix} i_2(t) \\ i_2(t) \\ \vdots \\ i_{n-1}(t) \end{bmatrix}$$

$\vec{i}(t)$ is a vector containing the currents in the damper bars and $\dot{\vec{i}}(t)$ is a vector containing the derivatives of these currents. As in our case every equation contains the derivatives of the currents of all damper bars we build an equation system of the following form:

$$\begin{aligned} \dot{\vec{i}}(t) &= B\vec{i}(t) + C \\ \vec{i}(t) &= A^{-1}B\vec{i}(t) + A^{-1}C \end{aligned} \quad (13)$$

The matrixes A, B and C are given on the next page. $L_{diff,i,j}$ is replaced with $L_{i,j}$ to make the equations more readable.

$$A = \begin{bmatrix} -L_{2,1} + L_{n,1} + L_{1,2} - L_{n,2} & -L_{2,1} + L_{n,1} + L_{2,2} - L_{n,2} & \cdots & -L_{n-1,1} + L_{n,1} + L_{n-1,2} - L_{N,2} \\ -L_{1,2} + L_{n,2} + L_{1,3} - L_{n,3} & -L_{2,2} + L_{n,2} + L_{2,3} - L_{n,3} & \cdots & -L_{n-1,2} + L_{n,2} + L_{n-1,3} - L_{N,3} \\ -L_{1,n-1} + L_{n,n-1} + L_{1,n} - L_{n,n} - L_{2,n-1} + L_{n,n-1} + L_{2,n} - L_{n,n} & \cdots & -L_{n-1,n(-1)} + L_{n,n-1} + L_{N-1,N} - L_{N,N} \end{bmatrix} \quad (14)$$

$$B = \omega \frac{\partial}{\partial \alpha} \begin{bmatrix} L_{1,1} - L_{n,1} - L_{1,2} + L_{n,2} + R_1/\omega & L_{2,1} - L_{n,1} - L_{2,2} + L_{n,2} - R_2/\omega & \cdots & L_{n-1,1} - L_{n,1} - L_{n-1,2} + L_{n,2} \\ L_{1,2} - L_{n,2} - L_{1,3} + L_{n,3} & L_{2,2} - L_{n,2} - L_{2,3} + L_{n,3} + R_2/\omega & \cdots & L_{n-1,2} - L_{n,2} - L_{n-1,3} + L_{n,3} \\ L_{1,n-1} - L_{n,n-1} - L_{1,n} + L_{n,n} + R_n/\omega & L_{2,n-1} - L_{n,n-1} - L_{2,n} + L_{n,n} + R_n/\omega & \cdots & L_{n-1,n-1} - L_{n,n-1} - L_{n-1,n} + L_{n,n} + R_{n-1}/\omega + R_n/\omega \end{bmatrix} \quad (15)$$

$$C = \frac{d}{dt} \begin{bmatrix} \Phi_{exc,1} - \Phi_{exc,2} \\ \Phi_{exc,2} - \Phi_{exc,3} \\ \Phi_{exc,n-1} - \Phi_{exc,n} \end{bmatrix} \quad (16)$$

c) Numerical resolution of the differential equations

The Runge-Kutta method was chosen for the numerical resolution of the differential equation system. The Runge-Kutta method allows the resolution of a differential equation system of the following form:

$$\begin{aligned}\dot{\vec{i}}(t) &= f(\vec{i}(t), t) \\ \vec{i}(0) &= \vec{i}^0\end{aligned}\quad (17)$$

In the following we will apply the 2nd order Runge-Kutta method (also called Heun method) to the differential equation system describing the currents in the damper bars (equation 13).

For calculation of the steady-state currents we have the following scheme:

$$\vec{i}^{k+1} = \vec{i}^k + \frac{h}{2}(p_1 + p_2) \quad (18)$$

With:

$$\begin{aligned}p_1 &= A^{k-1} B^k \vec{i}^k + A^{k-1} C^k \\ p_2 &= A^{k+1-1} B^{k+1} \left(\vec{i}^k + h p_1 \right) + A^{k+1-1} C^{k+1} \\ h &= t^{k+1} - t^k = \Delta t\end{aligned}\quad (19)$$

The exponent 'k' signifies the quantity at the time-step 'k'. The initial currents are chosen equal zero:

$$\vec{i}^0 = \begin{bmatrix} 0 \\ 0 \end{bmatrix}$$

2.5.3 Calculation of the no-load voltage

As in a no-load situation no current flows in the stator windings, the calculation of the no-load voltage, knowing the currents in the damper bars and in the field windings, is rather simple. The voltage induced in one conductor is given by the derivative of the flux linked to the conductor:

$$u_{ind_j} = \frac{d\phi_j}{dt} \quad (20)$$

As in the case of the damper bars, the flux linked to one stator conductor can be expressed as the sum of the contributions of the field windings and the 'n' damper bars:

$$\varphi_j = \varphi_{exc,j} + \sum_{k=1}^n \varphi_{k,j} = \varphi_{exc,j} + \sum_{k=1}^n L_{diff,k,j} i_k \quad (21)$$

All the necessary values are already calculated using magnetostatic finite element calculations (see section d) of paragraph 2.4.1). The following formula is used for the numerical derivation, where again the exponent 'k' signifies the quantity at the time-step 'k':

$$\frac{d}{dt} \varphi_j(t^k) \cong \frac{\varphi_j(t^k) - \varphi_j(t^{k-1})}{t^k - t^{k-1}} \quad (22)$$

Finally, the voltage induced in one phase can be calculated by summing up the voltages of the conductors forming the phase (according to the winding scheme of the machine).

In the case of the conductors on the stator the differential inductances and the values of flux linkage with the field windings have to be re-assigned to the conductors on the stator after a rotation of the rotor of one stator slot pitch (the conductors have to be 'shifted' to the next slot), then the values calculated for the same rotor positions can be re-used. Figure 7 shows the way the conductors have to be shifted for a given rotating direction.

This simple technique takes fully into account the rotational periodicity of the machine and allows to use the magnetic coupling, calculated only for some rotor positions within one stator slot pitch, for any position of the rotor. As the flux linkages and mutual inductances were calculated separately for each conductor and not for coils, any kind of winding scheme can be analyzed with the same flux linkage values and inductances.

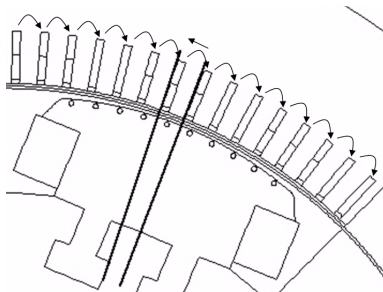


Figure 7: Shifting stator conductors

2.6 Practical application of the method

2.6.1 FEM calculations

Throughout this thesis the FEM calculations were carried out using the software Flux from Cedrat [11]. This software allows to define one project manually (for example simulation with only field windings supplied) and to generate automatically, based on this project, all other projects (simulations with field windings supplied and a test current in one damper bar). For the resolution of each project the position of the rotor can be parametrized using a sliding air band in the air gap.

The FEM calculations can therefore be highly automatized; only very little user interaction is necessary. The result files need no further pre-processing, they are directly used by the tool presented in the next paragraph.

2.6.2 Tool for solving the circuit equations

A tool for pre-processing the results of the FEM calculations and for solving the circuit equations as described in paragraph 2.5 was developed using the Delphi programming language.

This tool has a graphical user-interface which allows easy introduction of the necessary machine characteristics and of the location of the result files of the magnetostatic FEM calculations. The characteristics of a project can be saved in a text file which allows consulting or modifying the project later.

Figure 8: Tool for calculation of the no-load voltage

The program calculates in three steps the no-load voltage as well as the damper bar currents using the vector potential values directly from the FEM result files.

The three steps are the following:

1. Calculation of the mean value of the vector potential for each region of interest (stator conductors and damper bars) and calculation of the flux linked to each one of these regions for each FEM project and each rotor position.
2. Calculation of all differential inductances using the flux values obtained in step one.
3. Calculation of the damper bar currents and the no-load voltage using the flux linkage values and the differential inductances.

The results of each step (flux values, differential inductances, currents and voltages) are stored in text files; values once calculated must not be calculated again when re-opening a project.

Finally the damper bar currents and the phase and line voltages can be visualized. As these currents and voltages are also saved in text files (output of the third stage) they can be analyzed using another program (e.g. Matlab, Microsoft Excel) for example for calculation of the Fourier decomposition or for calculation of the Telephone Harmonic Factor (THF). Figure 9 shows the visualization of the results.

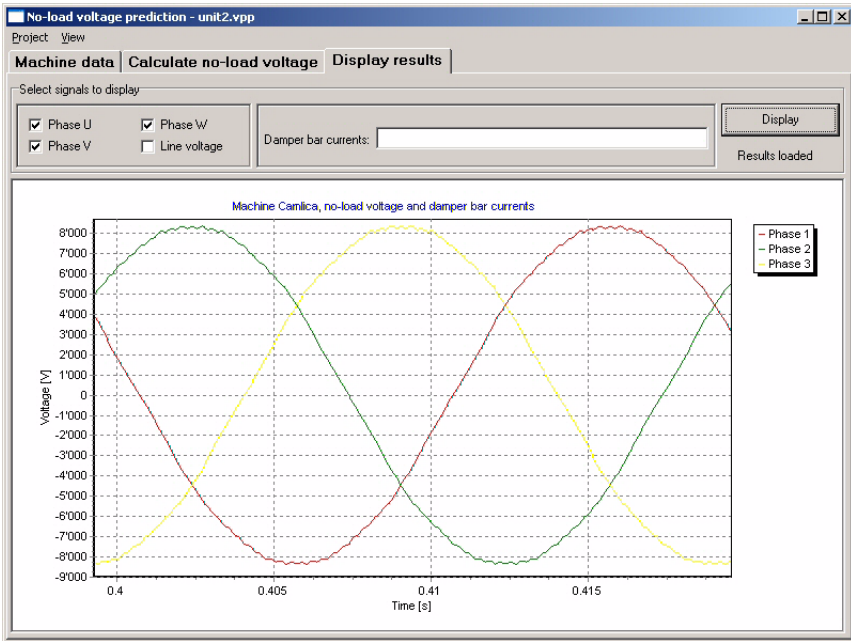


Figure 9: Visualization of the phase voltages

3 Verification and applications

3.1 Introduction

The method for prediction of the no-load voltage of salient-pole synchronous generators, described in chapter 2, was tested and verified on different examples (existing machines). For all examples the results obtained with the described method were compared to the results obtained with transient magnetic FEM simulations and in one case also to the measured no-load voltage of the real generator. In the following one verification on unit 1 and one application of the method on unit 2 are presented.

3.2 Verification on unit 1

3.2.1 Unit 1

Unit 1 is a very interesting example for the verifications. A measurement of the no-load voltage of this machine exists, as well as the THF calculated on the basis of this measurement.

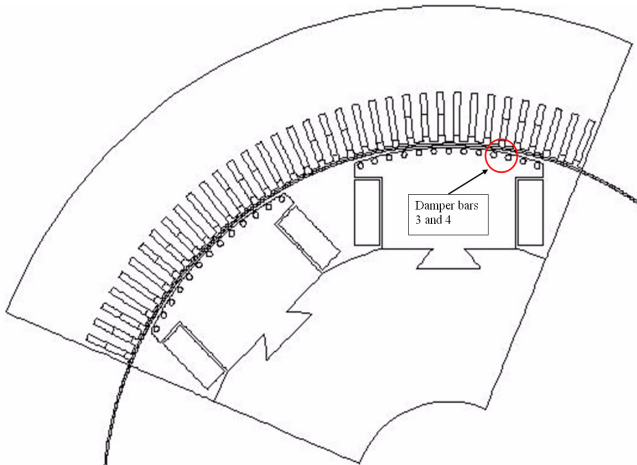


Figure 10: Geometry of unit 1

The principal characteristics of unit 1 are given in the list below and figure 10 shows its geometry. In figure 10 the positions of damper bars 3 and 4, for which a comparison is presented in the next paragraph, are indicated.

- Rated output [MVA]: 11
- Rated voltage [V]: 6300
- Rated frequency [Hz]: 50
- Rated speed [rpm]: 750
- Number of damper bars per pole: 13
- Number of stator slots per pole and per phase: 6
- Symmetrical poles
- Damper bars centered on pole shoes

One pole pair was used for modeling the machine. The differential inductances were calculated for 20 positions within one stator slot pitch. As there are 26 damper bars in the geometry considered, 540 magnetostatic FEM calculations were necessary.

3.2.2 Comparison of the results

a) Damper bar currents

Figure 11 compares the damper bar currents obtained with the described method and with a transient magnetic FEM simulation. A very good agreement of the currents can be observed. The method allows therefore a very precise prediction of the no-load losses due to damper bar currents.

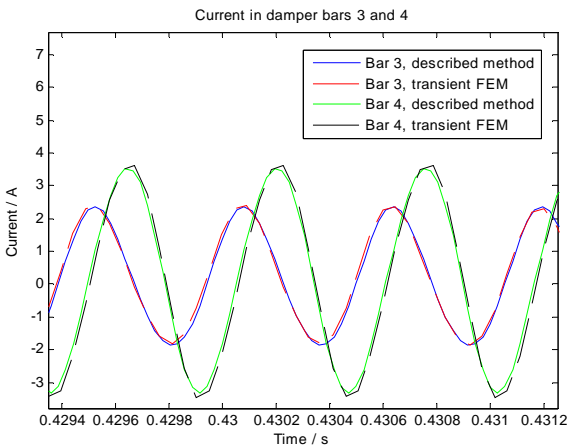


Figure 11: Currents in two adjacent damper bars

b) No-load voltage and THF

Figures 12 and 13 compare the line voltages, again obtained with the described method and with a transient magnetic FEM simulation. Again a very good agreement of the results can be observed; the curves are practically superposed.

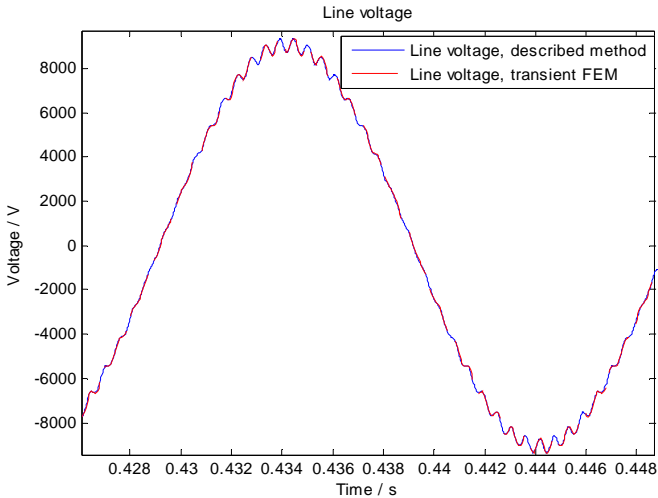


Figure 12: Line voltage

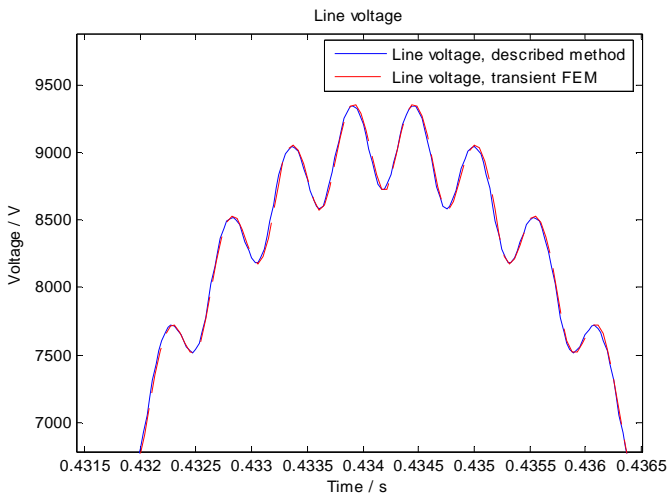


Figure 13: Line voltage, zoomed

Finally the Fourier decomposition of the no-load line voltages obtained with the described method and with a transient magnetic FEM simulation were compared to the Fourier decomposition of the measured no-load line voltage and the Telephone Harmonic Factors (THF) were calculated.

Figure 14 shows the comparison of the line voltage harmonics. The voltage of each harmonic is given in percent of the fundamental harmonic.

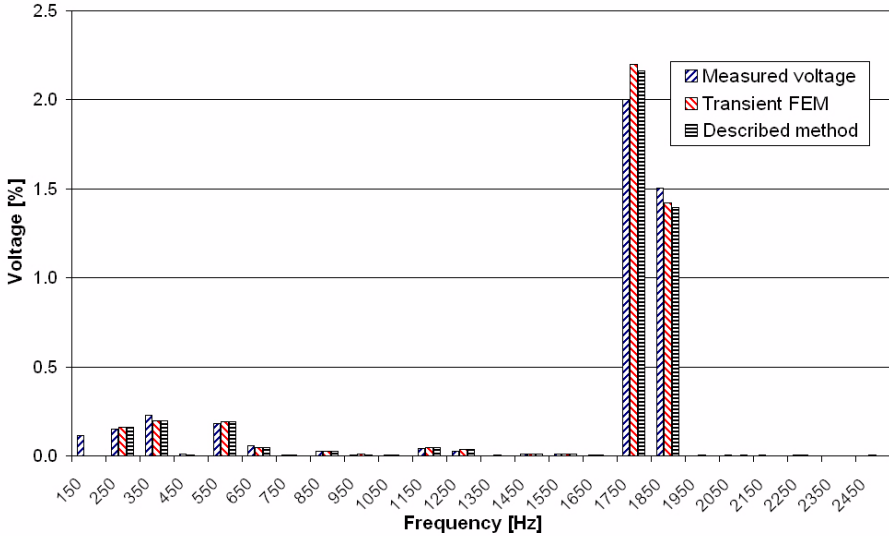


Figure 14: Comparison of line voltage harmonics

A very good agreement of the values of the harmonics calculated using the FEM and using the described method can be observed. These values are also close to the values of the measured harmonics.

The following table 1 compares the THF, calculated using the voltage harmonics obtained with the three methods. The THF was the requirement of the IEC 60034-1 standard for a practically sinusoidal no-load voltage waveform. Its definition is given in equation 23.

$$THF = \frac{1}{U} \sqrt{(U_1 \lambda_1)^2 + (U_2 \lambda_2)^2 + (U_3 \lambda_3)^2 + \dots + (U_n \lambda_n)^2} \quad (23)$$

The THF is thus a weighted sum of all frequency components of the no-load voltage; each harmonic component of the no-load voltage is weighted by a factor λ . The values of these factors are shown in figure 15.

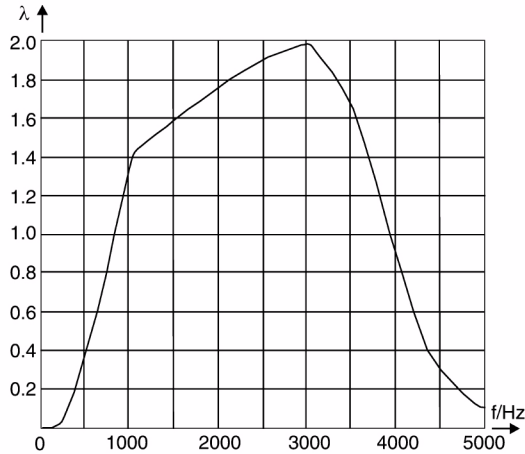


Figure 15: Weighting factors for THF calculation

The THF was replaced by the THD (Total Harmonic Distortion), which is defined as given in equation 24; nevertheless the THF is an important standard as it remained often in the machine specifications of the manufacturers.

$$THD = \frac{\sqrt{\sum_{k=2}^n U_k^2}}{U_1}, n = 100 \quad (24)$$

Again a very good agreement can be observed in table 1, with a relative difference of less than 3% between the THF calculated with the measured harmonics and the THF calculated from the harmonics obtained with the described method. This fast method allows therefore a rapid and precise verification of this value.

	Measured	FEM	Described method
THF [%]:	4.26	4.47	4.39

Table 1: Comparison of Telephone Harmonic Factors

3.3 Application to unit 2

Unit 2 is also an existing machine. With this example a possible application of the method will be demonstrated. As the described method is not very time-consuming, it can be used for comparison of different machine designs. It can also help to better understand some physical phenomena in the machine.

3.3.1 Unit 2

The principal characteristics of unit 2 are given in the list below and figure 16 shows its geometry.

- Rated output [MVA]: 31.5
- Rated voltage [V]: 10600
- Rated frequency [Hz]: 50
- Rated speed [rpm]: 750
- Number of damper bars per pole: 10
- Number of stator slots per pole and per phase: 5
- Symmetrical poles
- Damper bars shifted by $\pm\tau_s/4$ on pole shoe (τ_s being one stator slot pitch)

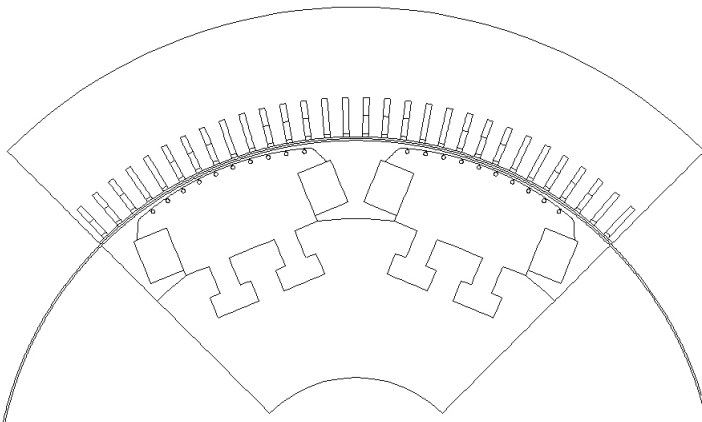


Figure 16: Geometry of unit 2

3.3.2 Comparison of two damper cage layouts

a) No-load voltage and damper bar currents for two cases

In the case of unit 2 two variants were compared:

1. The real machine with damper bars shifted by $\pm\tau_p/4$ on the pole shoes.
2. A hypothetical case with damper bars centered on the pole shoes.

For both cases the damper bar currents and the no-load voltage obtained with the described method were compared to those obtained with transient magnetic FEM simulations. The agreement of the results was as close as in the case of unit 1 (see paragraph 3.2.2), the following figure 17 shows the comparison of the no-load voltage harmonics for both cases.

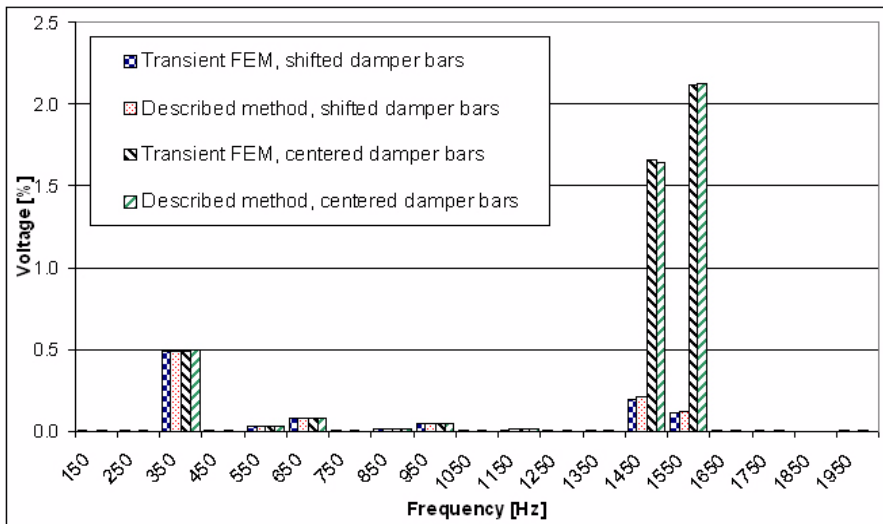


Figure 17: Comparison of line voltage harmonics

This result demonstrates the well known effect on the voltage harmonics of simply shifting the damper cage on the pole shoes. In the case with shifted damper cage the no-load voltage harmonics are dramatically reduced. The agreement of the results is again very good; the calculation with the described method took significantly less time (10 to 20 times less).

b) Analysis of the damper bar currents

The significant difference in line voltage harmonics of the two cases shown in figure 17 is a well known fact to every hydrogenerator designer and this knowledge is applied for a long time. Nevertheless it is not very straightforward to explain this difference. As the described method predicts also precisely the currents in the damper bars, it is possible to give a more profound explication of this phenomenon.

Figures 18 and 19 show the amplitudes and the phase angles of the fundamental harmonic component of the damper bar currents for the two cases (shifted and centered damper cage), calculated both with the described method. As can be seen, there is not much difference regarding the amplitudes of the currents, except for the high currents in the first and the last bar on each pole in the case of the centered damper cage. Regarding the phases, a significant difference can be observed. In the case of the shifted damper cage the currents in the bars on one pole are 'following' each other and one can observe the same distribution of the phases on both poles. In the case of the centered damper cage all currents in the bars on one pole have more or less the same phase angle and the phases of the currents on the second pole are shifted by 180° .

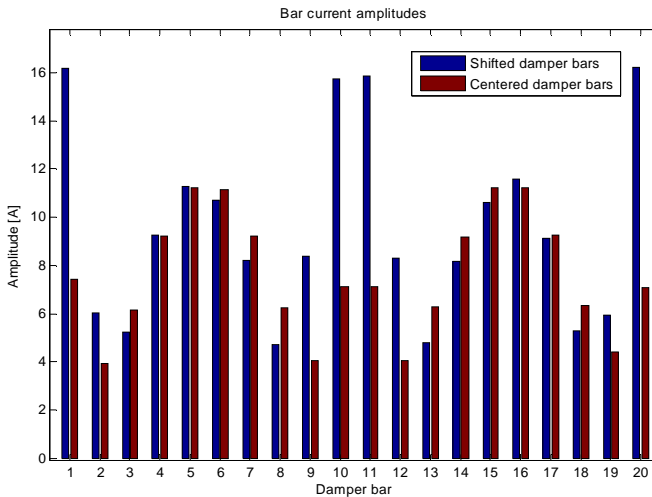


Figure 18: Amplitudes of damper bar currents

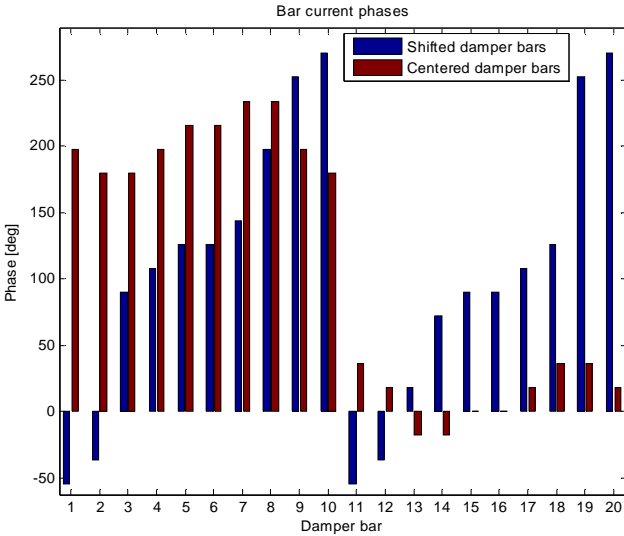


Figure 19: Phase angles of damper bar currents

These distributions of the damper bar currents lead to a significant current flowing from the bars on one pole to the bars on the second pole in the case of the centered damper cage. Figure 20 shows the evolution in time during one period of the slot pulsation field of the sum of the currents in the damper bars of each pole. The current flowing from one pole to another is much lower in the case of the shifted damper cage.

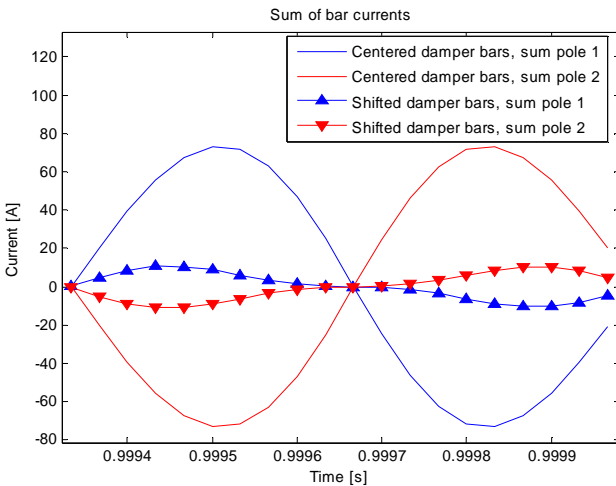


Figure 20: Sum of damper bar currents on each pole

The described distributions of the damper bar currents are the source of the air gap MMF shown in the figures 21 and 22. In those two figures the MMF is given in function of the position on the stator and in function of the time. Respectively one pole pair (position on the stator) and one stator slot period (time) is represented.

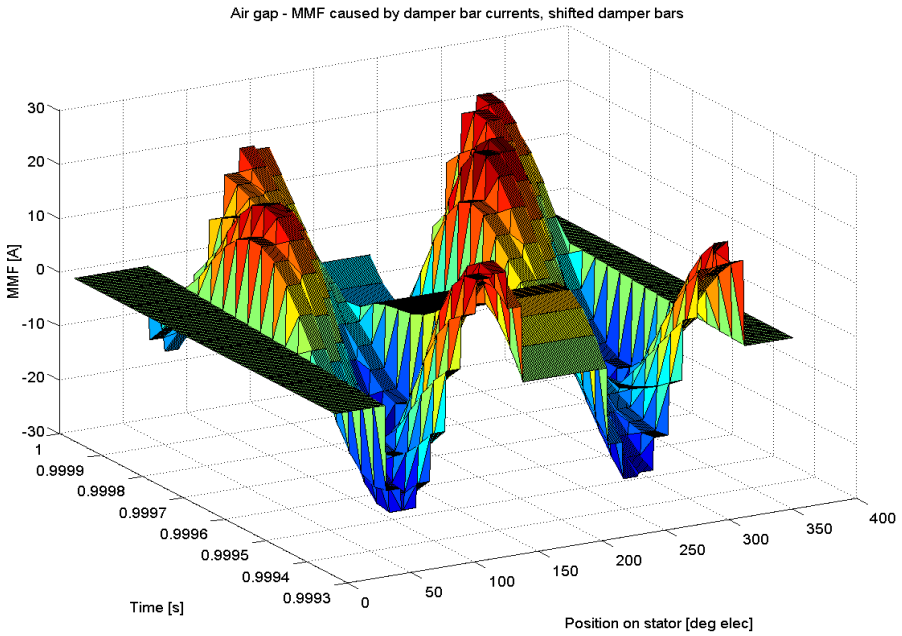


Figure 21: Air gap MMF, shifted damper bars

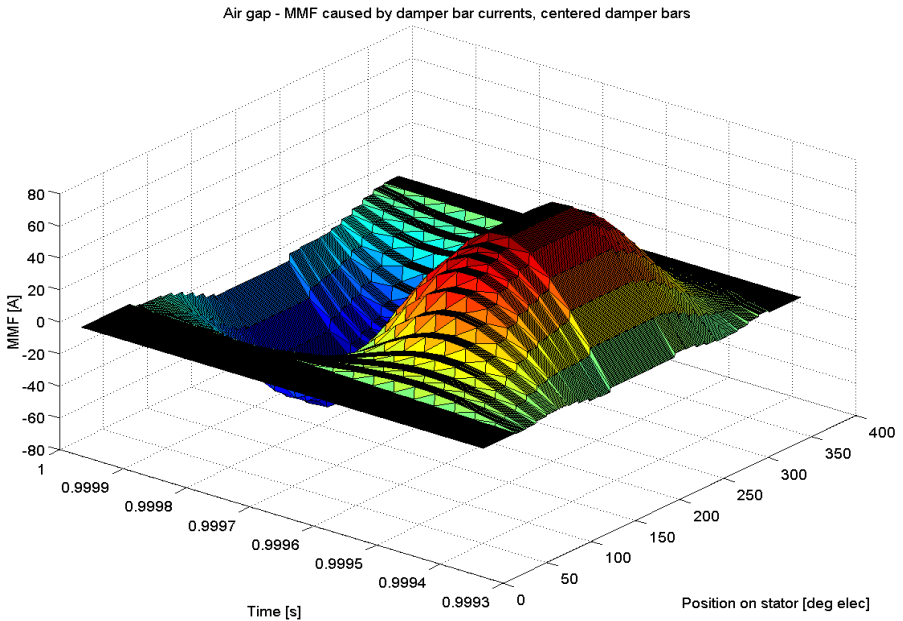


Figure 22: Air gap MMF, centered damper bars

In the case of the shifted damper bars a spatial periodicity of the MMF of twice the pole-pair period can be observed (the currents are circulating essentially on one pole). Thus, in the case of an integer number of stator slots per pole and per phase, the 'outward'- and 'return'-conductors of each coil on the stator 'see' exactly the same magnetic potential and therefore the effect of the MMF caused by the damper bar currents is cancelled out in each coil. This is not the case in the situation with centered damper bars, where a spatial periodicity of exactly one pole pair period can be observed (the currents are circulating on one pole pair).

3.4 Comparison of the simulation time

In the preceding paragraphs transient magnetic FEM simulations were used as a reference for comparing the results obtained with the described method. As already mentioned, the main drawback of transient magnetic FEM simulations is the simulation time. Especially for studies like the one presented in paragraph 3.3, where different machine geometries have to be simulated, simulation time is often prohibitive.

Because of the limited use of FEM calculations the described method is significantly faster than transient magnetic FEM simulations. The resolution of the differential equations takes only some minutes (typically 2 to 3 minutes) and the magnetostatic FEM calculations needed to obtain the differential inductances took from 40 minutes (unit 2) to a little bit more than 3 hours (unit 1). This compares to transient magnetic finite element simulations taking 40 hours (unit 2, study time limit 1s for reaching steady-state conditions) and more.

All calculations were performed on a desktop PC with Pentium 4 CPU (2.6GHz, HT) and 1GB of RAM, running Windows XP Professional.

4 Prediction of the damper bar currents and of unbalanced magnetic pulls in deformed synchronous machines

4.1 Introduction

This chapter describes a method for calculation of the circulating currents in the damper bars and of the unbalanced magnetic pulls due to various rotor and stator deformation conditions. This method is based on the method for prediction of the no-load voltage waveform presented in chapters 2 and 3. Generally the FEM is still used to calculate some values of magnetic coupling and electrical circuit equations are solved using the Runge-Kutta method. The possibility to calculate also the circulating currents in parallel circuits of the stator windings was investigated but not yet implemented. The principles for calculation of these stator currents are exactly the same as for calculation of the damper bar currents; adding this part later on to the damper bar current calculation should not be difficult. Some verifications concerning this part will be presented. The unbalanced magnetic pull calculation is based on [24].

An article describing the presented method was accepted for publication in the IET Electric Power Applications Journal [25].

4.1.1 Types of deformations

The aim of the method described in this chapter is to calculate the effects of any type of eccentricity or deformation on the damper bar currents and on the circulating currents in the stator parallel circuits. It is nevertheless helpful to classify the types of deformations according to some basic characteristics, last but not least to use a clear terminology throughout this report. The two main categories, static and dynamic deformation, as well as their sub-categories are defined in the following paragraphs. In a real machine it is of course likely to find a combination of these basic deformations; the described method allows to analyze all these cases. In the following, O_r will designate the center of the rotor and O_s the center of the stator.

a) Static deformation

The term static deformation will be used for any air gap deformation fixed with respect to the stator (figure 23). In the case of a 1st order static deformation (also called static eccentricity) O_r is fixed with respect to O_s , but it does not coincide with O_s . In the case of a higher order static deformation O_r coincides with O_s , but the stator is deformed. A 2nd order static deformation means an elliptic shape of the stator, 3rd order a triangular shape and so on.

These stator deformations depend generally on the type of fixation of the stator on the foundations and on the type of construction of the stator. Also stator deformations in vertical and horizontal machines may be different. Bulb type machines are specially liable to stator deformations.

Figure 23 shows the examples of 1st (left) and 3rd (right) order static deformations.

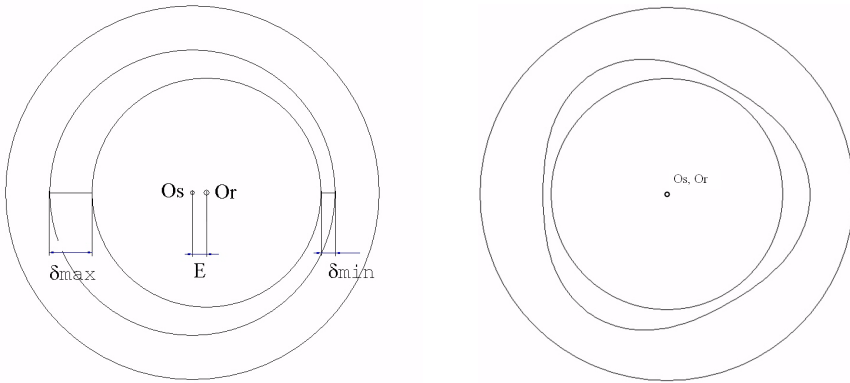


Figure 23: Examples of 1st (left) and 3rd (right) order static deformations

b) Dynamic deformation

In the case of a 1st order dynamic deformation (also called dynamic eccentricity) O_r rotates around O_s at the machine rotating speed (figure 24). In the case of a higher order dynamic deformation O_r coincides with O_s , but the rotor is deformed, typically because of displaced poles. Figure 24 shows the example of a 1st order dynamic deformation.

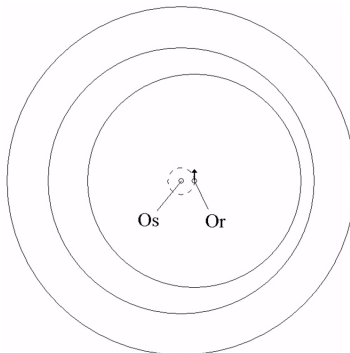


Figure 24: Example of 1st order dynamic deformation

4.1.2 Existing methods for eccentricity analysis

The physical effects of eccentricities are quite well studied, both theoretically and practically, in the case of induction machines. In [13] a way of detecting eccentricities in a medium-sized induction motor, based on a harmonic analysis of the stator currents is presented. An analytical approach to evaluate the performance of a three-phase induction motor under mixed eccentricity conditions is applied in [14]. In [15] coupled magnetic circuit simulations are carried out to quantify the line current harmonics under different combinations of load, pole pair numbers, rotor slots, and eccentricity conditions in induction machines. [16] explains in terms of harmonic field theory the influences affecting the unbalanced magnetic pull in eccentric induction machines. Experimental results are provided in order to explain the reduction in unbalanced magnetic pull due to iron saturation. A simple analytical model for prediction of the unbalanced magnetic pull in eccentric induction machines, taking into account the damping effects of a cage rotor in the case of a dynamic eccentricity, is presented in [17].

In the case of synchronous machines, and specifically in the case of large low speed salient-pole synchronous generators, the knowledge of the physical effects of eccentricities on the magnetic and electric circuits is considerably less complete. In [8] a salient-pole synchronous generator with dynamic eccentricity is modelled and simulated using a modified winding function theory. Also a modified winding function approach is applied in [18] for modelling dynamic air gap eccentricity in synchronous machines. In [7] this same approach is used and the relationships between stator-current-induced harmonics and dynamic air gap eccentricity are investigated. The FEM is used in [19] to compute the currents circulating in stator parallel circuits under faulty conditions. In [20] and [21] the effects of eccentricities on shaft signals of salient-pole synchronous machines are studied. Finally in [22] a computational model for calculating unbalanced magnetic pull in a two-pole turbogenerator in eccentricity conditions is developed.

In the case of the present thesis the above mentioned methods were not considered appropriate for the planned analysis of eccentricities. The method presented in chapters 2 and 3 was therefore extended to the study of machines in eccentricity conditions.

4.1.3 Extensions of the method described in chapter 2

The basic idea of the method described in chapters 2 and 3, computation of flux linkage values through 2D magnetostatic FEM calculations and resolution of the circuit differential equations, remains unchanged. Also the representation of the flux linkage values as the sum of the flux linkage caused by the field windings and the flux linkage caused by all other machine conductors for taking into account saturation is

not changed. Nevertheless some extensions will be introduced for the following reasons:

- Due to the uneven air gap the half or even the whole circumference of the machine has to be modeled for the FEM calculations, leading to a high number of finite elements.
- The longer cyclic periodicity (generally one whole rotor revolution) leads to a higher number of rotor positions for which the inductance and flux linkage values have to be calculated.
- Drawing a geometry of an deformed machine for the FEM calculations can be very time consuming (especially for higher order stator deformations).

The mentioned reasons all lead to a longer calculation time, either through a higher number of FEM calculations or through a higher number of finite elements, and lead therefore also to more result data. A simple numerical example for unit 2 presented in chapter 3 illustrates this fact. In the case of a third order stator deformation, combined with a dynamic eccentricity the whole machine has to be modeled. We have therefore:

- 120 stator slots
- 4 pole pairs
- 80 damper bars

If we keep the resolution of 20 rotor positions within one stator slot pitch, this leads to the following number of magnetostatic FEM calculations:

$$n_{\text{tot}} = (80+1) * 120 * 20 = 194400$$

If we take an average calculation time of 20s for one case (which is rather low, considering the high number of finite elements to expect for the whole geometry), the overall calculation time will be of 45 days and roughly 200GB of data will be created. These values can even be much higher for a machine with a higher number of poles. The study of bulb type machines is specially interesting as they are very liable to stator deformations.

For these reasons the hypothesis and simplifications described and verified in paragraph 4.2 are introduced. The complete method is summarized and verified in paragraphs 4.3 and 4.5; an application is presented in paragraph 4.6.

4.2 Hypothesis and simplifications

As mentioned above, some hypothesis and simplifications have to be admitted to calculate in a reasonable time the effect of rotor and stator deformations on unbalanced magnetic pulls, damper bar currents and circulating currents in the stator windings. These hypothesis and simplifications are explained in detail in the following paragraphs and the machines used for verification are briefly presented. As the method is based on the method for prediction of the no-load voltage, the hypothesis mentioned in paragraph 2.3 remain valid.

4.2.1 Machines used for verification

For systematical verification of the hypothesis and simplifications two machines were used, one hypothetical 4-pole machine called unit 3 and an existing 12-pole machine called unit 4. All verifications were carried out with transient magnetic FEM calculations. Other machines with higher number of poles were used for the verifications of the complete method, they will be presented in paragraph 4.5.1.

a) Unit 3

This salient-pole machine with only two pole pairs was «designed» based on unit 2 presented in paragraph 3.3.1. With only two pole pairs it is still possible to perform transient magnetic FEM calculations with the whole geometry for verifications in a reasonable time. The main data of this machine is given in the list below and figure 25 shows the geometry of the machine. The damper bars and stator slots, which will be used for comparisons in the following, are indicated in this figure.

- Number of pole pairs 2
- Rotational speed [rpm]: 1500
- Number of damper bars per pole: 8
- Number of stator slots per pole and per phase: 4
- Symmetrical poles
- Damper bars centered on the pole shoes

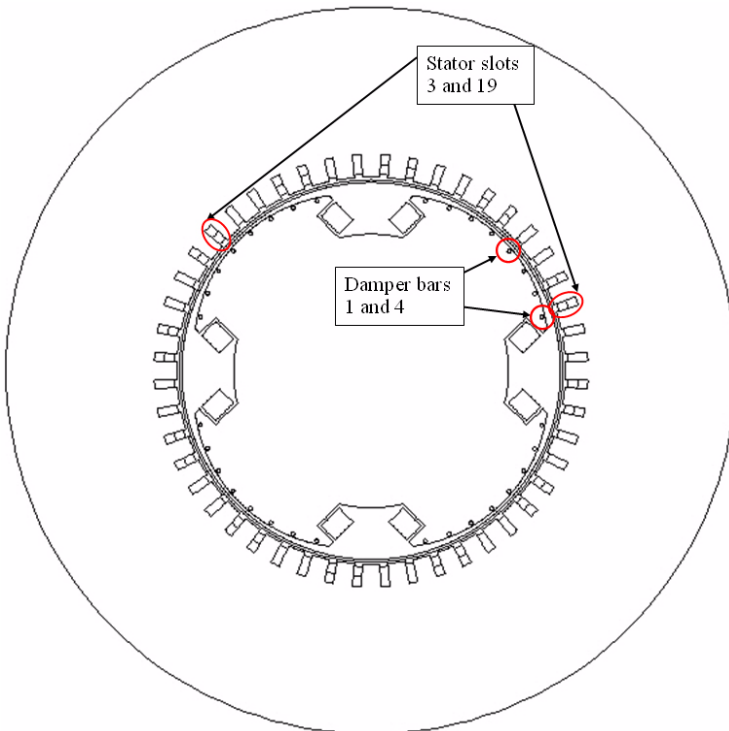


Figure 25: Geometry of unit 3

b) Unit 4

The second machine used for verification is unit 4. This machine was only used for simplified transient magnetic FEM calculations (without stator slotting, see also paragraph 4.2.2) as detailed simulations would have been too time consuming. The main machine data is given below and the geometry is shown in figure 26. The damper bars, which will be used for comparisons in the following, are indicated in this figure.

- | | |
|--|------|
| • Rated output [MVA]: | 15 |
| • Rated voltage [V]: | 5500 |
| • Rated frequency [Hz]: | 50 |
| • Number of pole pairs | 6 |
| • Rotational speed [rpm]: | 500 |
| • Number of damper bars per pole: | 7 |
| • Symmetrical poles | |
| • Damper bars centered on the pole shoes | |

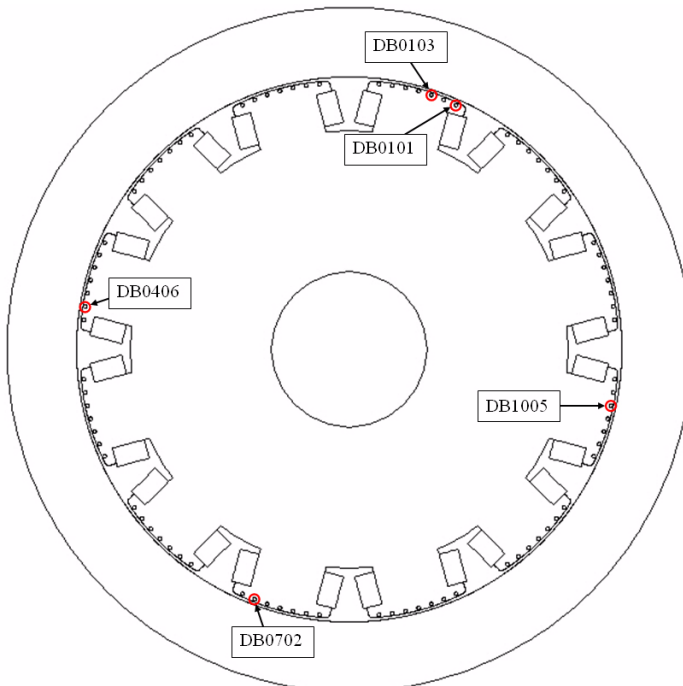


Figure 26: Geometry of unit 4

4.2.2 Neglect stator slotting

Stator slotting is one of the most important factors when calculating the no-load voltage waveform, but when one is only interested in the effects of rotor and stator deformations, the high frequency components in the currents and voltages are of no interest. On the contrary, these high frequency components increase significantly the sampling rate necessary to describe the phenomena.

When applying the method for prediction of the no-load voltage as described in chapter 2 the number of necessary FEM calculations is directly linked to the sampling rate and to the cyclic periodicity of the machine. In the case of a deformation the flux linkage and inductance values have to be calculated not only for some positions of the rotor within one stator slot pitch, but for a high number of rotor positions within a rotation of 360° in the worst case. This is due to the fact that there exists no more cyclic periodicity of one stator slot pitch, but a cyclic periodicity of 360° . A reduction of the sampling rate is therefore highly desirable. For this reason the stator slotting will be neglected. In the following paragraphs it will be demonstrated that the stator slotting has no effects on the consequences of any type of deformation.

a) Modification of the air gap according to Carter

The transformation of a slotted stator into a smooth stator is done using the Carter factor. The Carter factor describes the ratio between maximum field density in the air gap taking into account stator slotting and maximum field density of an idealized air gap field curve without stator slotting. The Carter factor k_c [29] can be calculated as follows:

$$k_c = \frac{B_\delta}{B_{max}} = \frac{\tau_s}{\tau_s - \gamma b_s} \quad (25)$$

With:

$$\gamma \approx 1 / \left(1 + 5 \frac{\delta}{b_s} \right) \quad (26)$$

Where:

- B_δ : maximum field density in the air gap with stator slotting
- B_{max} : maximum field density of the idealized air gap field curve
- τ_s : stator slot pitch
- b_s : stator slot opening
- δ : minimum air gap width of the slotted stator

The Carter factor can then be used to modify the air gap width in the case of a smooth stator so as to obtain the same fundamental harmonic component of the air gap field density as in the case of a slotted stator. The modified air gap width is obtained as follows:

$$\delta_{sm} = \delta \cdot k_c \quad (27)$$

Where:

δ_{sm} : corrected air gap width in the case of a smooth stator

It has to be mentioned that the Carter correction was developed for non-saturating stator iron ($\mu_r = const$ and $\mu_r \gg 1$). Nevertheless different verifications with machines with saturating stator iron showed that this correction provides good results also in the saturated case.

b) Stator conductors on smooth stator

In the case of a smooth stator the stator conductors can not be any longer placed at the same positions, embedded in the stator, as in the case of a slotted stator. The stator conductors have to be concentrated to a point on the interior stator surface in the case of a smooth stator; this leads to the same flux linkage values.

For calculation of the circulating currents in the parallel circuits of the stator windings the stator conductor mutual inductances have to be known. To calculate these inductances it is proposed to supply small air regions located at different positions in front of one pole pair with a test current and to calculate the mutual inductances of these regions with points distributed around the interior stator surface. The procedure is basically the same as the one used for the damper bar mutual inductances; the values obtained for the conductors in front of one pole pair can be re-used for the conductors in front of the other pole pairs. The program Flux used throughout this thesis provides the possibility to use small line air gap regions (see also paragraph 4.2.4) where a current density can be imposed. This feature can be used in this case.

4.2.3 Verifications concerning stator slotting

a) Carter correction of the air gap

Figure 27 shows the air gap field curves of unit 3 for the following cases:

1. Slotted stator
2. Smooth stator, unchanged air gap width
3. Smooth stator, air gap width corrected using the Carter factor

The following list presents the values of the fundamental harmonic component of the three curves, it demonstrates the effectiveness of the Carter correction.

- Slotted stator [T]: 1.0738
- Smooth stator, unchanged [T]: 1.1193
- Smooth stator, Carter correction [T]: 1.0747

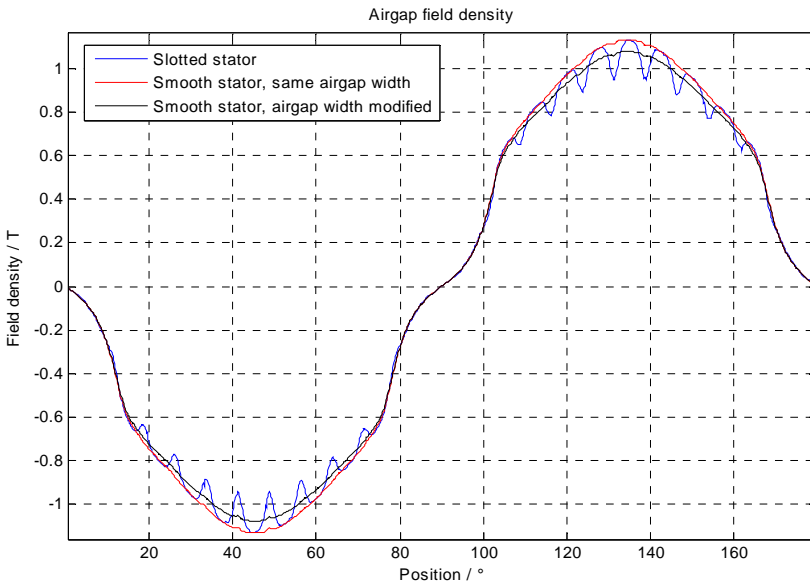


Figure 27: Air gap induction, Carter correction

b) Neglecting stator slotting

The effect of stator slotting on the damper bar currents has been investigated using unit 3. Transient magnetic FEM calculations have been performed on several examples. Figure 28 shows the currents in two damper bars in the case of a combined 1st order static and dynamic deformation with and without stator slotting. The two harmonic components due to the static eccentricity and due to the stator slots can be clearly distinguished in the case of the slotted stator; in the case of the smooth stator only the low frequency component remains. The low frequency component of the currents due to the eccentricity can therefore be calculated separately and be added up to the slot pulsation field component, calculated for example with the method described in chapters 2 and 3, if one is interested in the maximum current in a real machine (with stator slots).

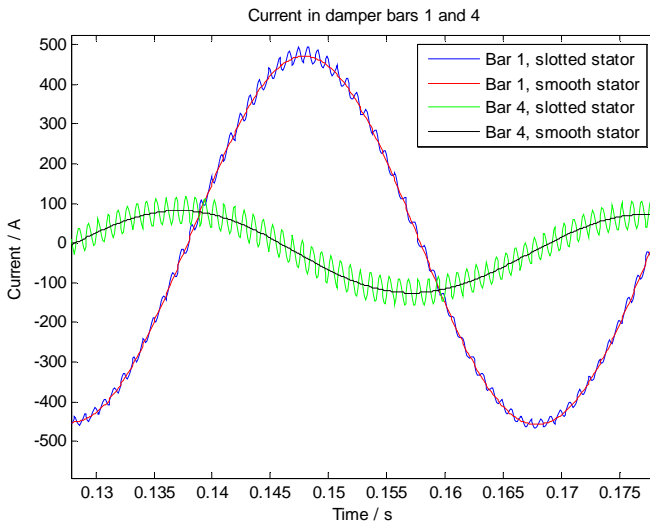


Figure 28: Damper bar currents, slotted and smooth stator

Figure 29 shows the flux linked with the interior and exterior conductors in two stator slots as well as the flux linked with the points on the interior stator surface at the same angular positions as the two slots. The effect of the dynamic eccentricity can be clearly seen. As expected, the three curves for each slot are nearly superposed, the hypothesis of concentrating the stator conductors to a point on the interior stator surface is therefore also verified.

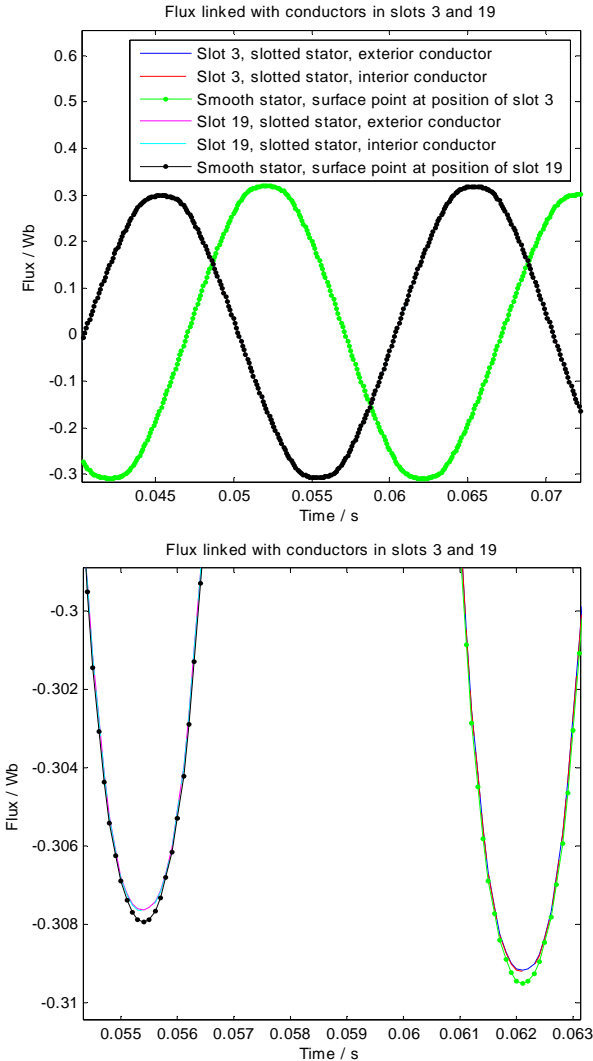


Figure 29: Flux linked with stator conductors, slotted and smooth stator

4.2.4 Modeling of the variable air gap

Another issue when studying eccentricities and deformations is the drawing of an eccentric machine for the FEM calculations. Even in the case of a smooth stator surface a higher order static deformation is not easy to draw. Furthermore, if the effects of several types of deformations are to be analyzed, a geometry has to be drawn for every case (and the corresponding FEM project has to be solved). In the following an easy to use method for modeling a variable air gap is presented.

a) Variable air gap representation for FEM calculations

The method chosen to model a variable air gap is based on the possibility in the FEM program Flux to introduce line regions representing a small air gap. The idea is to draw the whole geometry of the perfectly centered machine (without stator slots). The interior surface of the stator is then divided into line region segments representing variable air gaps. Figure 30 shows one line region segment in the case of unit 4.

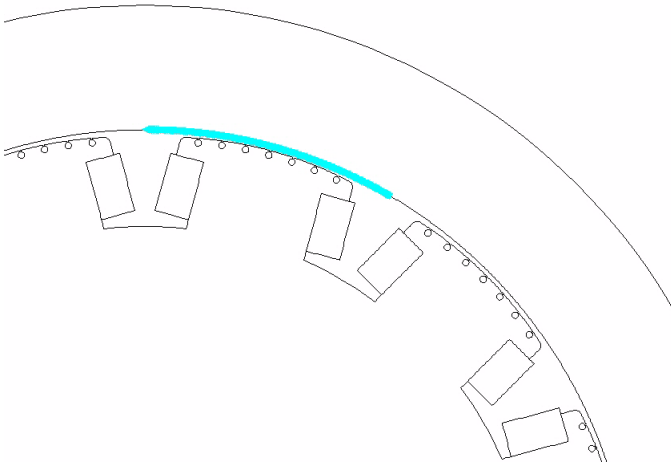


Figure 30: Line region segment

The number of segments depends on the order of stator and rotor deformation to be analyzed and on the precision required (spatial discretization of the air gap deformation). The choice of the number of air gap segments will be discussed in paragraph 4.5.5. The air gap width without additional air gap in the line regions should be chosen slightly smaller than the nominal air gap width, thus allowing to vary the air gap width in both directions (smaller and bigger than nominal air gap width).

This method can be used in the case of transient magnetic FEM calculations with rotating rotor. But one has to be aware of the discontinuities introduced by the air gap width varying abruptly from one segment to the neighboring segments. These discontinuities are especially important for small air gap widths and big air gap variations. As the voltage induced in the machine conductors is the derivative of the flux linked to the conductor, an abrupt variation of the flux linkage value due to an abrupt variation of the air gap width will cause a high value of induced voltage.

Figure 31 shows the current in one damper bar of unit 5 (main characteristics see paragraph 4.5.1). The simulated machine has a mean air gap width of 8.5mm and a 2nd order static deformation with an amplitude of 1mm was modeled. The discontinuity in the current is due to the abrupt variation of the air gap width from one segment to the neighboring segments. The number of air gap segments is equal to the number of poles, therefore the discontinuity is repeated with a frequency of 100Hz (machine rotating speed for 50Hz). With a less important deformation the discontinuity was also less important. As one will see in paragraph b) this problem will not be present in the proposed method.

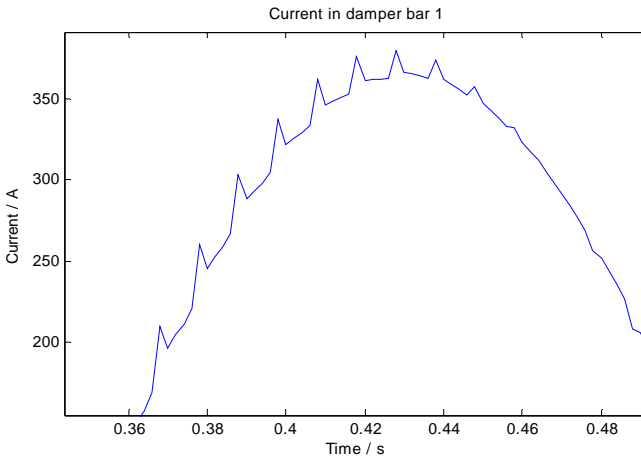


Figure 31: Discontinuity in damper bar current due to abrupt air gap width variation

b) Calculation of magnetic coupling without rotating the rotor

In the case of the method described in this chapter the flux linkage values of the machine conductors have to be calculated for different rotor positions using magnetostatic FEM calculations. Furthermore the interior stator surface is smooth and the air gap deformation is modeled with air gap segments located on the stator surface. Therefore the rotation of the rotor could be replaced by a modification of the air gap width values of the air gap segments according to each rotor position considered. One could say that the rotation of the rotor is replaced by a rotation of the air gap deformation.

Without rotating the rotor, the air gap distribution according to any combination of static and dynamic deformation and any rotor position can be represented by adjusting correctly the air gap width of each segment on the stator interior surface. The flux linkage values for any situation could thus be calculated without rotating the rotor. This technique also prevents the phenomenon of discontinuity described in paragraph a) as the air gap variations from one rotor position to the next one can be chosen much smaller (this means considering more rotor positions than air gap segments per revolution).

c) Representation of the effects of each air gap segment

Computing the flux linkage values for many combinations of air gap widths of the line regions (according to the number of rotor positions per revolution) would still lead to a very high number of magnetostatic FEM calculations. For this reason the influence of the air gap value of one single air gap segment on the different flux linkage values was studied.

Figure 32 shows the variation of flux linkage of the field windings with damper bar 3 on pole 1 in function of a variation of the air gap segment in front of each pole ('Pole 1' to 'Pole 12') in the case of unit 4 (12 air gap segments). The air gap width of each segment was varied from 0mm to 2mm while the air gap width of all other segment were fixed to 1mm.

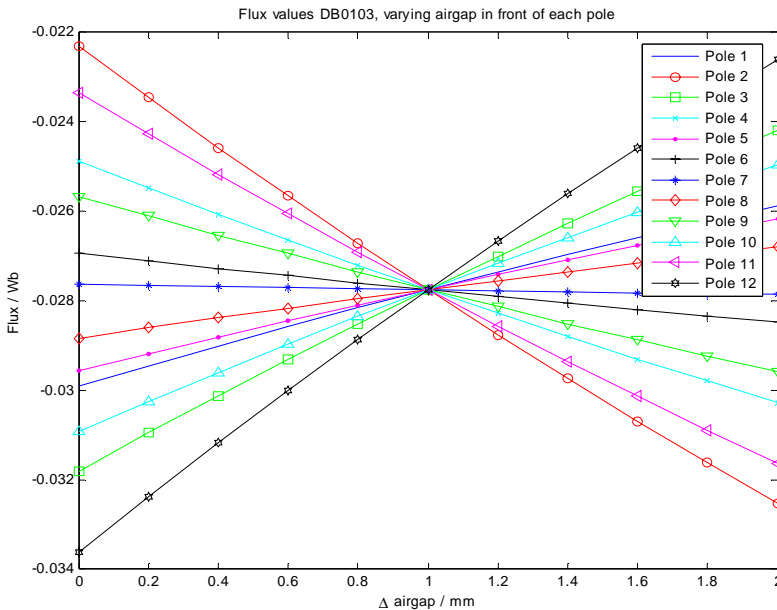


Figure 32: Flux linkage values in function of varying air gap in front of each pole

As expected, the variation of some segments influences the flux linkage value more than others, but generally the dependence seems to be quite linear in all cases.

In figures 33 and 34 the variation of the mutual differential inductances of damper bar 1 on pole 1 with bar 3 on the same pole (figure 33) and with bar 6 on pole 4 (figure 34) also in function of the air gap width of each segment is shown. Again the influence depends on the position of the air gap segment, but, also in the case of the differential inductances, the dependence appears to be quite linear.

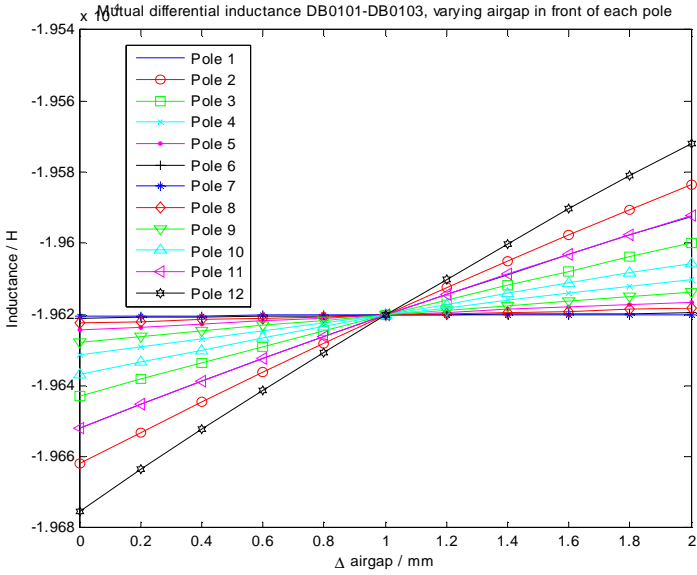


Figure 33: Mutual differential inductances in function of varying air gap in front of each pole

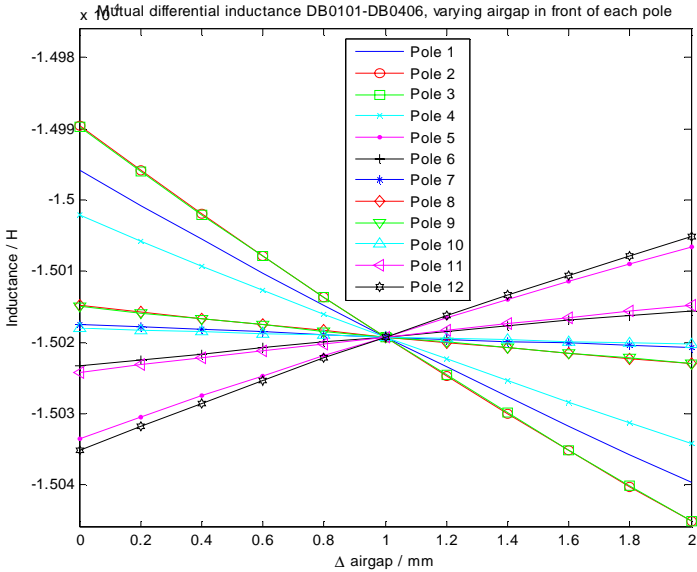


Figure 34: Mutual differential inductances in function of varying air gap in front of each pole

The fact to have an almost linear dependence of the flux linkage and differential inductance values in function of the air gap width of each line region segment does not surprise. For important variations of the air gap width the dependence would be exponential. But the small variations of the air gap considered in our case influence only slightly the saturation in the stator and the rotor and no other non-linear influencing factors are present, therefore only a slight non-linearity can be observed.

For this reason a good approximation of the influence of the air gap width of each line region segment on each flux linkage or differential inductance value for small air gap variations can be obtained using 1 or 2 linear segments as shown in figure 35. The red line shows the 2-segment approximation, one segment from the value at minimum air gap width to mean air gap width and one from mean air gap width to maximum air gap width. This approximation allows to determine the influence of each segment on each flux linkage or inductance value with two magnetostatic FEM calculations, one with maximum air gap for the considered segment and one with minimum air gap (mean air gap for all other segments). Additionally one FEM calculation has to be performed with mean air gap width for all segments. The green line shows an approximation using only one linear segment issued from a small air gap variation of the segment. This approximation provided also very good results (see also paragraph 4.5.5), allowing to reduce even more the calculation time. A more detailed description of the number of necessary FEM calculations with a numerical example will be presented in paragraph 4.4.1. The choice of maximum and minimum air gap values for the segments is discussed in paragraph 4.4.2.

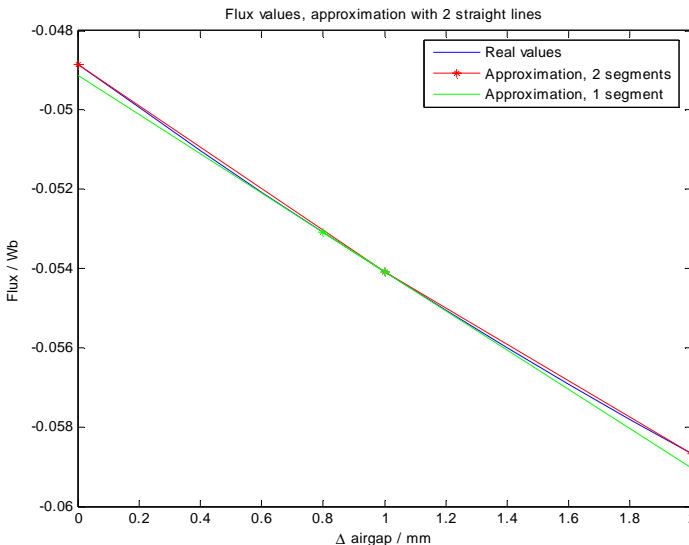


Figure 35: Linear approximation of flux values in function of the air gap width

d) Combination of the effects of each air gap segment

Furthermore the influence of a combination of different air gap widths of several segments on the flux linkage and inductance values was investigated. The influence of a combination of different air gap widths was described as a linear superposition of the influence of these air gap widths. Thus, knowing the linearized influence of each segment on each flux linkage or inductance value as described above, all flux linkage and inductance values for the air gap distribution according to any combination of static and dynamic deformation and any rotor position can be calculated.

This can be mathematically described as a first order Taylor approximation of an unknown function of several variables. Each flux linkage value (for a given static and dynamic deformation and rotor position) can be expressed as the sum of its value with mean air gap width for all line region segments and a corrective value for the actual air gap width of each segment (in this case linearization with one line segment):

$$\Phi_{exc,j} = \Phi_{exc,j}^* + \sum_{l=1}^N (k_{exc,j,l} \cdot \delta_l) \quad (28)$$

Where:

- $\Phi_{exc,j}$: flux linkage value (field winding - conductor 'j') for a given static and dynamic deformation and rotor position
- $\Phi_{exc,j}^*$: flux linkage value (field winding - conductor 'j') with mean air gap width for all line region segments (perfectly centered machine)
- $k_{exc,j,l}$: influencing factor of segment 'l' on this flux linkage value, in [Wb/mm]
- δ_l : difference from the mean air gap value for segment 'l' (positive or negative), in [mm]

The same applies for the mutual differential inductance values:

$$L_{diff_{i,j}} = L^*_{diff_{i,j}} + \sum_{l=1}^N (k_{i,j,l} \cdot \delta_l) \quad (29)$$

Where:

- $L_{diff_{i,j}}$: mutual differential inductance value (conductor 'i' - conductor 'j') for a given static and dynamic deformation and rotor position
- $L^*_{diff_{i,j}}$: mutual differential inductance value (conductor 'i' - conductor 'j') with mean air gap width for all line region segments (perfectly centered machine)
- $k_{i,j,l}$: influencing factor of segment 'l' on this mutual differential inductance value, in [H/mm]
- δ_l : difference from the mean air gap value for segment 'l' (positive or negative), in [mm]

The influencing factors $k_{i,j,l}$ and $k_{exc,j,l}$ are nothing else than the slopes of the line segments as shown in figure 35 (green line). In the case of a linearization of the influence of the air gap segments with two line segments (red lines in figure 35), there will be two different values for $k_{i,j,l}$ and $k_{exc,j,l}$ according to a positive or a negative value of δ_l .

e) Resolution of the circuit equations

The flux linkage values and differential inductances calculated for a given case (given rotor and stator deformations and given number of rotor positions per revolution), as described in paragraph d), can then be used in the equations described in paragraph 2.5.2. The resolution of the electrical circuit equations remains the same as in the case of the method for calculation of the no-load voltage presented in chapters 2 and 3. The only difference lies in the way the flux linkage and inductance values are calculated. In both cases the magnetostatic FEM is used but in the first case with different rotor positions and in the second case with varying air gap segments.

4.2.5 Verifications of the air gap modeling

a) Representation of air gap deformations using line region segments

A first verification was carried out to make sure a simulation using line region segments on the interior surface of the stator to represent the variable air gap under deformation conditions provides the same results as a simulation with a deformed geometry. This was verified with several examples and varying numbers of air gap segments, always using transient magnetic FEM simulations with deformed geometries or with air gap segments. In the following the case of a combined 1st order static and dynamic eccentricity in unit 3 presented in paragraph 4.2.1 is shown. The interior stator surface was divided into 48 line region segments. Figures 36 and 37 show the currents in two damper bars and the flux linked with conductors in two stator slots (points on interior stator surface) in the two different cases. In all cases the curves match very well; the representation of the variable air gap using line region segments on the interior stator surface is therefore verified.

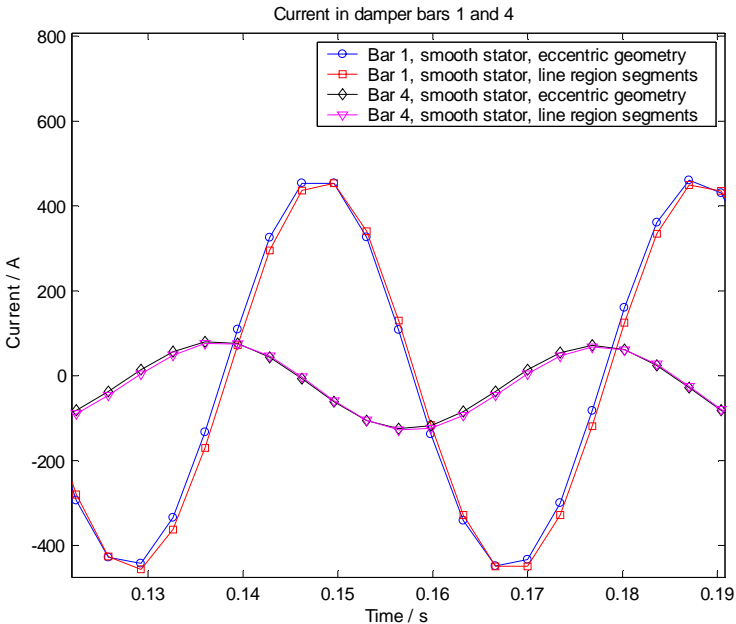


Figure 36: Currents in two damper bars

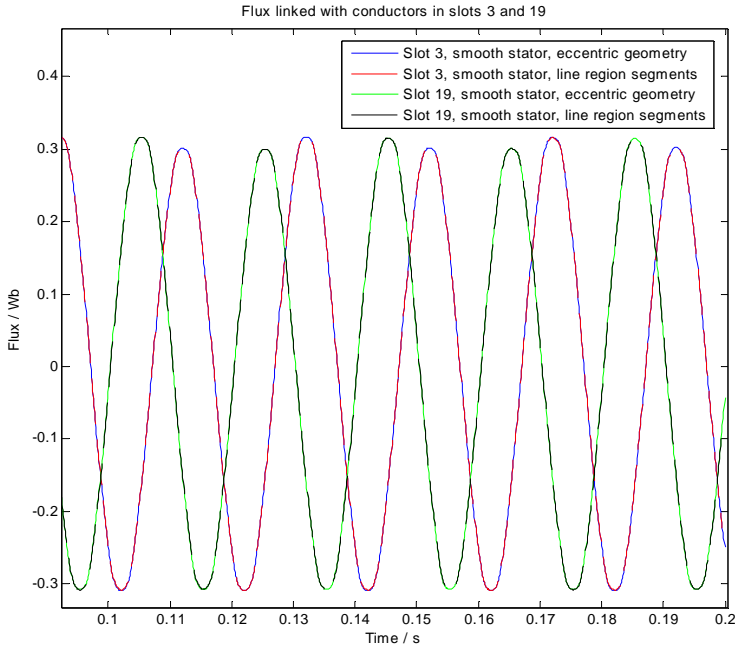


Figure 37: Fluxed linked to conductors in two stator slots

b) Linear superposition of the influences of several air gap segments

For verification of the linearization and of the linear superposition of the effects of each line region segment on the flux linkage and inductance values, as described at the end of paragraph 4.2.4, unit 4 was used. The interior stator surface was divided into 12 line region segments; the air gap value of each one could be adjusted to 0.4mm, 0.7mm, 1.0mm, 1.3mm and 1.6mm. Using magnetostatic FEM calculations the flux linkage values of the field windings with several damper bars and stator conductors (points on the stator surface) were calculated for all possible combinations of air gap width values of the segments 1, 2, 6 and 10, the air gap values of the other segments remaining at 1mm (see figure 38). The same operation was repeated for the mutual differential inductances of several damper bars and stator conductors with bar 1 on pole 1.

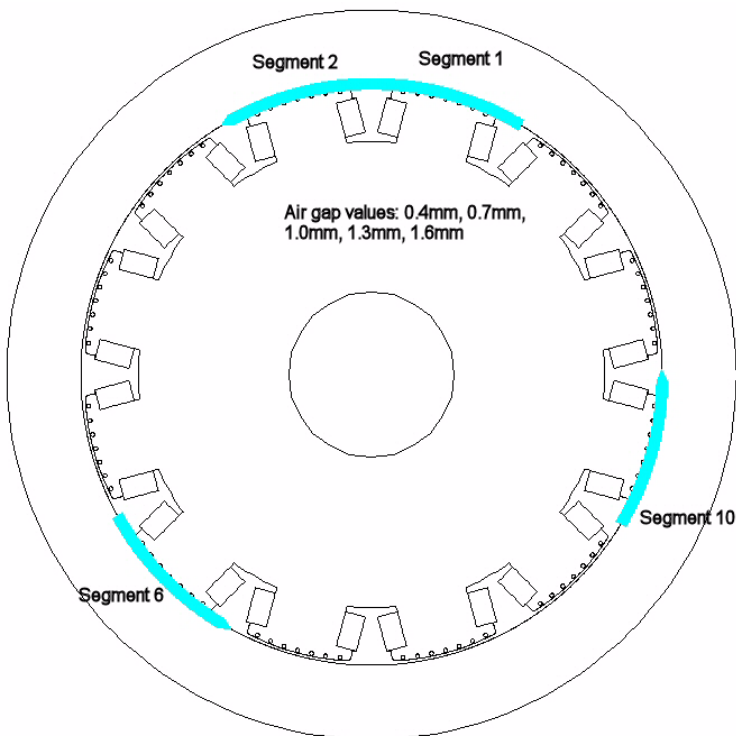


Figure 38: Air gap values of different segments

The same values were then calculated using only the values of the influencing factors and the flux linkage and inductance values for a constant air gap width of 1mm (as described in paragraph 4.2.4, equations 28 and 29). Table 2 shows the flux linkage values for some of the possible combinations of air gap widths of the 4 segments. Only the flux values of the first 10 lines were used for calculating the linearizations and then the flux values of the 615 following lines.

δ , segment 1 [mm]	δ , segment 2 [mm]	δ , segment 6 [mm]	δ , segment 10 [mm]	Flux value [Wb]
1	1	1	1	-9.664668e-003
0.4	1	1	1	-9.667097e-003
1.6	1	1	1	-9.662304e-003
1	0.4	1	1	-6.379331e-003
1	1.6	1	1	-1.270605e-002
1	1	0.4	1	-9.108732e-003
1	1	1.6	1	-1.017936e-002
1	1	1	0.4	-1.143475e-002
1	1	1	1.6	-8.026022e-003
0.4	0.4	0.4	0.4	-7.598026e-003
0.4	0.4	0.4	0.7	-6.692197e-003
0.4	0.4	0.4	1	-5.821375e-003
0.4	0.4	0.4	1.3	-4.983516e-003
0.4	0.4	0.4	1.6	-4.176744e-003
0.4	0.4	0.7	0.4	-7.878273e-003
0.4	0.4	0.7	0.7	-6.971513e-003
0.4	0.4	0.7	1	-6.099793e-003
0.4	0.4	0.7	1.3	-5.261071e-003
0.4	0.4	0.7	1.6	-4.453450e-003

Table 2: Combinations of air gap values of different segments

The flux linkage and inductance values obtained through the linear superposition approach were compared to the values directly obtained from the magnetostatic FEM calculations. These comparisons are shown in the figures 39 to 42. In the figures only the positions of the conductors on the stator are indicated (not attributed to a stator slot). It has to be noted that these figures do not have any physical signification; they simply show the flux linkage values or inductances (y-axis) for different combinations of the air gap values of the 4 air gap segments (x-axis, the possible combinations are numbered from 1 to 625).

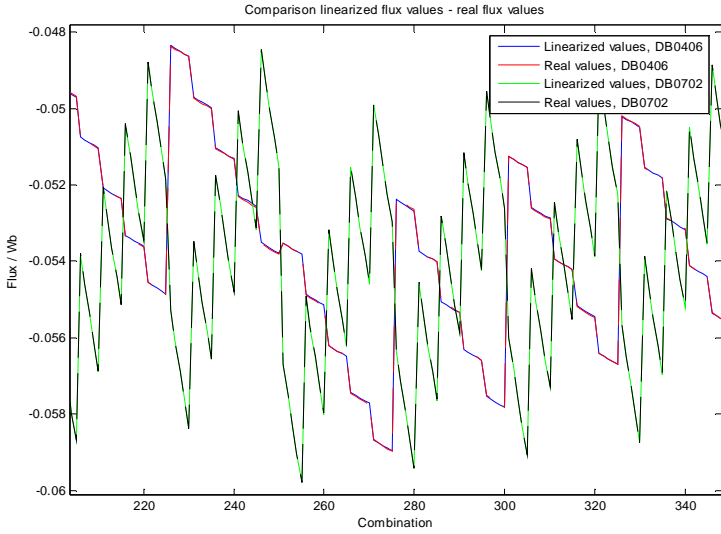


Figure 39: Linear superposition of linearized flux linkages with damper bars

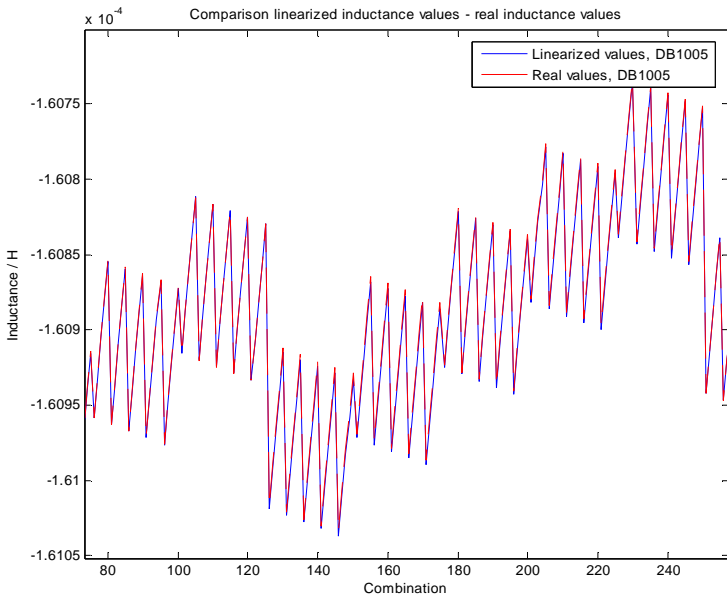


Figure 40: Linear superposition of linearized mutual inductances of damper bar 1 with other damper bars

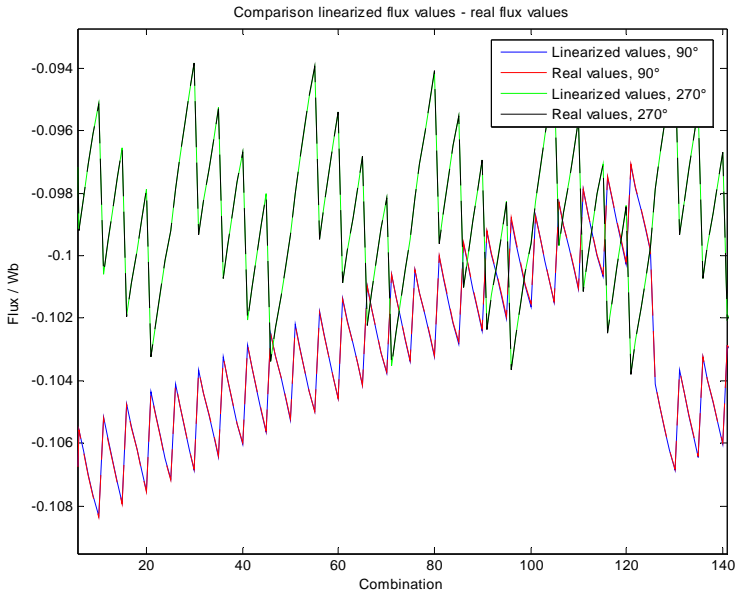


Figure 41: Linear superposition of linearized flux linkages with stator conductors

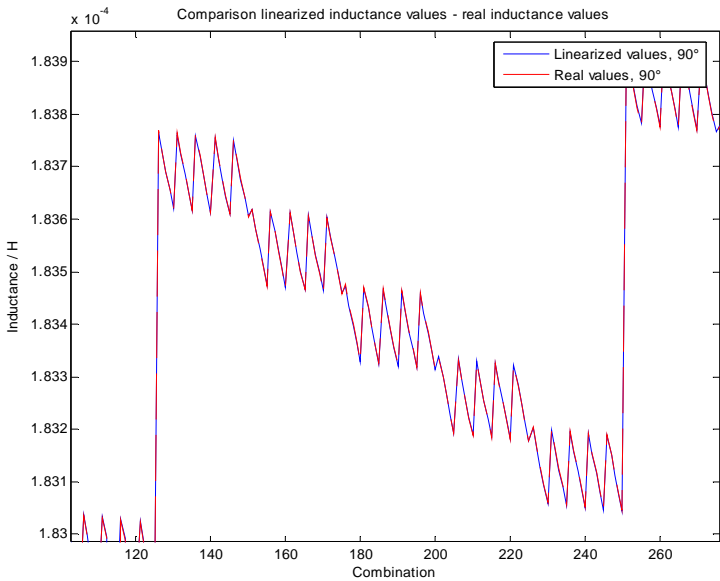


Figure 42: Linear superposition of linearized mutual inductances of stator conductors with damper bar 1

As can be seen on figures 39 to 42, the values obtained through linear superposition of the linearized effects of each segment agree very well with the real values. The maximum relative error for any case is about 1%.

Additionally to verifications of the different hypothesis presented in this paragraph the complete method was verified on several examples. Some of these comparisons of results from transient magnetic FEM simulations of machines with deformed geometries with results from the described method will be presented in paragraph 4.5.

4.2.6 Re-using inductance values

As already mentioned, in the case of an eccentric machine the whole geometry of the machine has to be modelled for the FEM calculations, generating a high number of finite elements.

Some calculation time can nevertheless be economized by re-using the flux linkage and inductance values calculated for one pole pair. In the described method the flux linkage and inductance values as well as the influencing factors for each air gap segment (as used in equations 28 and 29) are calculated only for the damper bars of one pole pair (mutual inductances with all bars on all pole pairs). These values can be re-used through re-attribution for all other damper bars.

4.3 Unbalanced magnetic pull calculation

4.3.1 Deformation of the air gap induction

An eccentricity situation induces a deformation of the air gap induction. The air gap induction, $B(\alpha_s, t)$, in an eccentered machine can very generally be expressed as the multiplication of the air gap induction of the centered machine multiplied with two modulation functions, Λ_s and Λ_r , expressing the static and dynamic deformations respectively.

$$B(\alpha_s, t) = \left(\sum_v^{\hat{v}} \hat{B} \sin(v(\alpha_s - \Omega t) + v\phi) \right) \Lambda_s(\alpha_s) \Lambda_r(\alpha_s, t) \quad (30)$$

With:

$$\Lambda_s(\alpha_s) = 1 + \sum_{\eta}^{\eta} \varepsilon_s \sin(\eta\alpha_s + \eta\phi_s) \quad (31)$$

$$\Lambda_r(\alpha_s, t) = 1 + \sum_{\kappa}^{\kappa} \varepsilon_r \sin(\kappa(\alpha_s - \Omega t) + \kappa\phi_r) \quad (32)$$

Where:

- \hat{B} : amplitude of the harmonic v of the air gap induction of the centered machine
- α_s : position on the stator
- ε_s : relative amplitude of the harmonic η of the static air gap deformation
- ϕ_s : phase angle of the harmonic η of the static air gap deformation
- ε_r : relative amplitude of the harmonic κ of the dynamic air gap deformation
- ϕ_r : phase angle of the harmonic κ of the dynamic air gap deformation

Considering only the fundamental harmonic of the induction of the centered machine ($v = p$, where p is the number of pole pairs) and modulation functions for a 1st order static and a 1st order dynamic eccentricity ($\eta = 1, \kappa = 1$) one can easily calculate the resulting air gap induction. Neglecting the terms with the factor $\varepsilon_s \cdot \varepsilon_r$, ε_s and ε_r being normally in the range of some percents, one can observe that each one of the two

eccentricities introduces two rotating waves with orders $p-1$ and $p+1$. This situation is summarized in table 3.

	static eccentricity		dynamic eccentricity	
	rotating speed	frequency induced on stator	rotating speed	frequency induced on stator
wave of order $p-1$	$\frac{n_s p}{p-1}$	f_1	n_s	$\frac{f_1(p-1)}{p}$
wave of order $p+1$	$\frac{n_s p}{p+1}$	f_1	n_s	$\frac{f_1(p+1)}{p}$

Table 3: Rotating waves caused by 1st order eccentricities

It can be observed that the rotating waves due to the static eccentricity induce voltages with the fundamental frequency, whereas the waves due to the dynamic eccentricity induce voltages with different frequencies. This effect can be seen very clearly for example in figures 54 and 56.

4.3.2 Unbalanced magnetic pull calculation

As the unbalanced magnetic pulls are due to the deformation of the air gap induction, their calculation is based on the air gap induction. The method described in this chapter allows to calculate the voltages induced at different positions on the stator bore. The air gap induction at these positions can then be obtained through equation 33.

$$B(\alpha_s, t) = \frac{U_{\alpha_s}(t)}{v l_i} \quad (33)$$

Where:

$U_{\alpha_s}(t)$: voltage induced at position α_s on the stator bore.

v : speed of the rotating magnetic field

l_i : ideal length of the machine

The magnetic pressure can then be calculated for these positions on the stator bore:

$$\sigma(\alpha_s, t) = \frac{B^2(\alpha_s, t)}{2\mu_0} \quad (34)$$

Where:

$\sigma(\alpha_s, t)$: magnetic pressure at the position α_s on the stator bore

And finally the unbalanced magnetic pulls are obtained through integration of the magnetic pressure on the whole circumference.

$$F(t) = l_i r \int_0^{2\pi} \sigma(\alpha_s, t) d\alpha_s \quad (35)$$

Where:

- F(t) : unbalanced magnetic pull in function of time
 r : bore radius

If the general description of the air gap induction as given in equation 30 is introduced in equations 34 and 35, one can observe that only the 1st order static and dynamic eccentricities lead to an unbalanced magnetic pull. All the contributions of other components or of combinations of other components of the deformation of the air gap induction are either negligible compared to the contribution of the 1st order eccentricities or are cancelled out through the integration in equation 35.

4.4 Summary of the method

The method described in this document can be summarized very briefly in 6 steps as follows:

1. Calculation of the flux linkage values and mutual differential inductances for a perfectly centered rotor and not deformed stator and of the influencing factors of each air gap segment on each one of these values (as used in equations 28 and 29) using the magnetostatic FEM without rotation of the rotor.
2. Reading the result files of the FEM calculations and storing only the necessary data. The FEM result files can then be deleted or archived.
3. Calculation of the flux linkage values and mutual differential inductances for a chosen case (chosen static and dynamic air gap deformation) and a chosen number of rotor positions per revolution using equations 28 and 29.
4. Solving the electrical circuit equations using the values calculated in step 3 as described in paragraph 2.5.2.
5. Calculation of the voltages induced at several points on the interior stator surface using the damper bar currents calculated in step 4.
6. Calculation of the unbalanced magnetic pulls using the voltages calculated in step 5 according to paragraph 4.3.2.

In the following some more details are given regarding some specific points and also regarding the practical application of the method.

4.4.1 Number of FEM calculations

The number of magnetostatic finite element calculations depends on the following parameters:

- number of air gap segments (spatial discretization of the air gap deformation)
- number of linear segments for representation of the influence of each segment on the flux linkage and inductances values (paragraph 4.2.4)
- number of damper bars on one pole pair

As can be seen the number of FEM calculations does not depend on the number of rotor positions per revolution (time discretization). This is due to the fact that all magnetostatic FEM calculations are carried out without rotation of the rotor. The rotor rotation is introduced later on, when preparing the flux linkage and inductance values for a given case.

Knowing the above mentioned values the necessary number of FEM calculations can be obtained as follows: $n = (b+1)*(s*ls+1)$, where b is the number of damper bars on one pole pair, s the number of air gap segments and ls the number of linear segments for representation of the influence of each air gap segment. For a typical example of a machine with a high number of poles, where $b = 8$, $s = 38$ and $ls = 1$, this results in $n = 351$ FEM calculations. The only limiting factor regarding machines with high number of poles is therefore the high number of finite elements in the FEM model, because the whole geometry of the machine has to be represented. This means a high calculation time for each case and also much data created.

4.4.2 Description of the calculation steps

a) FEM calculations

The preparation of the FEM calculations is somewhat simplified by the fact that the stator slots are neglected, this reduces the stator to two circles. It is recommended to define only one FEM project manually and derive all the others from this one. Typically the project with only field windings supplied can be created manually; all other projects can then be derived by simply supplying each time one damper bar. The important points concerning the preparation of the FEM projects are the following:

- The geometry of the whole machine (complete circumference) should be represented.
- No sliding air gap band is required as there will be no rotation of the rotor.
- The real non-linear characteristics of the magnetic materials should be used.
- The currents in the field windings and the damper bars are introduced as uniformly distributed current densities.
- All segments should have the same air gap width. Typically 1mm in the case of a linearization of the influence of each segment using two linear segments or 0mm in the case of a linearization using only one linear segment.
- The meshing of the air gap segments should be chosen accordingly if one wants to calculate the induced voltages in stator conductors and the unbalanced magnetic pulls (more details regarding this point is given in [23]).

Once the $b+1$ FEM projects are defined (b being the number of damper bars on one pole pair), their parameterized resolution has to be prepared. In the case of a parameterized resolution using the software Flux, one has the possibility to solve the same FEM project several times using different values for some parameters. In our case the parameters are the air gap widths of each air gap segment. The values for the parameters are chosen so as to obtain the values for the linearization of the influence of each air gap segment. The following values are recommended:

- One linear segments: 0mm (reference value) and 0.2mm
- Two linear segments: 0mm, 1mm (reference value) and 2mm

These values have to be introduced for every FEM project and for every air gap segment. The reference [23] points out a fast and easy way of doing this. The FEM projects can then be solved in batch mode; this can generally be done in less than one

night even for machines with a high number of poles. It is pointed out that this step does not depend on the type of deformation to be analyzed. It has therefore to be carried out only once and its results can be re-used for the analysis for any kind of deformation.

b) Calculation of flux linkage and inductance values

The flux linkage and inductance calculation is based directly on the results of the above mentioned FEM simulations, applying equations (28) and (29). These value are calculated for a certain number of rotor positions within one rotor revolution. The number of rotor positions can be chosen independently from the number of air gap segments. For each position the air gap value of each segment has to be adjusted in function of the rotor position and of the static and dynamic air gap deformations. The choice of the number of rotor positions will be discussed in paragraph 4.5.5.

c) Resolution of differential equations

Based on the Kirchhoff laws differential equations are formed exactly in the same way as described in paragraph 2.5.2 (but this time including all damper bars of the machine). They can also be solved using a numerical method (e.g. Runge-Kutta) as described in this same paragraph.

d) Calculation of the unbalanced magnetic pulls

For calculation of the unbalanced magnetic pulls the voltages induced at several points on the interior stator surface are used as described in paragraph 4.3.2 and in [24]. Generally 15 equally distributed points were chosen and the voltages were calculated exactly as described in paragraph 2.5.3.

4.4.3 Tool for practical application of the method

A user friendly industrial application of the method described in this document was an important goal of this thesis. Therefore the described method was implemented in a graphical tool using the Delphi programming language. This tool allows a convenient industrial application of the method. Comparative studies of different eccentricity situations can be carried out in a comfortable way.

The necessary FEM calculations were described in paragraph 4.4.2; the tool uses directly the FEM result files for computation of the damper bar currents and unbalanced magnetic pulls for a given deformation. It is prepared for easy integration of the calculation of the currents in stator parallel circuits. In the following the use of this tool is very briefly presented, more information on this subject can be found in [23].

a) Generalities

The program has a graphical user interface, allowing easy introduction of the project data. A project can be saved to a file and opened again. The different calculation steps are activated by buttons and dialog boxes are used for selecting the input and output files.

b) Introduction of machine data

The necessary machine data is introduced on the first page of the tool, shown in figure 43.

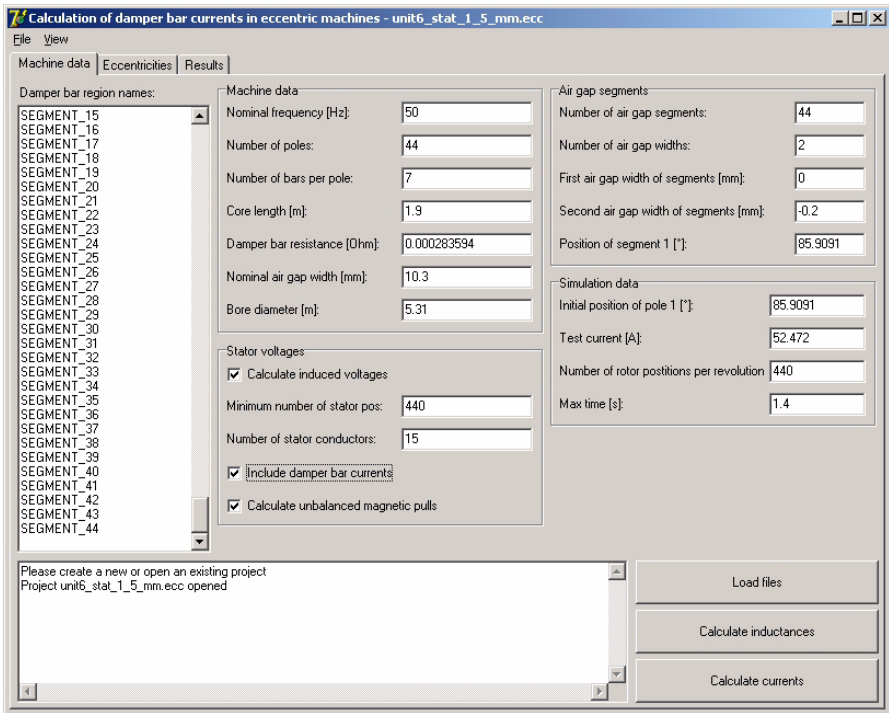


Figure 43: Introduction of machine data

This data is very easy to put together as soon as the FEM projects are defined. As one can see it is also possible to calculate the voltages induced in conductors located on the interior stator surface. The user can choose if he wants to calculate the unbalanced magnetic pulls (based on the voltages) and if he wants to include the damper bar currents (damping effects) in the voltage and unbalanced magnetic pull calculations. This functionality allowed also the verification of the induced voltages and will

simplify the extension of the method to the calculation of the currents in parallel circuits of the stator windings.

c) Description of the deformation

On the second page of the tool, shown in figure 44, the eccentricity situation to be studied can be described.

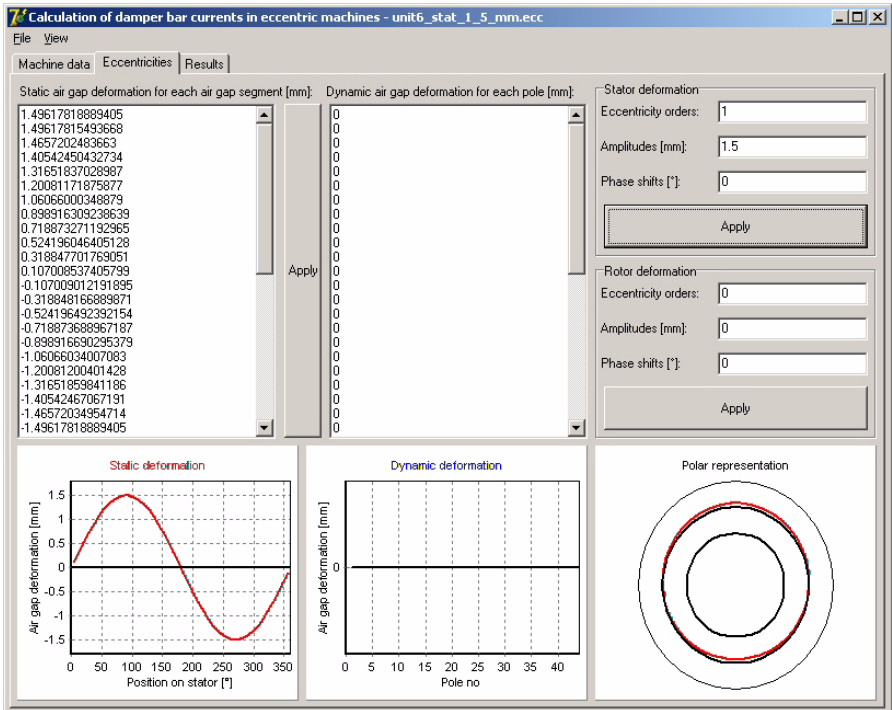


Figure 44: Introduction of deformation data

The data concerning static and dynamic air gap deformations can be entered separately. The deformations can either be described by Fourier series using amplitude and phase for each harmonic order or as series of air gap deformation values for each segment or each pole respectively. This allows an easy description of any eccentricity situation. A Carter correction of the air gap width for taking into account the missing stator slots (see also paragraph 4.2.2) could also be introduced at this place by adding a constant air gap increase on the whole circumference (this will affect the precision of the results). The considered eccentricity condition is graphically represented at the bottom of the page.

d) Calculation of the damper bar currents, stator voltages and unbalanced magnetic pulls

The calculation of the damper bar currents, stator voltages and unbalanced magnetic pulls is done in 5 steps using this tool:

1. Reading the FEM result files and extraction of the necessary data.
2. Calculation of the flux linkage and inductance values for a given number of rotor positions and given static and dynamic air gap deformations.
3. Computation of the damper bar currents using the values calculated in step 2.
4. Computation of the stator voltages using the values calculated in step 2 and the currents calculated in step 3.
5. Computation of the unbalanced magnetic pulls using the voltages calculated in step 4.

The 3 buttons on the first page of the tool (figure 43) correspond to these steps (steps 3 to 5 correspond to the 3rd button). The results of each one of these steps are written at the end of the calculation of the step in a text file. As the first step does not depend on the deformations which will be analyzed, it can be carried out only once and the result files of the FEM calculations can be deleted afterwards. For each eccentricity situation one is interested in, steps 2 to 5 can then be carried out using the output file of step 1. The output file of step 1 is not very big (<50MB) and the execution of steps 2 to 5 do not take much time (<1h). It is therefore easy to analyze different eccentricity situations for a given machine. Also the damping effects of the damper cage on the unbalanced magnetic pulls (see [28]) can be analyzed easily by carrying out steps 3 to 5 twice, once considering the damper bar currents in the voltage calculation and once without damper bar currents.

e) Visualization of the results

The last page of the tool allows the visualization of the results. As the results are also written in text files, they can be analyzed further (calculation of losses, etc.) using a more appropriate tool (e.g. Matlab, Microsoft Excel).

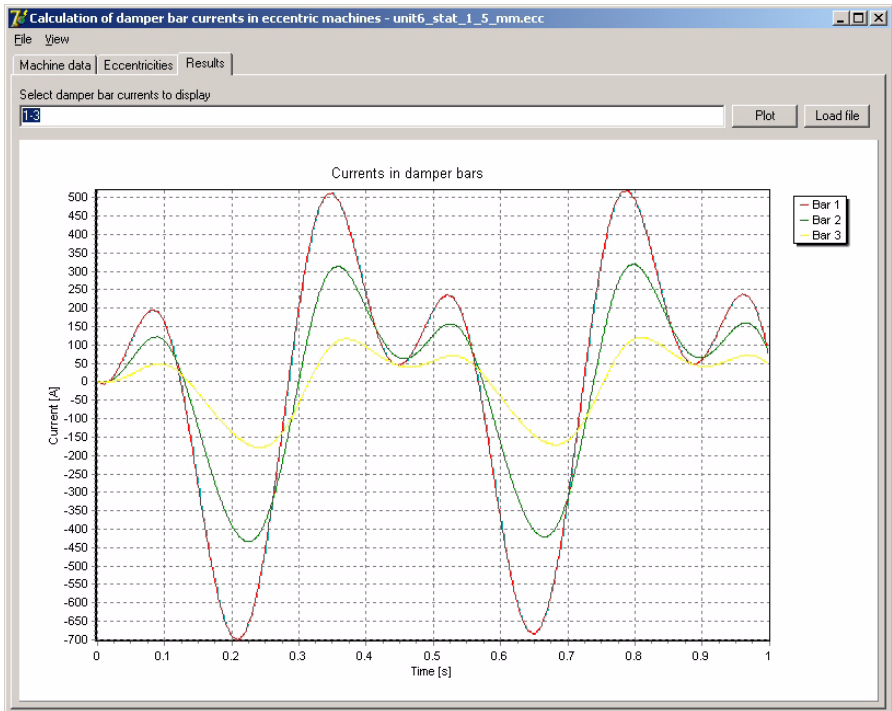


Figure 45: Visualization of the results

4.4.4 Calculation of additional losses due to eccentricities

As will be shown in paragraph 4.5.2, the precision of the damper bar currents calculated with the presented method is very good. This allows also a precise prediction of the Joule losses due to eccentricities. The calculation of the Joule losses, knowing the evolution in time of the currents in all damper bars is straightforward.

$$P(t) = \sum_j R_j i_j(t)^2 \quad (36)$$

As mentioned in paragraph 2.3 it is proposed to use the damper bar resistance for the corresponding frequency (calculated for example according to [12]) in the differential equations. The adaptation of the resistance in function of the expected frequency (frequency of the slot pulsation field or of the air gap deformation) proved to have very little influence on the calculation of the damper bar currents, the damper circuit being essentially inductive. The damper bar currents can therefore be predicted with high precision even when the DC-resistance of the damper bars is used. The resistance adaptation has nevertheless much influence on the calculation of the Joule losses and should therefore be taken into account at this stage.

For the calculation of the total losses it is proposed to calculate separately the currents and losses due to the eccentricities and due to the stator slotting. Both components of the losses should be calculated with the damper bar resistance according to the corresponding frequency. This proved to be an acceptable simplification in all cases.

As already mentioned in paragraph 2.5.2 the leakage inductances and resistances of the short-circuit rings are not taken into account. The presented method could nevertheless be improved easily by taking into account these inductances and resistances. This improvement would require a modification of the system of differential equations described in paragraph 2.5.2.; the process of resolution would remain exactly as it is. This modification would improve the precision of the results especially in the case of very short machines.

4.5 Verifications

Additionally to the verifications of the different hypothesis, the complete method described in this chapter was verified. All verifications were carried out on low speed alternators (see paragraph 4.5.1) because they are the most sensitive to eccentricity conditions. In the following some of these comparisons with transient magnetic FEM simulations are presented. Also the limits of precision of the method were investigated; the results of these investigations are presented at the end of this paragraph. All the simulations presented in the following were started from zero initial conditions (no currents in the damper bars). The simulated time was always chosen as

a compromise between reaching a stabilized state and duration of the transient magnetic FEM simulations carried out for comparison.

4.5.1 Machines used for verifications

The following two existing machines with high number of poles were used for comparison with transient magnetic FEM simulations.

a) Unit 5

The main characteristics of this bulb type machine as well as a picture of some poles are given in the following. In figure 46 the positions of damper bars 1 and 3, for which comparisons will be presented in the following, are indicated.

- Rated output [MVA]: 32.6
- Rated voltage [V]: 10500
- Rated frequency [Hz]: 50
- Number of pole pairs 38
- Rotational speed [rpm]: 78.94
- Number of damper bars per pole: 4
- Symmetrical poles
- Damper bars centered on the pole shoes

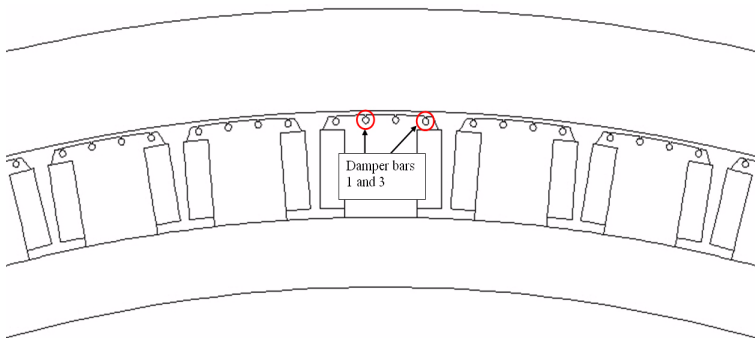


Figure 46: Geometry of unit 5

b) Unit 6

The main characteristics of this bulb type machine as well as a picture of some poles are given in the following. In figure 47 the positions of damper bars 1 and 3, for which comparisons will be presented in the following, are indicated.

- Rated output [MVA]: 47.37
- Rated voltage [V]: 10500
- Rated frequency [Hz]: 50
- Number of pole pairs: 22
- Rotational speed [rpm]: 136.36
- Number of damper bars per pole: 7
- Asymmetrical poles
- Damper bars shifted on the pole shoes

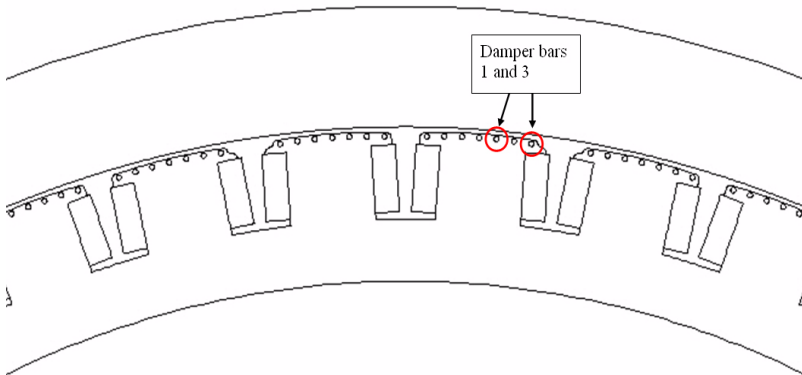


Figure 47: Geometry of unit 6

4.5.2 Damper bar currents

a) 1st order static eccentricity

The simplest and perhaps most common deformation condition is a first order static eccentricity. As described in paragraph 4.1.1 a first order static eccentricity corresponds to the case where the rotor is not centered within the stator.

The following figures show comparisons of the currents in 2 damper bars calculated with the described method and with the transient FEM in the case of a 1st order static eccentricity.

Figure 48 shows a comparison for unit 5 in the case of a 1st order static eccentricity of 0.8mm. As can be seen the currents match almost perfectly.

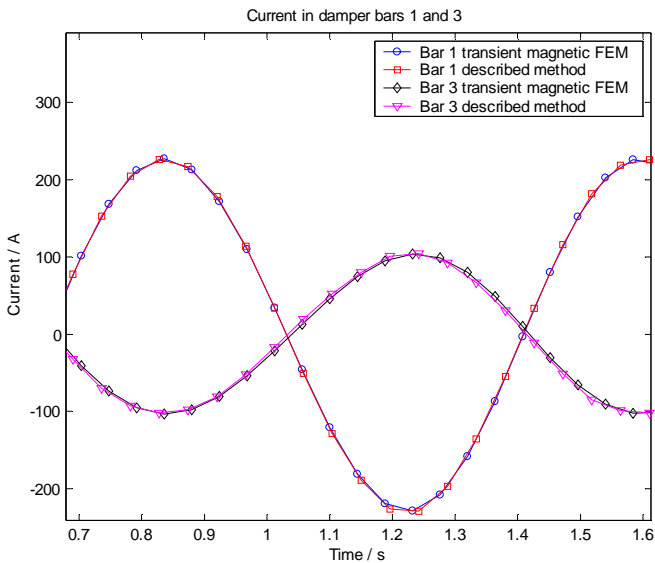


Figure 48: Damper bar currents, unit 5

Figure 49 shows this same comparison for unit 6 in the case of a 1st order static eccentricity of 1.5mm. For the transient magnetic FEM calculations the eccentricity was modeled using air gap segments; the effect of the discontinuous air gap variation in rotation, as mentioned in paragraph 4.2.4, can be observed (due to displaying of a limited number of points, only some samples are disturbed). If this effect is neglected the currents match also in this case very well.

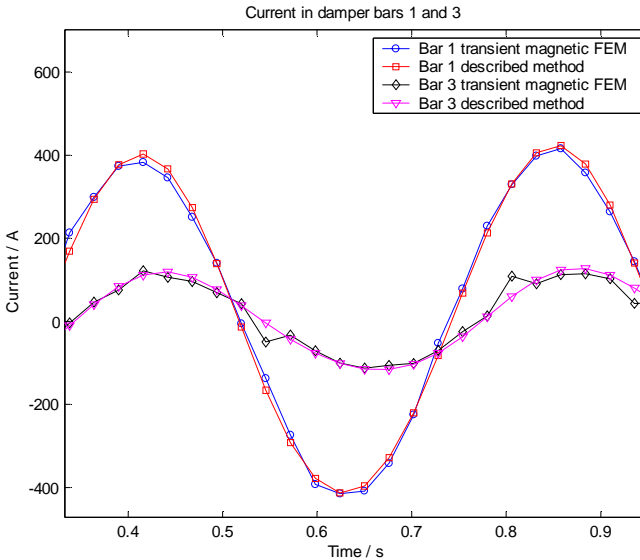


Figure 49: Damper bar currents, unit 6

These examples demonstrate the precision which can be achieved using the described method. In the case of unit 6 (minimum nominal air gap width: 10.3mm) an eccentricity of 1.5mm corresponds to almost 15% of the minimum air gap width which is already a considerable value.

b) Higher order static deformations

The transient FEM simulations for comparison of cases with higher order static deformations were all performed using air gap segments to represent the variable air gap. Therefore some parasitic high order harmonics will always be present in the damper bar currents computed by the transient magnetic FEM (again due to displaying of a limited number of points, only some samples are disturbed).

Figure 50 shows the currents in two damper bars of unit 5 in the case of a 2nd order static deformation of 1.0mm. Again the currents match well. One can observe, as expected, a fundamental harmonic with a frequency 2 times higher than in the case of a 1st order eccentricity (see figure 48). It can also be observed that the amplitude of the current is almost 2 times higher, in spite of an increase in amplitude of the deformation only from 0.8mm to 1.0mm. This is due to the voltage induced in the damper bars depending on the derivative in time of the flux linked to the bars.

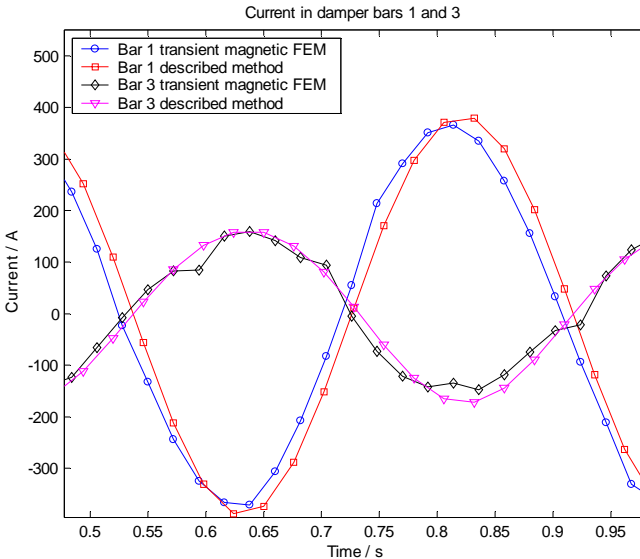


Figure 50: Damper bar currents, unit 5

Figure 51 shows a comparison of the damper bar currents of the same machine in the case of a combined 1st and 3rd order static deformation with amplitudes of 0.9mm and 0.4mm respectively. The two frequency components can be distinguished clearly.

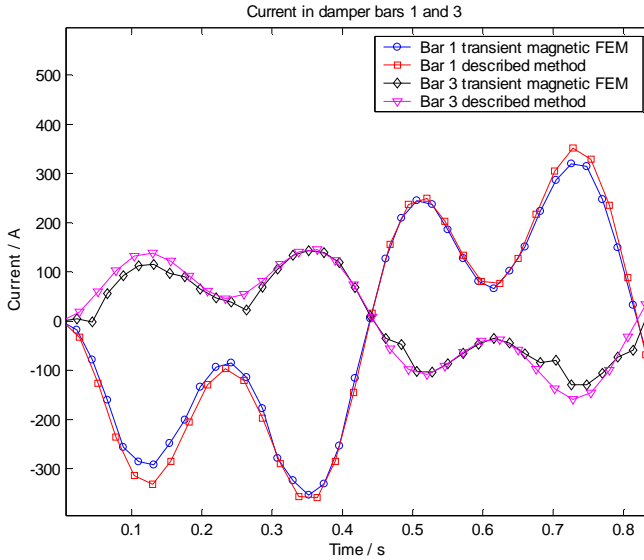


Figure 51: Damper bar currents, unit 5

The third example, shown in figure 52, is unit 6 in the case of a mixed 1st and 2nd order static deformation with amplitudes of respectively 0.4mm and 0.8mm. The curves match well and also in this case the two frequency components can be distinguished clearly.

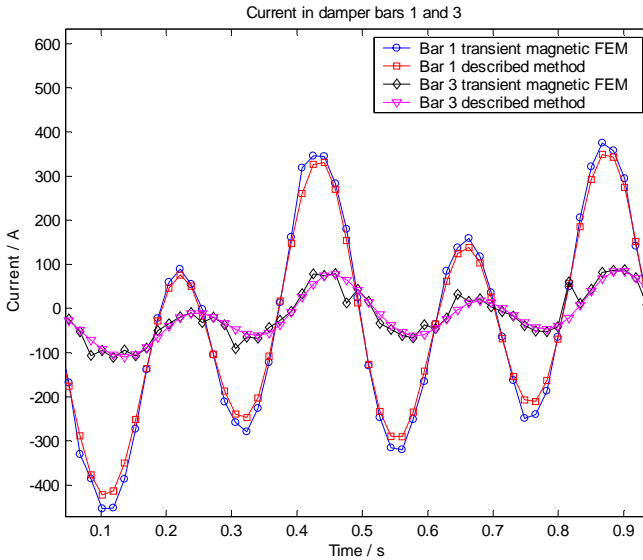


Figure 52: Damper bar currents, unit 6

c) Combined static and dynamic deformation

The case of combined static and dynamic deformations was also verified. Figure 53 shows the same damper bar currents in unit 6 as figure 49 but this time in the case of a combined 1st order static and dynamic eccentricity with amplitudes of 1.5mm and 0.7mm respectively. One can see that the dynamic eccentricity has practically no influence on the damper bar currents; the precision is still quite good. An explication for the slightly higher error will be given in section b) of paragraph 4.5.3.

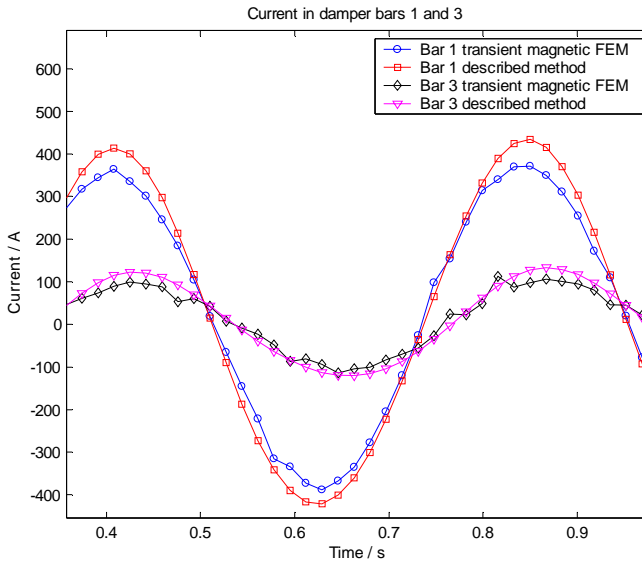


Figure 53: Damper bar currents, unit 6

4.5.3 Induced stator voltages

The voltages induced in conductors at different positions on the stator were also verified. The goal of this was to check if an extension of the method to the computation of the currents in parallel paths of the stator windings is possible. In the following the voltages induced computed using the described method are compared to the voltages obtained with the transient magnetic FEM. In the case of the transient FEM calculations the flux linked to points on the stator was extracted for every time step and the voltage was calculated using an Euler scheme for derivation of the flux.

In paragraph 4.5.4 the unbalanced magnetic pull calculation, which is based on the induced stator voltages, will be verified separately.

a) Static deformations

In the case of a static deformation, the only effect of the deformation is to change the amplitude of the induced voltages. There should be no additional frequencies due to the deformation in the spectrum of the induced voltages.

This phenomenon can be observed in the case of unit 5 (1st order static eccentricity of 0.8mm) and unit 6 (1st order static eccentricity of 1.5mm) in figures 54 and 55; the curves are practically superposed and the difference in amplitude can be clearly seen.

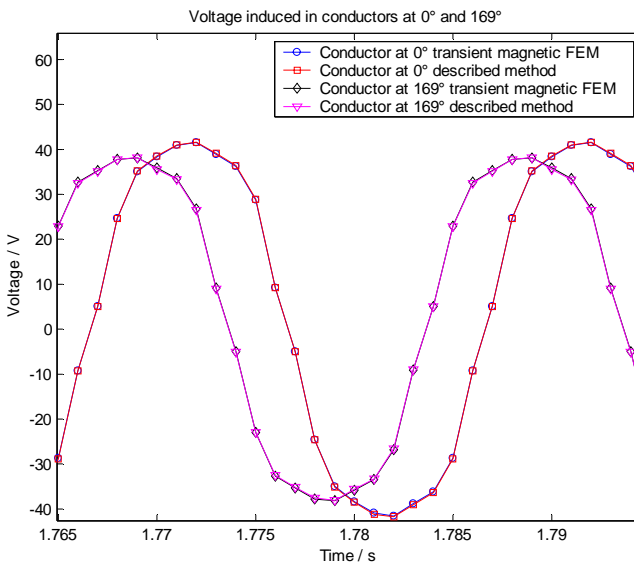


Figure 54: Stator voltages, unit 5

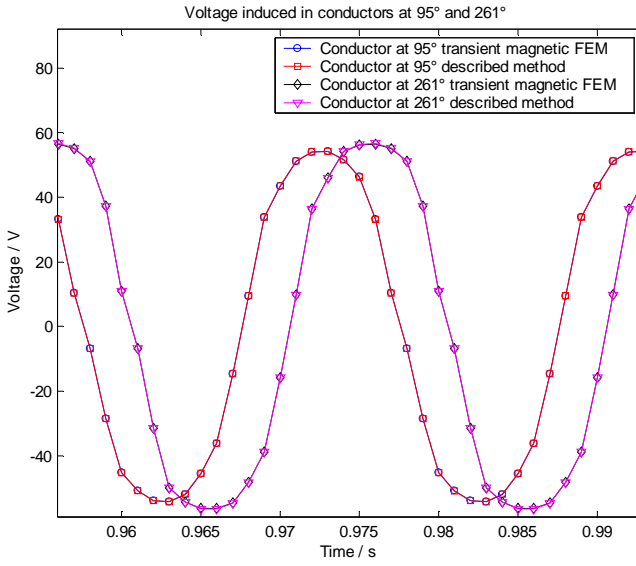


Figure 55: Stator voltages, unit 6

b) Dynamic deformations

Figures 56 and 57 show a comparison of the voltage induced in one conductor of unit 5 and unit 6 in the case of a 1st order dynamic eccentricity of 1.0mm and 0.7mm respectively. The effect of the dynamic eccentricity on the voltages can be seen very clearly.

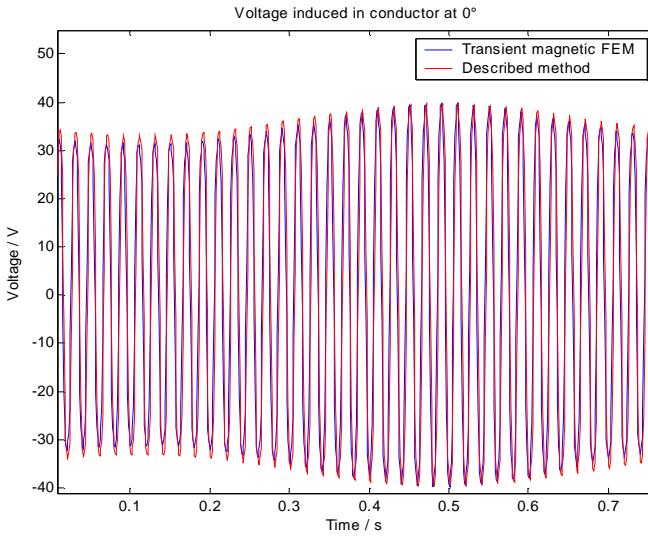


Figure 56: Stator voltages, unit 5

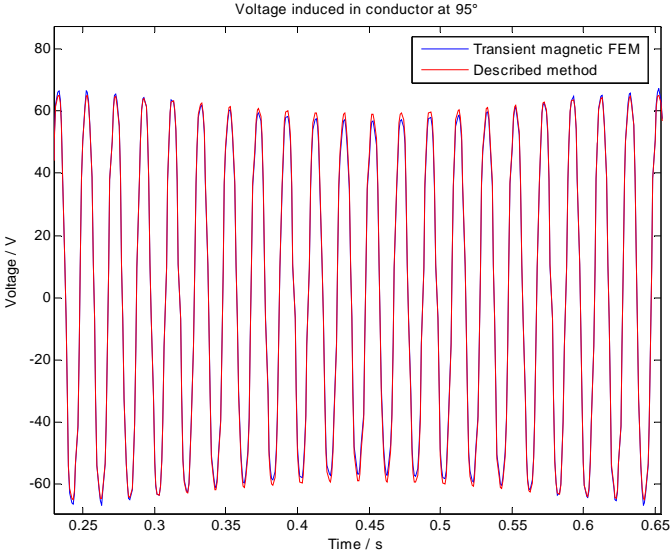


Figure 57: Stator voltages, unit 6

As in the case of the damper bar currents with presence of a dynamic eccentricity (section c) of paragraph 4.5.2) a slightly higher error can be noticed. A certain discrepancy in the amplitudes of the low frequency component due to the eccentricity (1.32Hz and 2.27Hz) is present for both machines. The amplitude calculated with the described method is lower than the amplitude calculated with the transient FEM. This can be explained by the different ways of modeling the dynamic air gap deformation. For the transient FEM simulations the dynamic air gap variation is modeled with air gap line segments in the pole bodies (see figure 58). In the described method the air gap variation is modeled with air gap segments at the interior stator surface (as described in paragraph 4.2.4).

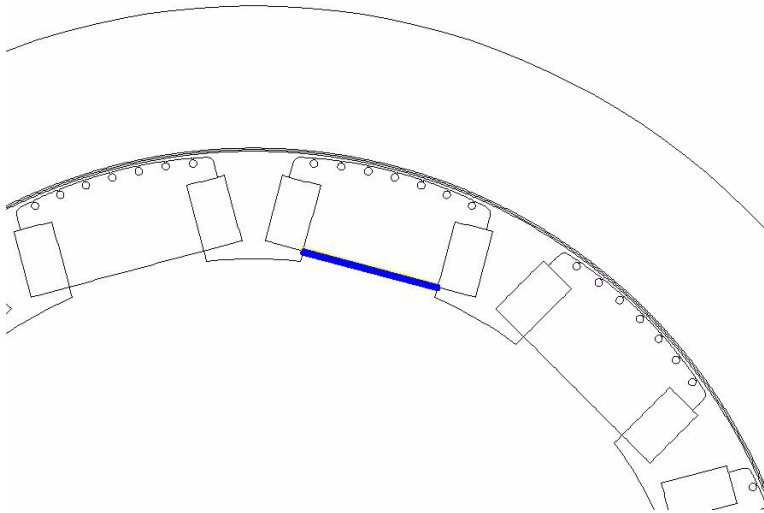


Figure 58: Air gap segment in pole body

In table 4 the relative dynamic eccentricity was evaluated as described in [24]. As can be seen, the air gap deformation is over-estimated by the transient magnetic FEM simulations. These relative eccentricity values, shown in the last two columns, should in any case be lower than the values of the geometric eccentricity, shown in the middle column, due to the damping effects of the iron saturation. The representation of the dynamic air gap deformation used in the case of the transient magnetic FEM simulations does not seem to be the best choice for modeling a dynamic air gap deformation. It is therefore questionable if this kind of transient magnetic FEM simulation can be taken as reference for comparisons regarding a dynamic eccentricity. Additional information concerning this point is provided in paragraph 4.5.4.

	Geometric eccentricity [mm]	Geometric eccentricity [%]	Relative eccentricity FEM [%]	Relative eccentricity descr. meth. [%]
Unit 5	1.0	11.11	11.6	8.4
Unit 6	0.7	6.80	7.7	4.7

Table 4: Dynamic eccentricity evaluation

c) Combined static and dynamic deformations

The following figure 59 compares the voltages in two opposite conductors of unit 6 in the case of a combined 1st order static and dynamic eccentricity with amplitudes of 1.5mm and 0.7mm respectively. The same observations as in the preceding paragraphs can be made.

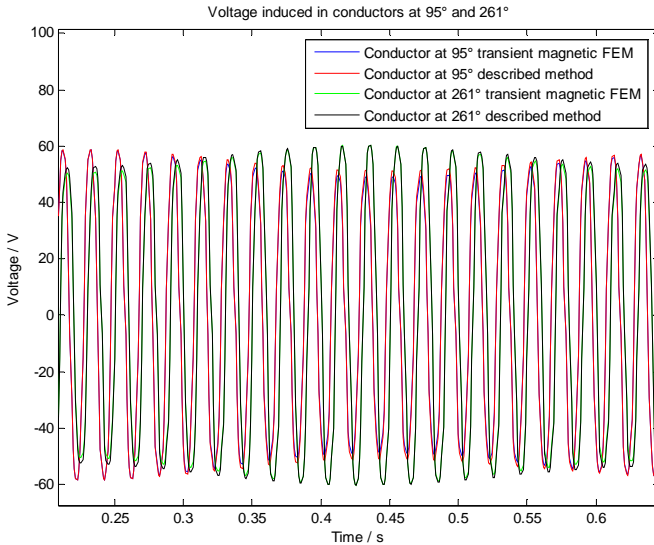


Figure 59: Stator voltages, unit 6

4.5.4 Unbalanced magnetic pulls

The unbalanced magnetic pulls as well as relative deformations calculated according to [24] with voltages obtained with the described method were compared to the unbalanced magnetic pulls and deformations calculated with voltages obtained with the transient magnetic FEM. This was done in the case of unit 6 with a static eccentricity of 1.5mm, with a dynamic eccentricity of 0.7mm and with a combination of both. Additionally the case of a combined 1st and 2nd order static deformation with values of 1.5mm and 1.0mm respectively was calculated with the described method only. Finally the case with static eccentricity was repeated without taking into account the damper bar currents (no rotor damping). The following table summarizes the results; the values on the left are from the transient magnetic FEM the values on the right from the described method.

	Static pull Amplitude [kN]	Static pull Phase [°]	Dynamic pull Amplitude [kN]	Dynamic pull Phase [°]
Static ecc.	163.6 / 169.6	325.4 / 326.2	6.0 / 6.0	- / -
Dynamic ecc.	0.3 / 16.0	- / -	328.1 / 190.0	12.7 / -3.5
Combined ecc.	157.3 / 165.6	321.4 / 327.4	254.8 / 182.3	13.7 / -4.1
Static 1st and 2nd order ecc.	- / 172.9	- / 322.1	- / 6.0	- / -
Static ecc. without damper cage	393.2 / 390.5	270.2 / 269.3	- / -	- / -

Table 5: Comparison of unbalanced magnetic pulls (FEM / described method)

In the case with static eccentricity a good agreement of the amplitudes and of the phases of the static pulls can be observed. The calculated dynamic pull is very low and due to a transient component in the damper bar currents.

The dynamic eccentricity case compares less well. This does not surprise as already the comparison of the voltages was not very satisfying. As already pointed out in paragraph 4.5.3, the method for modeling a 1st order dynamic eccentricity used for the transient magnetic FEM simulations does not seem to be an appropriate choice. Therefore additional comparisons were carried out. Figure 60 shows the unbalanced magnetic pulls due to 1st order dynamic eccentricities of different values and due to 1st order static eccentricities of the same values without rotor damping (without currents in the damper cage). All values were calculated with the described method. For the same value of eccentricity the pulls should be the same, as it is exactly the same air gap deformation only that this deformation is in one case rotating with the rotating speed of the rotor and in the other case fixed with respect to the stator. The

fact that the values match very well shows that the dynamic unbalanced magnetic pull values calculated with the described method should be quite correct. It is clear that this comparison is not a measure for the precision of this calculation.

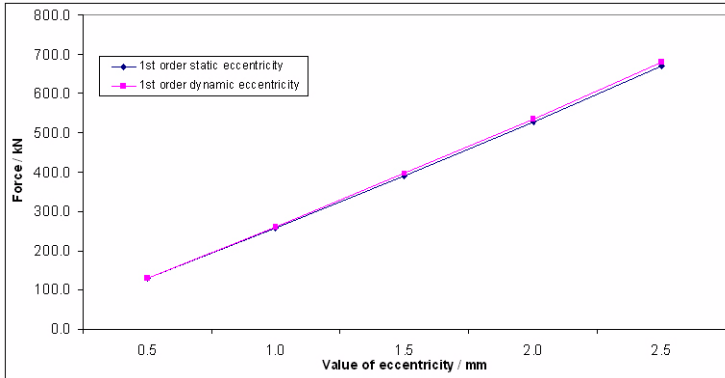


Figure 60: Comparison of static and dynamic unbalanced magnetic pulls

The combined eccentricity case demonstrates very well the fact that static and dynamic eccentricities are almost independent. As expected, the values of the pulls are only very little lower than in the first two cases, except for the dynamic pull calculated with the voltages from the transient FEM. This is again a sign for the unappropriateness of the chosen FEM modeling method.

The case of the combined 1st and 2nd order static deformation shows very well that there is no influence of the 2nd harmonic on the 1st. As expected, the presence of a 2nd harmonic in the static deformation does not influence the result.

The last line of the table shows the same case as the first line but this time without taking into account the damper bar currents. The values of amplitude and phase of the static pull match very well. This example shows that the damping effect of the damper bar currents is taken into account very precisely.

The unbalanced magnetic pull calculation was successfully verified on several machines with a high number of poles. On machines with a low number of poles the precision was less satisfying.

4.5.5 Limits of precision of the presented method

The consequences of the hypothesis adopted in the described method are, as expected, a limited domain of validity of the method. The main factors for this limitation are:

- Spatial discretization of the air gap deformation (number of air gap segments).
- Temporal discretization for the resolution of the circuit equations (number of rotor positions per revolution).
- Linearization of the influence of each air gap segment.
- Linearization around a chosen operating point of the influence of the iron saturation.

In the following the impact of these simplifications will be studied and the limits of validity of the proposed method will be estimated.

a) Influence of the number of air gap segments

The number of air gap segments is a measure for the spatial discretization of the air gap deformation. In general one can say that the higher the order of the air gap deformation the higher the number of segments should be chosen. With the following examples the necessary number of segments to model a given deformation will be determined.

The following figures compare the currents in the damper bars 1 and 3 of unit 5 for two different types of deformation and different numbers of air gap segments.

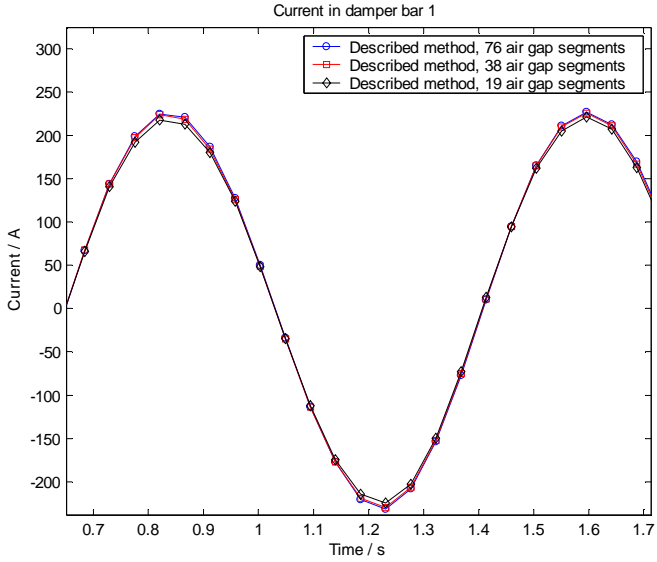


Figure 61: Unit 5, current in damper bar 1, 1st order static eccentricity

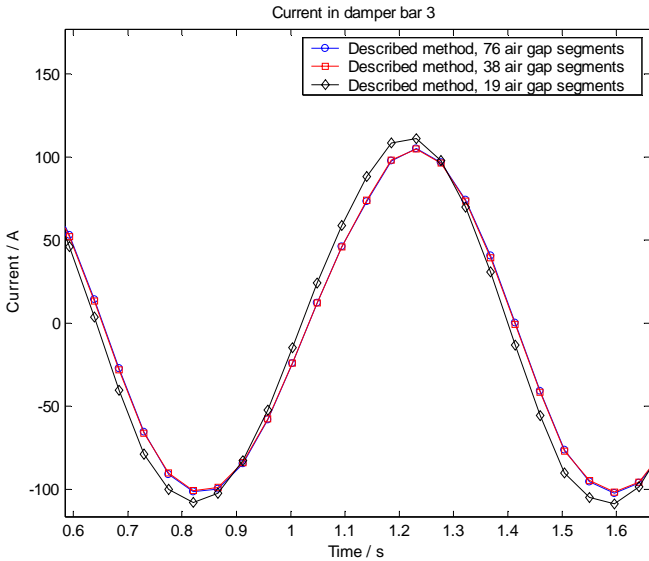


Figure 62: Unit 5, current in damper bar 3, 1st order static eccentricity

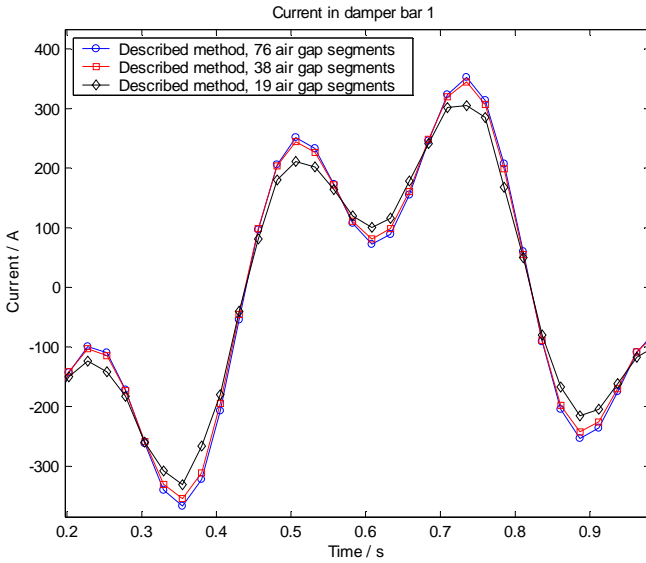


Figure 63: Unit 5, current in damper bar 1, combined 1st and 3rd order static deformation

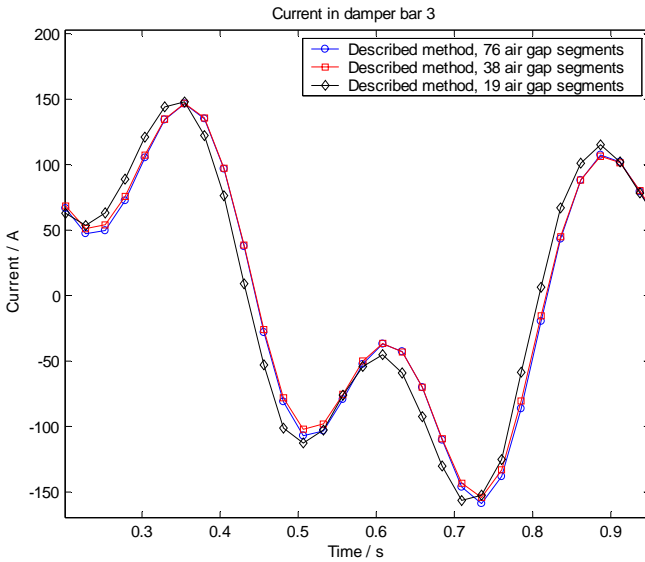


Figure 64: Unit 5, current in damper bar 3, combined 1st and 3rd order static deformation

The example of the 1st order eccentricity shows that with only 19 segments the precision is already significantly lower than with 38 or 76 segments, but there is almost no difference between 38 and 76 segments. The precision in the case of a 3rd order deformation with only 19 segments is even worse but there is still not an important difference between 38 and 76 segments.

As expected the spatial resolution of the representation of the air gap variation (number of air gap segments) has some influence on the precision of the results. Choosing a too low number of air gap segments can in some cases even result in completely wrong results. After analysis of several examples it is recommended to choose a number of at least 40 air gap segments for the analysis of 1st and 2nd order deformations. For the analysis of higher order deformations it is recommended to choose more air gap segments.

b) Influence of the number of rotor positions per revolution

The number of rotor positions per revolution determines the time resolution for the Runge Kutta algorithm, solving the differential equations. Choosing a too low time resolution can lead to very low precision or even to diverging results.

The influence of the number of rotor positions per revolution was tested on unit 5 with an air gap representation with 76 segments. Figure 65 shows the current in the first damper bar in the case of a combined 1st and 3rd order static deformation for different numbers of rotor positions per revolution.

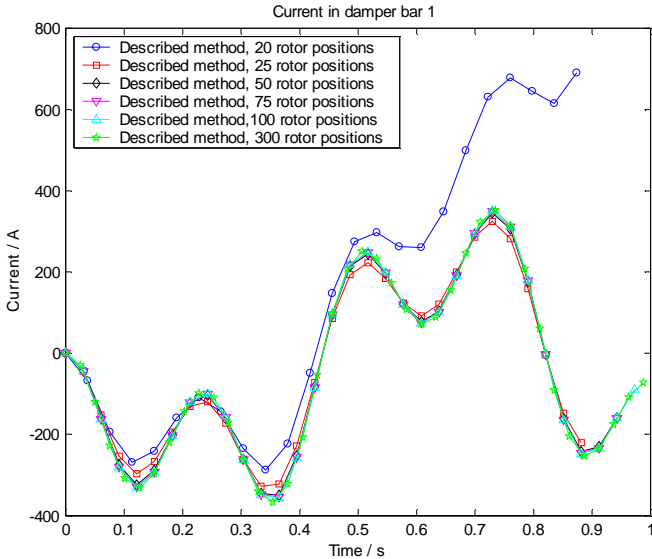


Figure 65: Unit 5, current in damper bar 1, combined 1st and 3rd order static deformation

As can be seen the precision of the results remains very precise down to 50 rotor positions per revolution. The precision is clearly lower with 25 position per revolution and the results diverge with 20 positions per revolution.

Generally it is recommended to use at least 10 to 20 times the highest order of static deformation considered rotor positions per revolution. This means for a 3rd order deformation as shown in the example at least 30 rotor positions per revolution.

If one is also interested in the unbalanced magnetic pulls a second condition concerning the number of rotor positions per revolution has to be respected. As the unbalanced magnetic pull calculation is based on the induced stator voltages, the time resolution has to be chosen so as to represent correctly the fundamental harmonic of the induced voltage (generally 50Hz or 60Hz). It is recommended to chose the number of rotor positions per revolution in this case at least equal to 20 times the number of pole pairs. This condition is generally more severe than the first one (machines with high number of poles and low orders of the static deformation).

c) Amplitudes of air gap deformations and linearization with one or two line segments

Due to the linearization of the influence of each air gap segment and due to the use of the differential inductances the precision of the described method is limited for important air gap deformations. Concerning the linearization of the influence of each air gap segment one has the possibility to choose between 1 or 2 linear segments (see also paragraph 4.2.4); this has also an influence on the precision of the results.

In the following figures the current in damper bar 1 of unit 5 in the case of 1st order static eccentricities with values of 0.8mm, 1.7mm, 2.5mm, 3.5mm and 4.5mm is assessed. On each figure the current obtained from the transient magnetic FEM is compared to the current calculated with the described method with 1 or 2 linear segments for representation of the influence of each air gap segment. It is mentioned that 4.5mm corresponds to about 50% eccentricity in this machine.

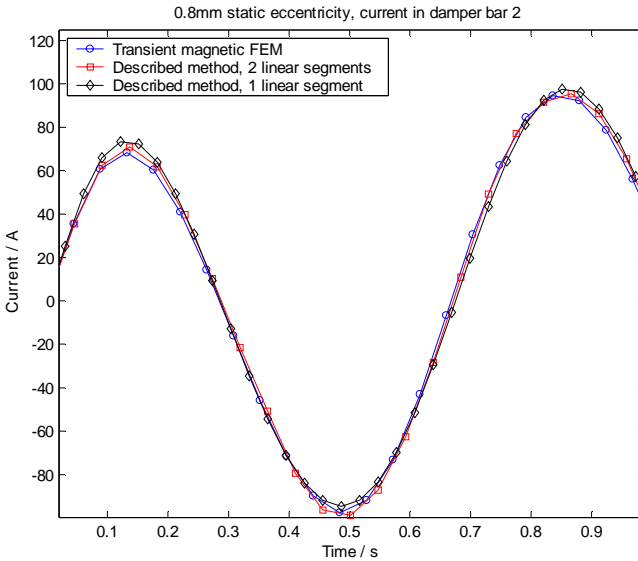


Figure 66: Unit 5, current in damper bar 2, 1st order static eccentricity of 0.8mm

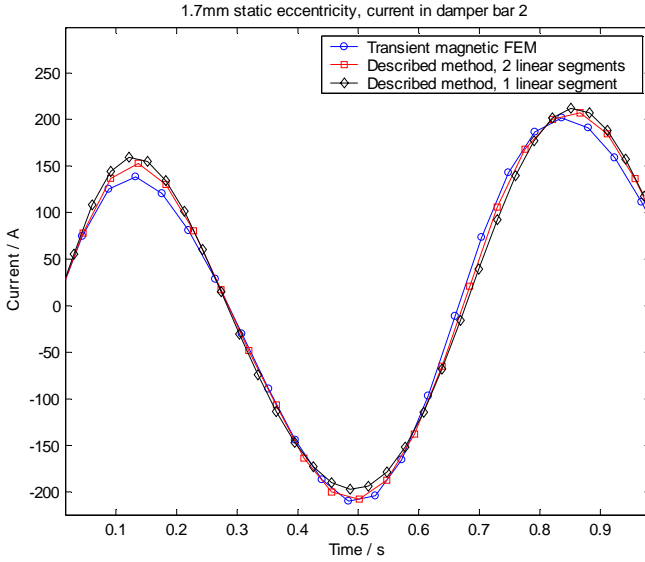


Figure 67: Unit 5, current in damper bar 2, 1st order static eccentricity of 1.7mm

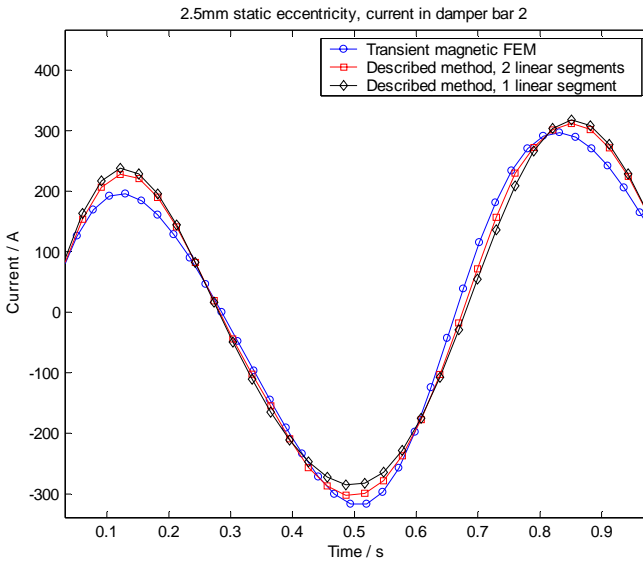


Figure 68: Unit 5, current in damper bar 2, 1st order static eccentricity of 2.5mm

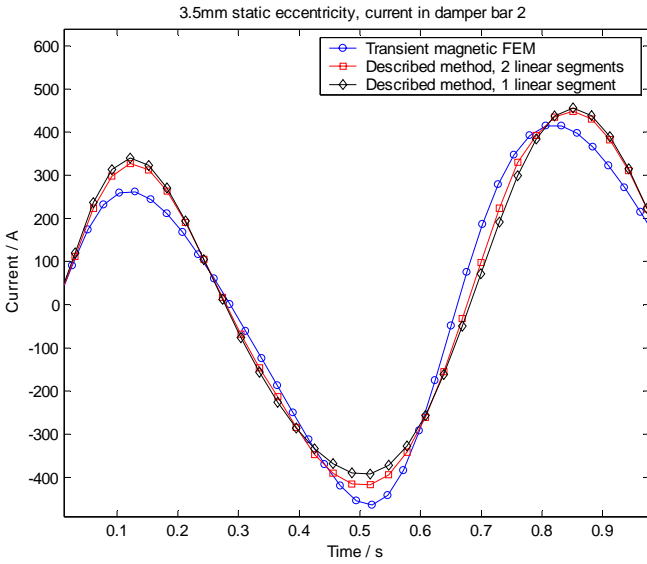


Figure 69: Unit 5, current in damper bar 2, 1st order static eccentricity of 3.5mm

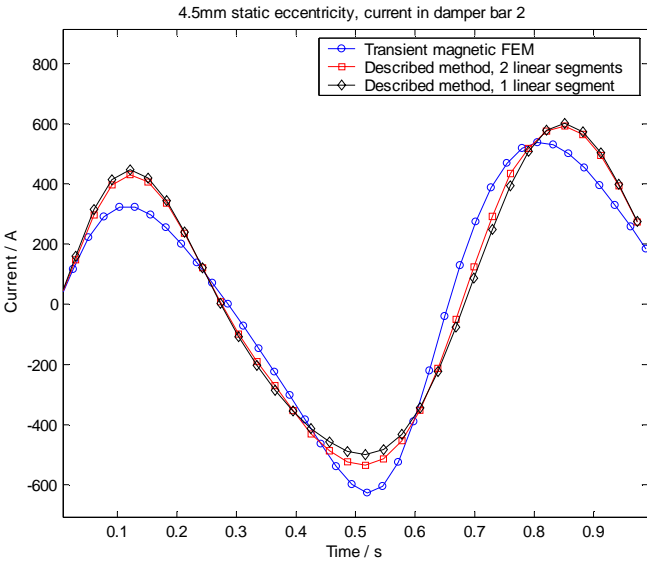


Figure 70: Unit 5, current in damper bar 2, 1st order static eccentricity of 4.5mm

The non linear increase of the amplitude of the currents with increasing amplitude of the deformation due to the iron saturation can be observed clearly. The precision of the results is, as expected, decreasing with increasing amplitude of the deformation. There is not much difference in precision between a linearization of the influence of each air gap segment with 1 or 2 linear segments. Even in the case of an eccentricity of 50% the results remain quite precise.

d) General assessment of the limits of precision

In the preceding paragraphs the expected limits of precision of the described method were investigated. These limitations are not severe and have no impact on an industrial application of the method. For industrial application only deformations with relatively low amplitudes and orders are of interest; severely damaged machines with strong deformations are of no interest in the case of this study and will be analyzed with other methods.

4.6 Application example

4.6.1 Unit 5, geometries with 3 and 4 damper bars

Unit 5 presented in paragraph 4.5.1 was recently refurbished. The pole shoes were exchanged against pole shoes with only 3 damper bars with bigger diameter. The rest of the pole shoe shape remained unchanged. Figure 71 shows the old (left) and the new (right) pole shoe.

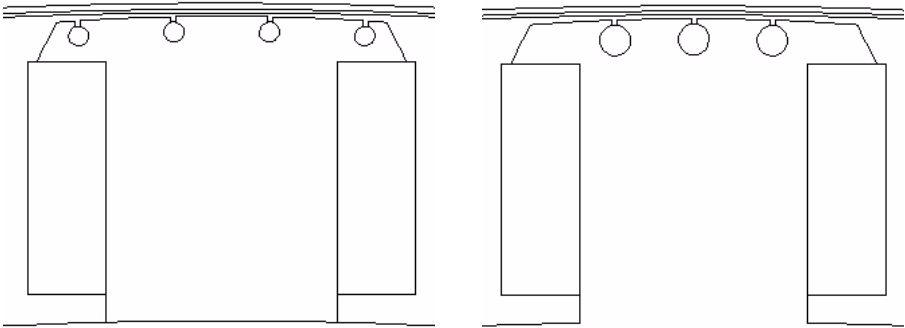


Figure 71: Unit 5, old (left) and new (right) pole shoe shape

The method described in this chapter was used to investigate the damping effects and the Joule losses of the two different damper cage designs. As already mentioned the proposed method allows rapid calculation of the damper bar currents and unbalanced magnetic pulls for different deformation cases. Figures 72 and 73 show the evolution

of the unbalanced magnetic pull and of the damper cage Joule losses in function of the value of a 1st order static eccentricity for the two damper cage designs.

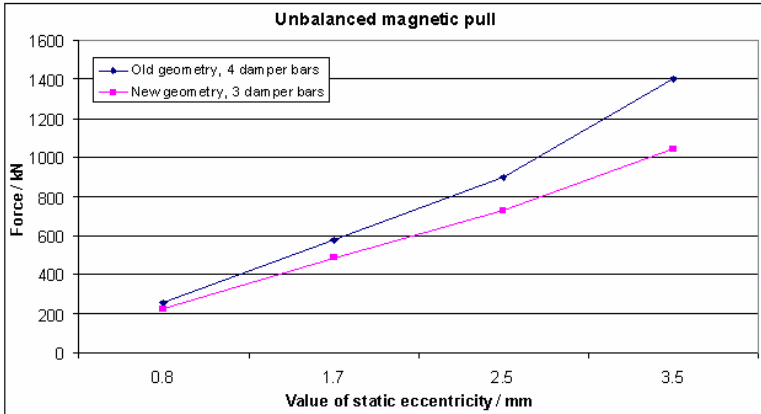


Figure 72: Comparison of unbalanced magnetic pulls

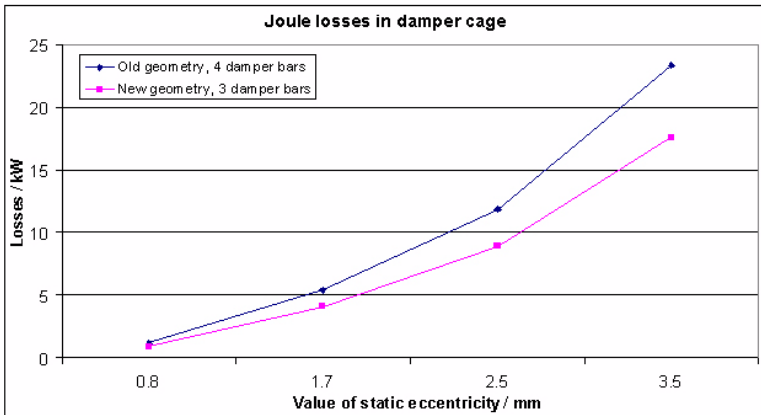


Figure 73: Comparison of damper cage Joule losses

As can be seen the new damper cage design is in both regards considerably better. The Joule losses are about 28% lower and the unbalanced magnetic pull is up to 29% lower.

This application demonstrates the advantages of the proposed method; the comparison of different eccentricity situations was possible in a relatively short time (about 30 minutes per case, based on the flux values of the initial magnetostatic FEM calculations), allowing an eloquent judgement of the two designs.

5 Outlook

The very simple basic principle used in the two presented methods, calculation of the magnetic coupling of the electric conductors using the magnetostatic FEM and resolution of electrical circuit equations makes best use of both worlds. The FEM is used in a limited way only for taking into account the complex geometry of the magnetic domain and its non-linearities and the numerical resolution of the analytical equations guarantees a short calculation time. This basic principle was applied to solve two different problems, the calculation of the no-load voltage of perfectly centered salient-pole synchronous machines and the calculation of unbalanced magnetic pulls and of the additional damper losses due to eccentricities in this same type of machine. The extensions and modifications proposed in the following paragraphs would allow to enhance the precision of the results, to calculate additional values or to apply this basic principle to solve other problems.

5.1 Calculation of circulating currents in stator parallel circuits and equipotential connections

The method for calculation of the damper bar currents and the unbalanced magnetic pulls in eccentricity conditions could be extended to include also the calculation of the currents in parallel circuits and equipotential connections of the stator and to take into account their damping effects in the unbalanced magnetic pull calculation.

This extension would work on exactly the same principles as the method presented in this document. One basic condition, the value of the voltages induced in the stator conductors, was already verified and the tool implementing the existing method is prepared for this extension.

Additionally the mutual inductances of the stator conductors should be calculated accordingly to the same principles as were applied for the determination of the mutual inductances of the damper bars. The system of differential equations described in paragraph 2.5.2 should then be adapted accordingly and could be solved in the same way as for the calculation of the damper bar currents.

Including this extension, the described method will be a very complete and convenient tool for the analysis of low speed hydrogenerators in eccentricity conditions.

5.2 Calculation for other operating points

The simple basic principle used in the two presented methods allows to take into account precisely the complex geometry of salient-pole synchronous generators, as well as the non-linearity of the magnetic circuit for a given operating point.

In the presented methods the chosen operating point was the no-load operation at rated voltage. It could also be imagined to calculate the flux linkage values and mutual differential inductances for other operating points, for example for rated output at rated voltage and rated power factor. As long as only calculations in steady-state conditions are considered, the cyclic periodicity of the machine can be considered in the same way as described in this report. This method would allow to carry out very complex investigations. The only condition is that the machine is in steady-state conditions (imposed main flux), but different types of defects could be analyzed (e.g. eccentricities, partial short-circuits in field windings, broken damper bars, asymmetrical steady-state conditions, etc.) in different operating conditions.

This basic principle constitutes in fact an advanced model for electric machine calculation. More generalized methods based on this same principle could also be used for more general electric machine calculations. There is still some potential that could be investigated.

6 Conclusion

The starting point of this thesis was the desire to analyze large low speed synchronous generators in eccentricity conditions. Of specific interest were the damping effects of the damper cage and the Joule losses in the damper cage due to different eccentricity situations. An inventory of the currently used methods for analysis of electrical machinery showed that the existing methods were either too slow or not precise enough for the kind of study in consideration.

The present thesis proposes therefore two combined numerical and analytical methods. The first one allows a fast calculation of the damper bar currents and of the voltage waveform in no-load conditions of perfectly centered, large salient-pole synchronous generators. The second one allows the determination of the damper bar currents and of the unbalanced magnetic pulls in no-load conditions of large low speed salient-pole synchronous generators in eccentricity conditions.

The presented methods are based on the same principles and therefore also on very similar hypothesis. They are both based on magnetostatic FEM calculations and on the resolution of electrical circuit differential equations. Therefore the methods take into account saturation and rotor damping effects, as well as the real geometry of the machines. They are much faster than transient magnetic FEM simulations (10 to 20 times faster) but provide the same level of precision. The described methods were successfully tested and verified on several existing hydrogenerators by comparison with results from transient magnetic FEM simulations.

Due to the very good level of precision the methods can be used for precise prediction of the no-load losses in the damper cage, of the harmonics in the no-load voltage (THF calculation) and of the unbalanced magnetic pulls. The first method allows to analyze the influence of different damper cage layouts, different pole shoe positions and shapes, magnetic wedges in the stator slots, as well as different winding schemes on the no-load voltage harmonics and on the no-load losses. The second one permits the assessment of the Joule losses and of the damping effects of different damper cage designs in different eccentricity situations.

For convenient industrial application both methods were implemented in documented tools with graphical user interfaces. The tools work directly with the result files provided by the commercially available FEM software Flux from Cedrat.

7 Bibliography

- [1] A. Schwery, G. Traxler-Samek, E. Schmidt, "Application of a Transient Finite Element Analysis with Coupled Circuits to Calculate the Voltage Shape of a Synchronous Generator", Proceedings of the 10th IEEE Conference on Electromagnetic Field Computation (CEFC), 2002
- [2] K. Weeber, "Design of Amortisseur Windings of Single-Phase Synchronous Generators Using Time-Stepping Finite Element Simulations", International Conference on Electrical Machines (ICEM), 1998
- [3] G. Traxler-Samek, A. Schwery, E. Schmidt, "Analytic Calculation of the Voltage Shape of Salient Pole Synchronous Generators Including Damper Winding and Saturation Effects", Proceedings of the 15th International Conference on Electrical Machines (ICEM), 2002
- [4] W. Janssen, "Ueber den Einfluss der Nutschlitz auf die Spannungskurvenform von Vollpolsynchrongeneratoren", Archiv für Elektrotechnik 77, 1994
- [5] K. Brune, H. O. Seinsch, J. Steinbrink, "Conducted emission of synchronous generators and its dependence on design features", Electrical Engineering 85, 2003
- [6] A. M. Knight, H. Karmaker, K. Weeber, "Use of a Permeance Model to Predict Force Harmonic Components and Damper Winding Effects in Salient-Pole Synchronous Machines", IEEE Transactions on Energy Conversion, Vol. 17, No. 4, 2002
- [7] H. A. Toliyat, N. A. Al-Nuaim, "Simulation and Detection of Dynamic Air-Gap Eccentricity in Salient-Pole Synchronous Machines", IEEE Transactions on Industry Applications, Vol. 35, No. 1, 1999
- [8] I. Tabatabaei, J. Faiz, H. Lesani, M. T. Nabavi-Razavi, "Modeling and Simulation of a Salient-Pole Synchronous Generator With Dynamic Eccentricity Using Modified Winding Function Theory", IEEE Transactions on Magnetics, Vol. 40, No. 3, 2004
- [9] S. Williamson, A. F. Volschenk, "Time-stepping finite element analysis for a synchronous generator feeding a rectifier load", IEE Proc. - Electr. Power Appl., Vol. 142, No. 1, 1995
- [10] J. Gyselincx, L. Vandeveld, J. Melkebeek, W. Legros, "Steady-State Finite Element Analysis of a Salient-Pole Synchronous Machine in the Frequency Domain", Proceedings of the 7th International Conference on Modeling and Simulation of Electric Machines, Converters and Systems, 2002
- [11] Flux, Cedrat, Grenoble, France, www.cedrat.com
- [12] R. Tuschak, "Stromverdrängung von in kreisförmigen Nuten gebetteten massiven Leitern", Period Polytech Electr Eng 1, 1957, Pages 27 – 51
- [13] A. M. Knight, S. P. Bertani, "Mechanical Fault Detection in a Medium-Sized Induction Motor Using Stator Current Monitoring", IEEE Transactions on Energy Conversion, Volume 20, Issue 4, December 2005, Pages 753 – 760
- [14] S. Nandi, R. M. Bharadwaj, H. A. Toliyat, "Performance Analysis of a Three-Phase Induction Motor Under Mixed Eccentricity Condition", IEEE Transactions on Energy Conversion, Volume 17, Issue 3, September 2002, Pages 392 – 399
- [15] S. Nandi, S. Ahmed, H. A. Toliyat, "Detection of Rotor Slot and Other Eccentricity Related Harmonics in a Three Phase Induction Motor with Different Rotor Cages", IEEE Transactions on Energy Conversion, Volume 16, Issue 3, September 2001, Pages 253 – 260
- [16] D. G. Dorrell, "Experimental Behaviour of Unbalanced Magnetic Pull in 3-Phase Induction Motors with Eccentric Rotors and the Relationship with Tooth Saturation", IEEE Transactions on Energy Conversion, Volume 14, Issue 3, September 1999, Pages 304 – 309
- [17] D. G. Dorrell, "Calculation of Unbalanced Magnetic Pull in Small Cage Induction Motors with Skewed Rotors and Dynamic Rotor Eccentricity", IEEE Transactions on Energy Conversion, Volume 11, Issue 3, September 1996, Pages 483 – 488
- [18] N. Al-Nuaim, H. A. Toliyat, "A Novel Method for Modeling Air-Gap Eccentricity in Synchronous Machines Based on Modified Winding Function Theory", IEEE Transactions on Energy Conversion, Volume 13, Issue 2, June 1998, Pages 156 – 162

- [19] A. Foggia, J.-E. Torlay, C. Corenwinder, A. Audoli, J. Hérigault, "Circulating Current Analysis in the Parallel-Connected Windings of Synchronous Generators under Abnormal Operating Conditions", International Conference on Electric Machines and Drives (IEMD), Seattle, USA, May 1999, Pages 634 – 636
- [20] J. S. Hsu, J. Stein, "Effects of Eccentricities on Shaft Signals Studied Through Windingless Rotors", IEEE Transactions on Energy Conversion, Volume 9, Issue 3, September 1994, Pages 564 – 571
- [21] J. S. Hsu, J. Stein, "Shaft Signals of Salient-Pole Synchronous Machines for Eccentricity and Shorted-Field-Coil Detections", IEEE Transactions on Energy Conversion, Volume 9, Issue 3, September 1994, Pages 572 – 578
- [22] R. L. Stoll, "Simple computational model for calculating the unbalanced magnetic pull on a two-pole turbogenerator rotor due to eccentricity", IEE Proceedings on Electric Power Applications, Volume 144, No. 4, July 1997, Pages 263 - 270
- [23] S. Keller, "Calculation of damper bar currents in eccentered salient-pole synchronous machines - users manual", LME internal report, August 2006
- [24] M. Tu Xuan, J.-J. Simond, R. Wetter, S. Keller, "A Novel Air-Gap Monitoring System For Large Low Speed Hydro-Generators", Proceedings of the IEEE-PES Annual Meeting, June 2006, Montréal
- [25] S. Keller, M. Tu Xuan, J.-J. Simond, "Large Low Speed Hydrogenerators - UMP and Additional Damper Losses in Eccentricity Conditions", accepted for publication in the IET Electric Power Applications Journal
- [26] M. Bissonnette, M. Cloutier, "Air gap measuring system", Proceedings of the 1st International Machinery Monitoring and Diagnostic Conference, Las Vegas, USA, 1989, Pages 261 - 267
- [27] S. Keller, M. Tu Xuan, J.-J. Simond, "Computation of the no-load voltage waveform of laminated salient-pole synchronous generators", IEEE Transactions on Industry Applications, Volume 42, Issue 3, May-June 2006, Pages: 681 - 687
- [28] J. Chatelain, M. Tu Xuan and B. Kawkabani, "Damping of the unbalanced magnetic pull in machines with rotor eccentricity by using windings with parallel paths", Beijing International Conference on Electrical Machines (BICEM), Beijing, China, August 1987.
- [29] K. Vogt et al., "Elektrische Maschinen - Berechnung rotierender elektrischer Maschinen", VEB Verlag Technik Berlin, 2. Auflage, 1974, Pages 187 - 196

8 Glossary

Symbol	Unit	Description	Page
L_{ij}	H	mutual inductance of conductors 'i' and 'j'	10
ϕ_j	Wb	flux linked with conductor 'j'	10
i_i	A	current in conductor 'i'	10
$\phi_{exc,j}$	Wb	flux linked with conductor 'j', caused by the field winding	12
$\Delta\phi_{k,j}$	Wb	small flux variation due to the current in conductor 'k'	12
$L_{diffk,i}$	H	mutual differential inductance of conductors 'k' and 'j'	12
τ_s	m	stator slot pitch	13
$\phi_{exc,k,j}$	Wb	flux linked with conductor 'j' caused by the field winding and conductor 'k'	14
R_j	Ω	resistance of conductor 'j'	16
$\vec{i}(t)$	A/s	vector of the derivatives of the currents in the damper bars at time 't'	18
$\vec{i}(t)$	A	vector of the currents in the damper bars at time 't'	18
\vec{i}^k	A	vector of the currents in the damper bars at time step 'k'	20
$h, \Delta t$	s	length of the time step	20
u_{ind_j}	V	voltage induced in conductor 'j'	20
U_i	V	harmonic component of order 'i' of the no-load voltage	28
λ_i	1	weighting factor for THF calculation	28
O_r	1	rotating center of the rotor	38
O_s	1	rotating center of the stator	38
k_c	1	Carter factor	44
B_δ	T	maximum field density in the air gap with stator slotting	44
B_{max}	T	maximum field density of the idealized air gap field curve	44
b_s	m	stator slot opening	44
δ	m	minimum air gap width of the slotted stator	44
δ_{sm}	m	minimum air gap width of the smooth stator after Carter correction	45
$\phi^*_{exc,j}$	Wb	flux linked with conductor 'j' caused by the field winding in the perfectly centered machine	55
$k_{exc,j,l}$	Wb/mm	influencing factor fo segment 'l' on the flux linkage between field winding and conductor 'j'	55
δ_l	mm	difference from the mean air gap width for segment 'l'	55
$L^*_{diff,i}$	H	mutual differential inductance of conductors 'i' and 'j' in the perfectly centered machine	56

$k_{i,j,l}$	Wb/mm	influencing factor fo segment 'l' on the mutual differential inductance of conductors 'i' and 'j'	56
\hat{v}_B	T	amplitude of the harmonic v of the air gap induction of a centered synchronous machine	64
η_{ε_s}	1	relative amplitude of the harmonic η of the static air gap deformation	64
η_{ϕ_s}	$^{\circ}$	phase angle of the harmonic η of the static air gap deformation	64
κ_{ε_r}	1	relative amplitude of the harmonic κ of the dynamic air gap deformation	65
κ_{ϕ_r}	$^{\circ}$	phase angle of the harmonic κ of the dynamic air gap deformation	65
$U_{\alpha_s}(t)$	V	voltage induced at position α_s on the stator bore	65
v	m/s	speed of the rotating magnetic field	65
l_i	m	ideal length of the machine	65
$\sigma(\alpha_s, t)$	Ws/m ³	magnetic pressure at position α_s on the stator bore	65
$F(t)$	N	unbalanced magnetic pull in function of time	66
r	m	bore radius	66

Curriculum vitae

Identity

Name: Keller Stefan
Date of birth: 21 May 1978
Nationality: Swiss
Email: stefan.keller@a3.epfl.ch

Education

1999 - 2003 Swiss Federal Institute of Technology Lausanne EPFL, Faculty of electrical engineering
1998 - 1999 Swiss Federal Institute of Technology Zurich ETHZ, Faculty of electrical engineering
1991 - 1998 Kantonsschule Hohe Promenade Zurich, Languages and Literature

Professional experience

2003 – present Doctoral assistant, EPFL, Laboratory for Electrical Machines (LME)
2000 – 2003 Assistant, EPFL, programming course and electronics laboratory
2000 Internship (13 weeks), Silicon Graphics manufacturing SA Cortaillod (CH)
1998 Internship (7 weeks), Grob AG Männedorf (CH)

Publications

«Large Low Speed Hydrogenerators - UMP and Additional Damper Losses in Eccentricity conditions», S. Keller, M. Tu Xuan, J.-J. Simond
Accepted for publication in the IET Electric Power Applications Journal

«An Original Inductive Air-Gap Monitoring System for Large Low Speed Hydro-Generators», J.-J. Simond, M. Tu Xuan, R. Wetter, S. Keller
Encontro Nacional de Monitoramento, November 2006, Foz do Iguaçu, Brazil

«A novel air-gap monitoring system for large low speed hydro-generators», M. Tu Xuan, J.-J. Simond, R. Wetter, S. Keller
IEEE PES General Meeting, June 2006, Montréal, Canada

«Computation of the no-load voltage waveform of laminated salient-pole synchronous generators», S. Keller, M. Tu Xuan, J.-J. Simond
IEEE Transactions on Industry Applications, Volume 42, Issue 3, Mai-June 2006, Pages 681-687

«Prediction of the no-load voltage waveform of laminated salient-pole synchronous generators», S. Keller, M. Tu Xuan, J.-J. Simond
IEEE IAS Annual Meeting, October 2005, Hong Kong, China

«Synchronous generator no-load voltage prediction using a combined analytical and FEM approach», S. Keller, M. Tu Xuan, J.-J. Simond
6th International Symposium on Advanced Electromechanical Motion Systems (Electromotion), September 2005, Lausanne, Switzerland